UNIVERSITÀ
DEGLI STUDI
FIRENZE

DOTTORATO DI RICERCA IN
Scienza Biomediche
Indirizzo in Oncologia Sperimentale e Clinica

CICLO XXVI

COORDINATORE Prof. Dello Sbarba Persio

Development of new therapeutic strategies for hERG targeting in leukemia cells

Settore Scientifico Disciplinare MED/04

Dottorando
Dott.ssa Falsini Sara

Tutore
Prof. Arcangeli Annarosa

Coordinatore
Prof. Dello Sbarba Persio

Anni 2011/2013

Principal aims of the thesis

hERG as a molecular and pharmacological target?

Leukemia represents a type of cancer very heterogeneous in the modality of development and also in the capability to respond to various treatments. In fact notwithstanding the remarkable progress attained in these last decades, a considerable percentage of patients still fail in response to standard drug treatments (chemotherapy or radiotherapy).

In fact many patient cases have an unfavorable outcome due to unpredictable development of the pathology, non specific distribution of drug, inadequate drug concentrations reaching the target, intolerability and development of multi-drug resistance. The advent of genomic technologies allowed to develop data that address the molecular profile of cancer for each patient, thus laying the foundation for the development of a personalized therapy. The molecular profile allows to evidence biomarkers, including mutated and overexpressed genes, as well as genes encoding fusion proteins (for example bcl-abr in chronic myeloid leukemia, CML).

Since many years, research in our laboratory underlined the importance of human *ether a-gò-gò* related gene (hERG) potassium channel activity in cancer, especially in leukemia. My thesis project fits on this research current in which are just demonstrated hERG role :

1. in the progression thought G1 phase of the acute myeloid leukemia (AML) cell cycle;
2. in migration and invasiveness from bone marrow to peripheral blood and AML diffusion into extramedullary organs;
3. in chemoresistance of acute lymphoblastic leukemia cells (ALLs) induce by the presence of bone marrow mesenchymal cells (MSCs).

For these reasons, hERG could be considered as a possible target in antineoplastic therapy and hERG inhibitors as a possible anticancer drugs. However the use of hERG blockers in clinical therapies is limited by the side effects induced in the patients. In fact $K_v11.1$ channels contribute to shape of action potential repolarization in ventricular heart myocytes. After depolarization, during the repolarization phase, they quickly recover from inactivation, thus transiently opening, they close again at the negative membrane potential. The most serious side effect induced by hERG inhibitors is caused by the prolongation of the cardiac repolarization and in turn in the extension of QT interval in the ECG. An uncontrolled QT interval lengthening can result in torsade de points (TdP), a ventricular arrythmia that may lead to ventricular fibrillation.

Our goal should be the development of new antineoplastic drugs, targeting hERG avoiding arrhtythmia and strengthening the positive effects of hERG inhibition, including reduction of leukemia invasiveness and chemoresistance induced by the presence of MSCs. In order to obtain these purposes we have attempted two different approaches: pharmacological and molecular.

The first of these approaches is based on the study of pharmacological effects of the hERG blocker, clarythromicin and its combinatorial effect with a conventional chemoterapic cytarabine, *in vitro* and *in vivo*. *In vitro* the experiments are conducted on acute promyelocitic leukemia cell line (HL60) in suspension and in co-colture with MSCs. We underline the effect of clarythromicin alone and its effect combined with cytarabine in HL60 and also in co-colture.

Presently, the experiments are conducted *in vivo* by Dr. Marika Masselli using acute promyleocitic leukemia cell line HL60-luc for imaging in NOD-SCID mouse. In particular the effect of clarytromycin alone and in combination with cytarabine has been studied.

The second approach is based on the development of new lipid based vectors for RNA interference (RNAi) targeting hERG. RNAi is an evolutionary conserved phenomenon whereby small double-stranded RNA regulates gene expression. The versatility of the RNAi mechanism has led to its exploitation for the treatment of diseases. However, many physiological obstacles stand in the way of successful and efficient use of RNAi as therapy. One of main challenges is the design of practical delivery reagents that are capable of protecting siRNA in circulation, as well as safely and efficiently delivering it to cytoplasm of appropriate cell types *in vivo*. A number of nonviral carriers have been used for potential *in vivo* delivery siRNA, including cationic polymers, peptides or liposomes and lipid-like materials that form complexes with negatively charged siRNAs by ionic interactions. Our attention is focused on four cationic surfactants namely: 12-3-12, 12-6-12, 12-12-12 and SH14, as possible delivery agents of siRNA. It is well established that cationic surfactants in aqueous solution self-assembly into micelles that are able to interact with the negative backbone of siRNA. Our attempt is the study of time-resolved complexation of siRNA and cationic surfactant micelles. This method allows to obtain informations not only on the aggregate internal structure and size but also of the timing necessary to obtain complexes with size useful for biological use.

First Part

Targeting hERG channels: a pharmacological approach through macrolide antibiotics

Chapter 1

1.1 Potassium channels

Voltage gated-like ion channels (VGICs) constitute the third largest group of signaling molecules encoded by the human genome, after protein kinases and G protein. [1] Within VGICs, K^+ channel genes represent the most extended superfamily with 78 members.
According to the IUPHAR classification K^+ channels can be divided into four structural types on the basis of their mode of activation and the number of transmembrane (TM) segments present in each channel subunits:

1. inwardly rectifying 2-TM K^+ channel (K_{ir});
2. two-pore, 4 TM (K_{2P});
3. calcium activated, 6 or 7 TM (K_{Ca});
4. voltage-gated, 6 TM (K_v)

1.1.1 Inwardly rectifying K+ channel

Inwardly rectifying K^+ (K_{ir})[2] currents are first identified in skeletal muscle.[3] They show greater flow of K^+ into the cell, rather than out of it. K_{ir} channels have been found in a wide variety of cells: cardiac myocytes[4], neurons[5], blood cells[6], osteoclasts[7], endothelial cells[8], glial cells[9], epithelial cells[10] and oocytes[11].
In 1993 the ATP-dependent K_{ir} channel ROMK1/K_{ir}1.1[12] and the ATP-dependent K_{ir} channel IRK1/K_{ir}2.1[13] were isolated, respectively from the outer medulla of rat kidney and from a mouse macrophage cell line respectively, and then characterized. Their primary structure is characterized by two transmembrane domains (TM1 and TM2),

linked by an extracellular pore-forming region (H5) and cytoplasmic amino (NH2)- and carboxy (COOH)- terminal domains. The H5 region permits the selective transport of K^+ ions thanks the signature sequence T-X-G-Y(F)-G which characterized only K^+ channel. The lack of the S4 voltage sensor region makes this channel insensible to membrane voltage and active at all membrane potential (**Figure 1.1, panel A**).
Inwardly rectifying channel are made up by four subunits each in a tetrameric complex. Actually 15 K_{ir} subunit genes have been identified and classified into seven subfamilies (K_{ir}1.x to K_{ir}7.x).

1) classical K_{ir} channels (K_{ir}2.x);
2) G-protein gated K_{ir} channel (K_{ir}3.x);
3) ATP-sensitive K^+ channels (K_{ir}6.x);
4) K^+-transport channel (K_{ir}1.x, K_{ir}4.x, K_{ir}5.x, K_{ir}7.x)

The simplicity and strong homology of the basic K_{ir} channel subunit allow for both homomeric and heteromeric combinations to form functional K_{ir} channels. Heteromeric assemblies generally occur within members of the same subfamily, for example, Kir 2.1 can associate with any one of other Kir2.x subfamily members. An exception is represented by Kir4.1 that aggregates with Kir5.1.
Many factors regulate pore opening kinetics and ion flux, such as ions, polyamines, nucleotides, lipids and a variety of intracellular proteins. Inward rectification of K^+ flux through K_{ir} channels result from the interaction between two intracellular substances, $Mg^{2+}$and polyamines.[14,15]
Other blockers most commonly used for K_{ir} channels are Ba^+ and Cs^+, also tetraethylammonium (TEA) and 4-aminopyridine (4-AP).[16,17]

1.1.2 Two-Pore Domain Potassium Channels

The family of two domain potassium (K_{2P})[18] channels includes fourteen members encoded by different genes. These members are divided into six subfamilies: TWIK, TREK, TASK, THILK, TALK and TRESK on the basis of sequence similarities and functional resemblance. However the members of different subfamilies show relatively low sequence similarity.[19] The 2 pore domain potassium channels are characterized by the same general structure. Each subunit contains two pore -forming regions arranged in tandem (P1 and P2) and four transmembrane segments (TM1-TM4) (**Figure 1.1, panel B**). Accordingly, K_{2P} subunits dimerize to constitute the functional selectivity filter containing four pore loop domains, a structure common to all known potassium channels. The hypothesis that K_{2P} channels give rise to background K^+ current, is well established. This current follows the Goldman-Hodgkin-Katz current equation[20] and regulates the resting membrane potential, as well as excitability of many kinds of cells.
These channels influence cell membrane potential and excitability and thereby modulate a variety of processes including hormone secretion, proliferation, and central nervous system (CNS) functions.

They play a central role not only in physiological conditions, but also in pathological processes, like cancer. The involvement of K_{2P} channel in tumor biology has recently discovered. The first evidence was demonstrated in breast cancer[21] where K_{2P}9.1(TASK3) is overexpressed. Other indications were provided in prostate cancer [22] and neuronal tumors.[23] In this field the development of new drugs to regulate K_{2P} channel activity has become urgent. Recently, ML308 has been identified as a novel inhibitor of the potassium channel, subfamily K, member 9 (KCNK9).[24] Other inhibitor of K_{2P} members are cations like Ba^{2+} or chloroform.

1.1.3 Calcium –activated potassium channel

The family of calcium-activated potassium channels[25,26] includes eight different members divided in two groups: the former, exhibiting large unitary conductance and gated by the cooperative action of membrane depolarization and internal concentration of Ca^{2+} , is termed BK_{Ca}; the latter displaying small conductance and gated exclusively by internal concentration of Ca^{2+} is called SK_{Ca}.[27]

BK_{Ca} channels are implicated in the regulation of smooth muscle tone,[28] in the microbial killing by leukocytes[29] and in the modulation of hormone and neurotransmitter release.[30] They are abundantly expressed in the most regions of the brain where BK_{Ca} channels contribute to repolarization of action potentials, mediate the fast phase of depolarization[31], shape the dendritic Ca^{2+} spikes[32] and influence the release of neurotransmitters. SK_{Ca} channels cover a wide range of activity from controlling uterine contractility[33], vascular tone[34], modulation of hormone secretion[35], control of cell volume in red blood cells[36], activation of microglia and lymphocytes[37,38], to regulation of excitability[39], synaptic signal transduction[40].

The BK_{Ca} channel core is a tetrameric assembly of α-subunits (BKα). Their primary structure comprises seven transmembrane domains (S0-S6) in between the short extracellular NH_2 terminus and the large intracellular COOH terminus. In turn the intracellular domain contains (i) four hydrophobic segments (S7-S10), (ii) two regulating conductance of K^+ (RCK) domains and (iii) a stretch of aspartate residues that are known as "Ca^{2+} bowl". Tertiary folding of these residues constitute the binding site for Ca^{2+}, whose occupancy is one of the two source of channel opening. The other modality of channel gating is membrane depolarization by movement of the voltage-sensing segment S2-4.[41] (**Figure 1.1, panel C**) Although tetramers of BK_{α} are functional, the majority of BK_{Ca} in the plasma membrane are associated with auxiliary β-subunits (BKβ) having a modulatory effect on gating, pharmacology, as well as on trafficking.

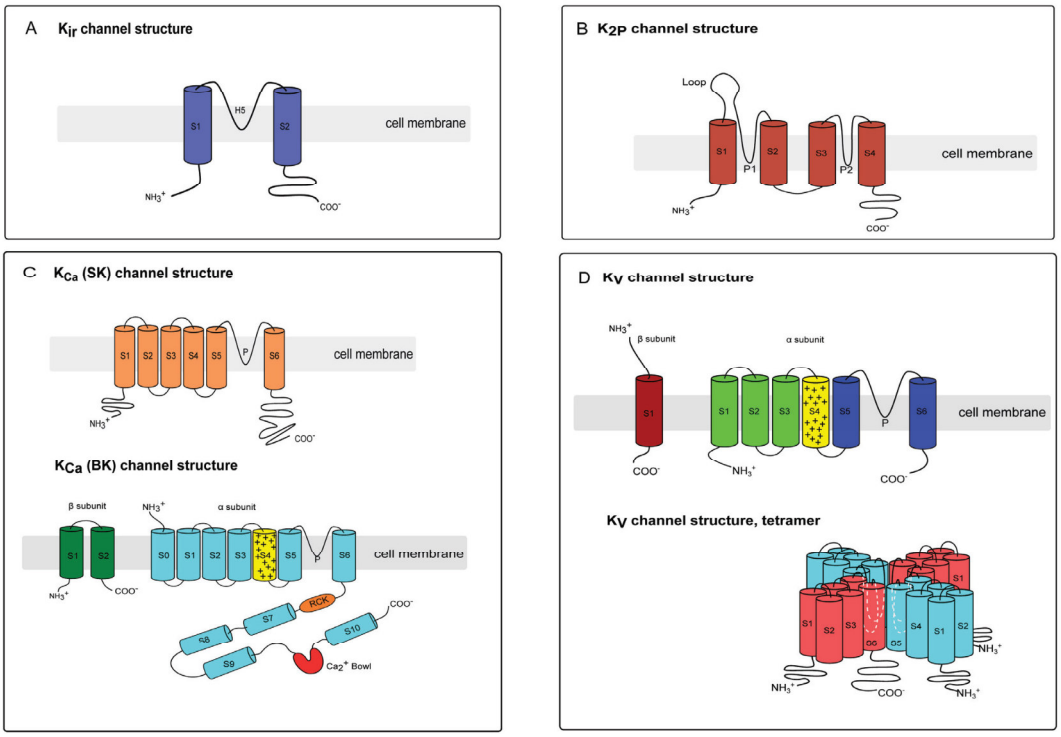

Figure 1.1: Molecular structure of potassium channels: α-subunit structure forming rectifying potassium channel (A); one of the two domain making K2P family (B); two different structures of the K_{Ca} family (C) and molecular structure of one subunit of K_v family and the functional tetramer (D).[42]

The SK_{Ca} channel is a tetrameric assembly of α-subunits (SKα). Their primary structure includes six transmembrane domain but lacks the voltage-sensing S4 segments. SKα gating is driven by a change in the intracellular Ca^{2+} concentration, through the binding of the C-terminal region with calmodulin.[43]

The most common BK_{Ca} blockers are TEA, charybdotoxin, a neurotoxin from the scorpion and quindine, an antiarrhythmic agent while SK_{Ca} are commonly blocked by apamina, a neurotoxin found in apitoxin, and by the tamapina toxin product from Indian Red Scorpion.[25]

1.1.4 Voltage gated potassium channel (K_v)

K_v channels represent the largest gene family in the K^+ channel group, they are encoded by 40 genes which are divided into 12 subfamilies including hERG which is the main focus of this thesis.

K_v channels are formed by four α-subunits arranged around a central pore as homotetramers and heterotetramers. Each subunit contains six transmembrane α-helical segments (S1-S6) and a membrane entering P-loop which contributes to form the ion conduction pore. S4 helix contains four positively charged arginine residues, as a

voltage sensor domain and determines the opening of the pore, pulling on the S4-S5 linker.[44-46] (**Figure 1.1, panel D**)

Because of K^+ concentration gradient across the plasma membrane, the opening of K_v channel results in an efflux of positive charge, which can serve to repolarize and hyperpolarize the membrane. In excitable cells such as neurons or cardiac myocytes, K_v channels, often expressed together with voltage-gated Na^+ and/or voltage-gated Ca^{2+} are involved in the repolarization after action potential firing.

Therefore K_v channel play an important role in Ca^{2+} signaling, volume regulation, secretion, proliferation and migration in both excitable or non-excitable cells.[47,-49]

K^+ efflux trough K_v channels is involved in the counterbalancing of Ca^{2+} influx in order to maintain an inward-rectifier Ca^{2+} current, necessary for cellular activation and migration. It is well established that K_v channels take part to large supramolecular complexes. The behavior of these complexes can be influenced by the channel in the absence of ion flow.

K_v channel activity is modulated by several molecules which could be divided in three categories: metal ions, organic small molecules (molecular weight of about 200-500 Da) and venom peptides (molecular weight 3-6 kDa).[50] These substances interfere with K_v channel function by blocking the ion-conducting pore from the external or internal side, or modifying channel gating binding the voltage sensor domain or auxiliary domain. For example peptide toxins bind either to the outer vestibule or the voltage sensor of K_v channels. Another examples are small agents, like tetrabutylammonium, d-tubocurarine and verapamil that block K_v channels occluding the inner pore or inserting their ammonium group into the ion permeation pathway. Correolide interact through its lipophilic domain, with S6 helix while with its polar acetyl group chelates K^+; in this way this nucleophilic molecules is able to block K_v.[51]

Another mechanism to modulate K_v channel with β-subunits is the disruption of the interaction between α- and β- subunits.[52]

1.2 hERG (human ether a-gò-gò related gene) K^+ channels.

The human *ether a-gò-gò* related gene (hERG) encodes pore forming subunit of a delayed rectifier voltage-gated K^+ (VGK) channel. This channel is variously referred to as I_{Kr}, hERG, K_v11. 1 or KCHN2. HERG is a member of one of the three subfamilies of the ether a-go-go family of VGK channels. Within the family of Kv11.x, there are three members, Kv11.1 (hERG), Kv11.2 (hERG2), and Kv11.3 (hERG3), but Kv11.1 is prevalently discussed in this thesis.

The family name *ether a gò-gò* was given by Kaplan and Trout in 1969 and was intended as a humorous reference to how the legs of mutant flies shake under ether anesthesia like the gò-gò dancers of the 1960s.[53]

The human KCHN2 gene are made of ~36kb in region q36.1 on chromosome 7. (**Figure 1.2**).

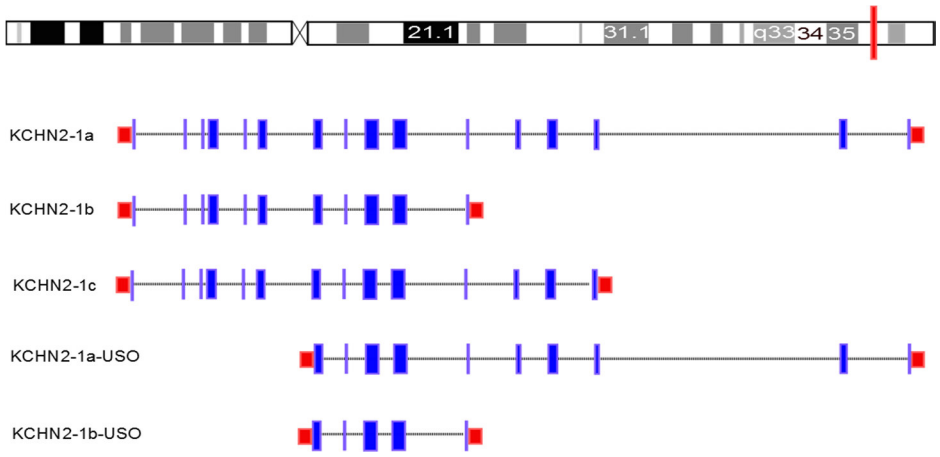

Figure 1.2: Genomic structure of KCHN2. Genome browser view of chromosome 7 q36.1. KCHN2 is transcribed in the reverse direction. Three alternative transcription start sites and two alternative termination sites give rise to five transcripts. 5'UTR and 3'UTR are shown in cyan and coding regions in blue.

It is transcribed in the reverse direction. Three alternative transcription start sites and two alternative termination sites give rise to five transcripts: KCHN2-1a, KCHN2-1b, KCHN2-1c (KCHN2-3.1), KCHN2-1a-USO and KCHN2-2a-USO.
KCHN2-1a contains 15 exons and corresponds to the longer transcript. KCHN2-1b has a transcription start site in intron 5, resulting in a transcript missing the first five exons of KCHN2-1a and containing an alternative exon 5b. KCHN2-1b is identical to KCHN2-1a from exon 6 onwards.
KCNH2-1c (KCNH2-3.1) has a transcription start site in intron 2. It lacks the first two exons and has six additional amino acids at the 5' end of exon 3 but for the rest, it is identical to KCHN2-1a. In addition to the termination site in exon 15, there is another 3'UTR end within intron 9 of the KCHN2-1a mRNA. Transcripts with this premature COOH-terminal truncation are called $hERG_{USO}$.
The KCHN2-1a transcript giving rise to a 1159-amino acid protein (hERG) contains six transmembrane (TM) segments (S1-S6). S1-S4 contains the voltage sensor domain (VSD) while S5-S6 loop contribute to forming the pore domain. Each subunit presents large cytoplasmic NH_2-terminal and COOH-terminal domains. The first one contains a Per-Arnt-Sim (PAS) domain that defines the *ether a gò-gò* subfamily of VGK channel. The COOH terminus contains a cyclic nucleotide binding domain (cNBD) which shows homology with the cNBD of CNG channels and hyperpolarization activated channel (HCN) (**Figure 1.3**).

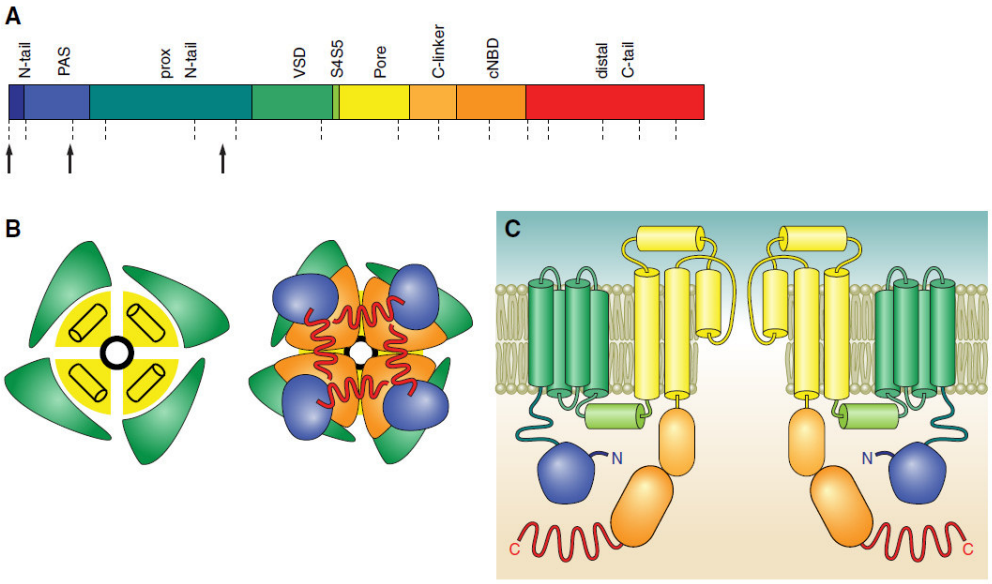

Figure 1.3: Topology and structure of K_v 1.1 chennels. Panel A shows a linear sequence of hERG-1a with domains color coded. Arrows indicate the transcription start sites, and dashed lines show the sites of exon-exon boundaries. Panels B shows the extracellular view (left) and intracellular view (right) of the tetrameric structure of Kv 11.1 channels. Panels C reported the topology of two opposing hERG-1a subunits color-coded as in A.

The functional channel is a tetramer where S5-S6 linker of each subunit surrounds the central pore, controlling the K^+ efflux.
Within KCHN2 gene exon 1 encodes the 5'UTR and first residues, which play an important role in deactivating regulation of the channel.
Exon 2 and exon 3 contain PAS domain. Exon 6 encodes the last portion of the cytoplasmic NH_2 terminus and first three transmembrane domain. Exon 7 encodes the fourth TM segment containing the positive residues acting as the principal voltage-sensing region within the VSD. The aminoacid bounding exon7/8 is the mostly conserved residues in all K^+ channels (Gly648 in hERG). Exons 8-10 encode the c-linker and cNBD domains while the remaining five exons encode the distal COOH-terminal domain.

1.2.1 hERG channel: operating mechanism.

hERG is expressed in a multiple tissues and cell types, including neural[54], smooth muscle[55] and tumor cells[56]. In the central nervous system of mammals, two other hERG channel genes are expressed (hERG2-3) and here heteromultimeric[57] channel complexes of all three subunits are be formed. However hERG is most highly expressed in the heart and disease where its function and dysfunction are best understood.
The action potential of human ventricular myocytes can be divided into five distinct phases. Phase 0 is characterized by activation of inward Na^+ current that triggers a rapid

depolarization of the membrane. Phase 1 repolarization starts and is due to the transient outward K^+ current (I_{to}). This phase proceeds rapidly in few milliseconds and is followed by phase 2 consisting of a much slower rate of repolarization, called plateau. The plateau is due to maintained inward Ca^{2+} current and because the outward K^+ current are slow to activate (slow delayed rectifier K^+ current) or exhibit strong rectification (inward rectifier K^+ current I_{K1} and rapid delayed rectifier K^+ current, I_{Kr}, conducted by hERG channels). In phase 3 repolarization terminates the action potential and returns the membrane potential to its resting level (phase 4). The most important component of phase 3 repolarization is the rapid delayed rectifier K^+ current (I_{Kr}) conducted by hERG channels. (**Figure 1.4**)[58]

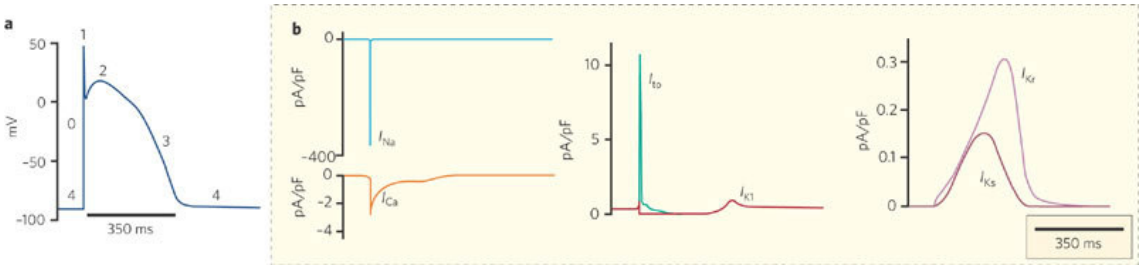

Figure 1.4: Simulated human ventricular action potential. a) At phase 0 an inward Na^+ current triggers a rapid depolarization of the membrane. In phase 1 repolarization proceeds rapidly, followed by a slower rate of repolarization in phase 2. The action potential ends in phase 3 and the membrane potential returns to the resting level during phase 4. b) Ion-channel currents involved during action potential. Phase 0 is mediated by activation of the inward Na^+ current, I_{Na}. Activation of the transient outward K^+ current, I_{to}, creates a brief and partial repolarization in phase 1. In phase 2 the plateau of the action potential is prolonged owing to a maintained inward current (I_{Ca}) conducted by L-type Ca^{2+} channels and because the outward K^+ currents are slow to activate (slow delayed rectifier K^+ current, I_{Ks}) or exhibit strong rectification (inward rectifier K^+ current, I_{K1} and rapid delayed rectifier K^+ current, I_{Kr}, conducted by hERG channels). Phase 3 repolarization is mediated by the outward currents I_{Kr} and I_{K1}. The resting potential between action potentials is called phase 4. Modelling courtesy of F. Sachse, University of Utah.

At negative membrane potential (about -80 mV) hERG channels are in non-conducting closed state. Depolarization of cell membrane to potential more positive than -60 mV induces channels to open and allows the outward diffusion of K^+ ions in accordance with its electrochemical driving force. As the membrane potential is progressively depolarized to more positive potential, channels enter another non conductive configuration called inactivated state. (**Figure 1.5**)

hERG gating is different from most K_v channels by two aspects.

First, inactivation is much faster than activation, this reduces outward conductance at depolarized potentials and prolongs phase 2 of the action potential.

Second recovery from inactivation is much faster than deactivation: this starts phase 3 repolarization of the action potential.

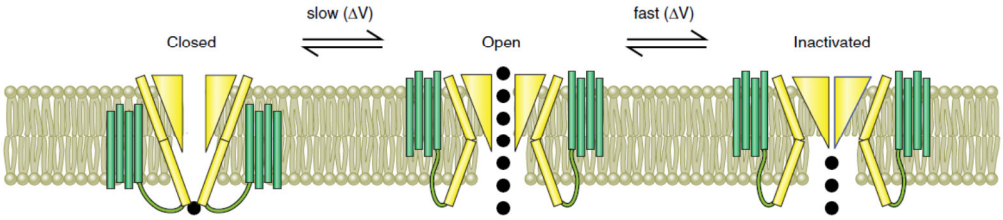

Figure 1.5: Gating of Kv11.1 channels. It shows the states of Kv11.1 channels: closed, open, or inactivated states. Transitions between them are voltage dependent, with the transition between the closed and open states being slower than transitions between open and inactivated states.

K_v11.1 mutations cause the Long QT Syndrome (LQTS) type 2. This syndrome is defined by the prolongation of the QT interval measured by a body surface electrocardiogram (ECG) and greatly increased risk of ventricular fibrillation. The QT interval is the time required for ventricular repolarization during a single cardiac cycle. The lack of repolarization increases the risk of torsade de pointes (TdP), a unique cardiac arrhythmia characterized by an ECG trace that resembles a waxing and waning sine wave. TdP can either revert to a normal sinus rhythm or degenerate into lethal ventricular fibrillation.

The most common hERG inhibitors are E4031, Way 123,398 and dofetilide. However Kv11.1 is blocked by many other compounds, such as antihistaminics (i.e. terfenadine), prokinetics (i.e. cisapride), antipsycothics (i.e. sertindole) and antibiotics (i.e. erythromycin). The chemical structure of these compounds confers them the capability to bind hERG channel pore at different points; these particularities could be exploited in order to reduced K^+ potassium current without provoking uncontrolled QT prolongation and ventricular fibrillation.

1.2.2 hERG channel under physiological and pathological conditions

VGC channels in general, and K_v11.1 channels in particular, have been implicated in the regulation of cell-cycle. hERG channels are expressed at high levels in early embryonic stages of quail neural crest and are replaced by inward rectifier currents during development.[59,60] It was found that the expression of hERG is particularly high in mouse embryonic heart and then downregulated during development.[61] The presence of hERG is also evidenced in cells undergone to dedifferentiation,[62] as well as in tissue samples from tumors where KCHN2 transcript and hERG protein expression is usually found to be more frequent than in the control tissue.[63] This phenomenon could explain the fact that the differentiated cells display a membrane potential more negative than -60mV while non differentiated cells are usually more depolarized.[64]

It was demonstrated in previous work from our group that the recorded membrane potentials of unsynchronized mammalian neuroblastoma cells vary cell-to-cell and these variations were attributed to different steady-state activation curves of K_{ir} inward

rectifier currents. Therefore it was first proposed that K_{ir} channels are a relevant target in the transformation process in cancer cells. Subsequently it was found that the mix of hERG subunits varies at different phases in the cell cycle of synchronized tumor cells. For example hERG-1b isoform is dominant during the S phase, while hERG-1a subunit during the G_1 phase. These results account for a correlation between biophysical parameters of K_{ir} and different phases of the cell cycle.[65]

Not surprisingly, the same ion-channels that are involved in cell proliferation, are also implicated in the process of apoptosis. For instance cell shrinkage, that characterizes the early steps of apoptotic cell death, is due to K^+ efflux. It is well established that potassium channels are involved in cytoskeleton reshaping and cell-cell interactions; these phenomena represent the initial step towards increased cell motility, a prerequisite for tumor invasion. In fact hERG has important implications for the invasiveness of cancers. In human colorectal cancer, it was found that hERG[66] regulates invasion of tumor cells and it is more expressed in metastatic cancers with a bad prognosis than in less aggressive cancers. [67]

This trend was observed in human leukemia cases, in which patients with hERG positive tumors have a higher mortality than in patients with hERG negative tumors.[68]

Furthermore, the interaction between K^+ channel and integrin plays a pivotal role in cancer cell migration since integrin is involved in cell adhesion through its interaction with fibronectin. It was found that in leukemic cell line FLG 29.1 fibronectin increases hERG current through the interaction with integrin. In turn, hERG activation leads to increased expression of $\alpha_v \beta_3$ integrins, indicating that hERG channels are involved both in ouside-in and inside-out signaling in these cells.

Further experimental evidences showed that interaction of hERG channels with β_1 subunit of the integrin receptor in leukemia and neuroblastoma cells could influence molecular signaling, such as tyrosine kinases and GTPases.

hERG and β_1 subunit of the integrin interaction appears in proximity of caveolin-1 indicating an involvement of lipids rafts/caveolae. It is also evident that focal adhesion kinase (FAK) associating with hERG becomes tyrosine phosphorylated after exposure of the cell to fibronectin; this effect could be blocked by Kv11.1 blockers.[69]

In solid tumors, hERG channels play an important role in new vasculature development outpacing the lack of oxygen. This mechanism is modulated by Kv11.1 channel gating which is activated under hypoxic conditions. It was also discovered that in glioblastoma multiforme, hERG channels are overexpressed and modulated by VEGF secretion that is critical for neoangiogenesis.[70]

1.3 Leukemia

Leukemia represents a group of hematological malignancies, characterized by clonal expansion of hematopoietic cells with uncontrolled proliferation, decreased apoptosis and blocked differentiation.

According to the disease progression and hematopoietic lineages involved, leukemia can be divided into acute or chronic forms:

- Acute leukemia, characterized by a rapid increase in the number of immature blood cells. Immediate treatment is required, in order to reduce the rapid progression and accumulation of the malignant cells, which migrate from the bone marrow environment to peripheral blood and spread rapidly to other organs of the body. Acute forms of leukemia are the most common forms of leukemia in children.
- Chronic leukemia, is characterized by the excessive build up of relatively mature, but still abnormal white blood cells. The progression of this chronic leukemia is slower than the acute form and occurs especially in older people, but can theoretically occur in any age group.

Traditionally, these malignancies are subdivided into:

- lymphoblastic or lymphocytic leukemias, where cancerous cell originates from marrow cells that normally differentiate in lymphocytes;
- myeloid or myelogenous leukemias, where tumor cells originate from marrow cells that normally form red blood cells, platelets and granulocyte (myeloid lineage).

Combining these two classifications provide a total of four main categories:

- Acute lymphoblastic leukemia (ALL) is the most common type of leukemia in young children. It affects also adults older than 65 years. Common treatments are chemotherapy and radiotherapy. The survival rates is higher in children (85%) than in adults (50%). Subtypes include precursor B acute lymphoblastic leukemia, precursor T acute lymphoblastic leukemia, Burkitt's leukemia and acute biphenotypic leukemia.
- Chronic lymphocytic leukemia (CLL) is diffuse prevalently in adults over the age of 55. It sometimes affects younger adults, but almost never occurs in children. The five-year survival rate is 75%. It is incurable, but there are many effective treatments. One subtype is B-cell prolymphocitic leukemia, a more aggressive disease.
- Acute myelogenous leukemia (AML) is more spread in adults than in children and occurs more commonly in men than in women. The five –year rate survival is 40% except for acute promyelocytic leukemia (APL), which is over 90%. Subtypes of these malignancies include APL, acute myeloblastic leukemia, and acute megakaryoblastic leukemia.
- Chronic myelogenous leukemia (CML) affects prevalently adults; only a small percentage of children is affected. Treatments is with imatinib (Gleevenec in United States, Glivec in Europe) or with other drugs (i.e. dasatinib). The five-year rate is 90%
- Hairy cell leukemia (HCL) affect prevalently adult men (80%). It is incurable, but easily tractable since survival is 96%-100% at ten years.

- T-cell prolymphocytic leukemia (T-PLL) is a very rare and aggressive leukemia affecting adults; somewhat more men than women are diagnosed with these disease. Despite its overall rarity, it is also the most common type of mature T cell leukemia. It is difficult to treat, and the median survival is measured in months.
- Large granular lymphocytic leukemia may involve either T-cells or NK cells, it is rare and indolent (not aggressive) leukemia.
- Adult- T leukemia is caused by human T-lymphotropic virus (HTLV) that infects CD4+ T-cells and replicates within them. HTLV immortalizes T-cells, giving them the ability to proliferate abnormally. Human T cell lymphotropic virus type I and II (HTLV-I/II) are endemic in certain areas of the word.

Leukemia is a treatable disease. Most treatments involve chemoterapy, medical radiation therapy, hormone treatments, or bone marrow transplant. The survival percentage depends on the type of leukemia, as well as the age of patient. Children are more likely to be permanently cured than adults. In 2010, globally, approximately 281500 people died for leukemia malignancy. In 2000, 256000 persons (adults and children) contracted leukemia, and 209000 died for it. This represents about 3% of the almost seven million deaths due to cancer in that year and about 0.35% of all deaths for any cause. Leukemia represent the 11^{th} most common cause of cancer-related death.
About one third of children affected by this cancer in general suffer from acute lymphoblastic leukemia. This type of leukemia is the second most common form of cancer in infants (under the age of 12 months) and in older children. Boys are somewhat more likely to develop leukemia than girls.

1.4 hERG role in leukemia

Leukemia originates from an abnormal and uncontrolled proliferation of blood stem cells within the bone marrow environment. During tumor development, these cells spread from the bone marrow to blood circulation, penetrating in extramedullary organs. Leukemia cells persistence in peripheral blood and subsequently their migration into organs, are considered unfavorable prognostic factors. In fact at these stages, patient response to chemotherapy is consistently reduced. In this field, biological researches strongly pushes to understand the molecular mechanisms regulating leukemia cell motility and transendothelial migration.
Research work conducted in our laboratory provides strong evidences that hERG channel activity is necessary for the progression of AML cells beyond the G1/S boundary.[71]
Subsequently it has been determined the crucial role of hERG1 channels in AML cell migration and invasion. This mechanism are activated by the formation of molecular complex composed by hERG1, vascular endothelial growth factor receptor-1 (VEGFR-1 or FLT-1) and β_1 subunit of integrin receptors. FLT-1 and hERG1B are constitutively

associated in leukemia cells and their assembly is potentiate by the signaling activated by VEGF. Therefore the recruiting of β_1 subunit in the complex FLT-1/hERG1B activates both MAPK and PI3K/Akt signaling pathways. hERG specifically inhibition confirm his role in FLT-1 dependent AML migration and invasion, and its presence in tumor confers a stronger malignancy.[72]

Therefore it has been demonstrated that bone marrow mesenchymal cells (MSCs) induce drug resistance in leukemic cells. It has been determined that activation of hERG1 channel induced by the presence of MSCs, is crucial in ALL chemioresistence. Co-colture experiments suggest that MSCs factor (SDF-1α) induces on the ALL plasma membrane, the expression of a signaling complex formed by hERG channels, the β_1 integrin subunit and the CXC chemokine receptor-4. The assembly of this molecular complex activates both the extracellular signal/related kinase 1/2 (ERK1/2) and the phosphoinositide 3-kinase (PI3K)/Akt prosurvival signaling pathways. Inhibition of hERG channel through silencing by siRNA or E4031 approaches evidence the reduction of ALL chemioresistance induced by the presence of MSCs.[73]

Recently it was found that hERG1B is up-regulated in comparison to hERG1A in ALL blasts, either B or T lineage.[74] As previously described hERG1 blockers can overcome chemoresistance both *in vitro* and leukemia mouse models. However hERG1 inhibitors could have a side effect on myocardial tissue. hERG1B overexpression in ALL patients may have clinical importance since hERG1B is expressed at low levels in human heart. For this reason, hERG1B targeting could be an approach for antileukemic therapy, avoiding adverse cardiac effect.

Chapter 2

2.1 Clarithromycin: current use in medicine

Clarithromycin is a macrolide antibiotic of second generation, used for the treatment of respiratory tract infections, sexually transmitted diseases and infections caused by *Helycobacter pylori* and *Mycobacterium avium* complex.

The first macrolide discovered is erythromycin that has been used since the early 1950s for the treatment of respiratory tract, skin and soft tissue infections in susceptible organisms, especially in patients who are allergic to penicillin. In order to improve pharmacodynamics, pharmacokinetics and tolerability, advanced macrolide antibiotics are synthetized by altering the erythromycin base. One of these new agents is clarithromycin, also known as Biaxin.

Clarithromycin or 6-methylerithromicin consists of a macrocyclic 14-memebered lactone ring with two sugar moieties: a neutral sugar, cladinose, and an amino sugar, desosamine. In comparison to erythromycin, clarithromycin shows a methoxy group in C-6 instead of hydroxil group. This substitution creates a more acid-stable antimicrobial compound and prevents degradation into an hemiketal intermediate, which results in improved oral bioavailability and reduced gastrointestinal intolerance.[75]

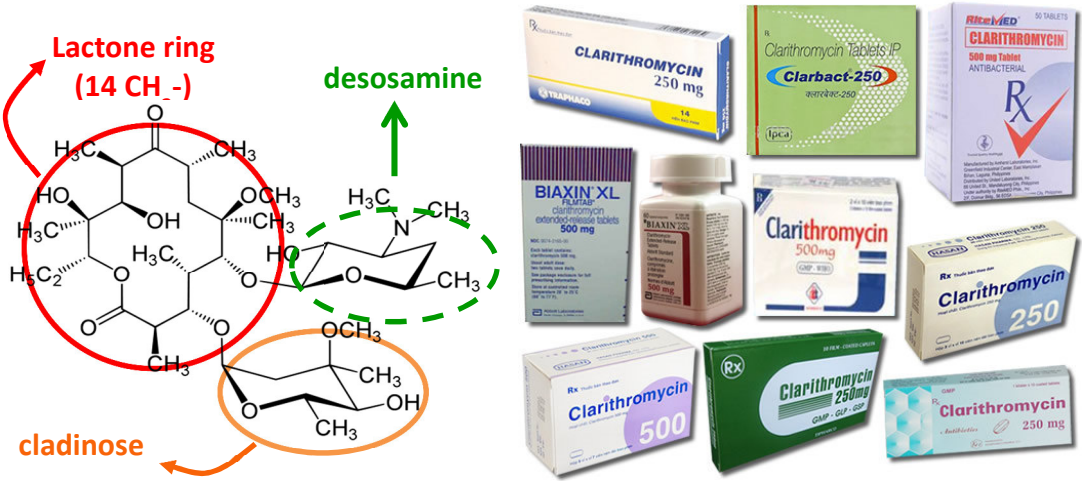

Figure 2.1: Chemical structure of clarythromicin (left) and some of its commercial forms (right).

These drug is available as immediate-release tablets (250 or 500 mg), extended-release tablets (500mg), and granules for oral suspension (125 or 250 mg/5mL) (**Figure 2.1**).
Clarithromycin is antibacterials drug and inhibits RNA-dependent protein synthesis. It binds the domain V in 23S ribosomal RNA of the 50s subunit of bacterial ribosome. Substantially, this macrolide blocks the translocation of aminoacyl transfer-RNA and polypeptide synthesis.[76,77]
This drug is metabolized in the liver by the cytochrome P450 3A4 (CYP3A4) enzymes into the active 14-hydroxy form and six additional products. Clarithromycin has a short half-life; however its metabolite, 14-hydroxy clarithromycin is nearly twice more active than clarithromycin against certain bacteria.[78,79]
30% - 40% of an oral dose of clarytromicyn is excreted in the urine either unchanged or as the active 14-hydroxy metabolite. The remainder is excreted into the bile. In patients with moderate and severe hepatic impairment, these dose should be reduced since clarythromycin is less metabolized into 14-hydroxy form which results in decreased peak plasma concentrations of the metabolite and increased renal excretion of unchanged clarithromycin.[80,81]
Clarithromycin is particularly effective against gram-negative bacteria.[79] Clarithromycin may be used to attenuate cardiac transplantation rejection via matrix metalloproteinase suppression.[82] Clarithromycin has been used to study inflammatory markers in chronic obstructive pulmonary disease (COPD).[83] It is used to study bacterial protein synthesis and peptide translation. It is effectively used for the treatment of the most frequently isolated bacterial causes of pharyngities, otitis media and sinutis. Various trials have demonstrated the efficacy of clarythromycin for treatment of lower respiratory tract infections, including acute brochitis, acute exacerbation of chronic brochitis (AECB), and common-acquired pneumonia.[84] It is also used as an antibiotic against *Helicobacter pylori* –associated peptic ulcer diseases, ulcer recurrence. Finally, it has been shown to be effective in preventing and treating disseminated MAC disease in HIV-infected patients.

2.2 Clarithromycin: mechanism of action

2.2.1 Clarithromycin: possible antineoplastic drug?

Clarithromycin is known to act not only as an antibiotics but also as a growth inhibitor of certain cancer cells. Treatments based on this drug are beneficial for unresectable non-small lung cancer patients and can increase the median survival of patients with advanced disease.[85] The effect of clarithromycin and its combination with carboplatin and cyclophosphamide cause a significant decrease in the death rate in F-344 rats inoculated with 13762 mammary adenocarcinoma cells.[86]
Therefore clarithromycin is well demonstrated as a potent inhibitor of tumor-induced angiogenesis. This effect is investigated *in vivo* using a mouse dorsal air sac model. The

inhibitory effect increased with the dose and 100mg/kg of clarithromycin administered intraperitoneally twice a day reduced the area of dense capillary network to about 30% that of the control.[87]

Presently patients affected by newly diagnosed multiple myeloma are treated with low-dose dexamethasone and lenalidomide with or without clarythromicin. Gay et al. demonstrated that survival percentage were significantly higher for the group treated with clarithromycin.[88-90]

Actually there are active studies of clarithromycin in patients. These include a phase II trial of single agent-clarithromycin in advanced stage indolent limphoma[91] or in combination with lenalidomide and dexamethasone in treating patients who have undergone stem cell transplant for multiple myeloma.[92]

Recently it has been demonstrated that clarithromycin inhibits autophagy. There are substantial evidences that the process of autophagy plays a key role in cancer development. In fact autophagy has been considered an adaptive response to starvation induced by stress, allowing cell survival in growth factor deprived environments. Inhibition of the early stage induces classical apoptosis, whereas inhibition of late stage autophagy results in the accumulation of autophagic vacuoles, followed by apoptosis. Inhibition of autophagy reduce tumor cell survival and increase the sensibility to chemotherapy.[93]

Nakamura et al. demonstrated that clarithromycin induces the inhibition of autophagy at late stage causing a significant induction of vacuoles in human myeloma cell lines.[94]

In turn clarithromycin restores the sensibility to chemoterapy through the autophagy inhibition in chronic myeloid leukemia. It is well established that tyrosine kinase inhibitors (TKIs) have revolutionized the treatment of CML since they block Bcr-Abl kinase. Recently, many studies have demonstrated that TKI like imatinib or dasatinib induce chemoresistance due to mutation on Bcr-Abl kinase domain or by inducing autophagy. Carella et al. describe a series of four patients with advanced CML whose disease was not adequately controlled by TKIs. They demonstrated that clarithromycin potentiates TKIs treatment restoring the sensitivity. Three of these patients during the treatments stopped clarithromycin and in all cases CML disease advance after clarithromycin discontinuation. When the macrolide is introduced again in the treatment, two of the three patients had improvement in disease burden. These are preliminary studies but they allow to underline the importance of clarithromycin in cancer treatment.[95]

The effect of clarithromycin is also evidenced on the K562 (CML cell line), where it increases the sensibility to dasantinib (TKI of second generation). In fact clarithromycin inhibits autophagy in a similar way to the late stage autophagy inhibitor ubiquinone. This effect is demonstrated by an increase in LC3-II protein levels and a concomitant increase in cellular vacuole formation. In conclusion, these studies demonstrate that autophagy may play a role in the resistance of CML cells to dasatinib therapy and treatment with clarithromycin restore the sensibility to the chemoterapy.[96]

Clarithromycin studies on CML are preliminary but they have important clinical implications. The restoring sensitivity to imatinib should not be very important after the

discovery of TKIs of second generation, such as dasatinib, nilotinib, bosutinib and/or ponatinib. In turn, there are instances where even the second generation TKIs are not so efficient, but in the presence of clarithromicyn their effects can be restored.

2.2.2 Reduction of potassium current in hERG potassium channel

Clarithromycin is a drug commercially used as antibiotics. Recently its pharmacological effect on hERG channel has been demonstrated.
At the beginning, results obtained from previous *in vitro* patch clamp studies indicate that clarithromycin blocks the human I_{Kr} in CHO (Chinese Hamster Ovary) cell line with relatively low efficacy (IC_{50}= 0.75 mM, Hill1 slope=1.7).[97]
In 2000, Stanat et al. obtained encouraging evidences that clarithromycin reduces hERG current on HEK293 stably transfected with hERG. These authors demonstrate that clarithromycin reduced hERG-encoded potassium current in a concentration dependent manner, higher drug concentrations produce both an increasing inhibition of the evoked current and an induction of a time dependent block during a depolarizing step. Clarithromycin reduces the amplitude of potassium current after depolarization and during hyperpolarization, until -40 mV. (**Figure 2.2, panel B**). **Figure 2.2 panel C** shows the sigmoidal curves in which increasing macrolide concentration induces a progressive reduction of the hERG potassium tail current.

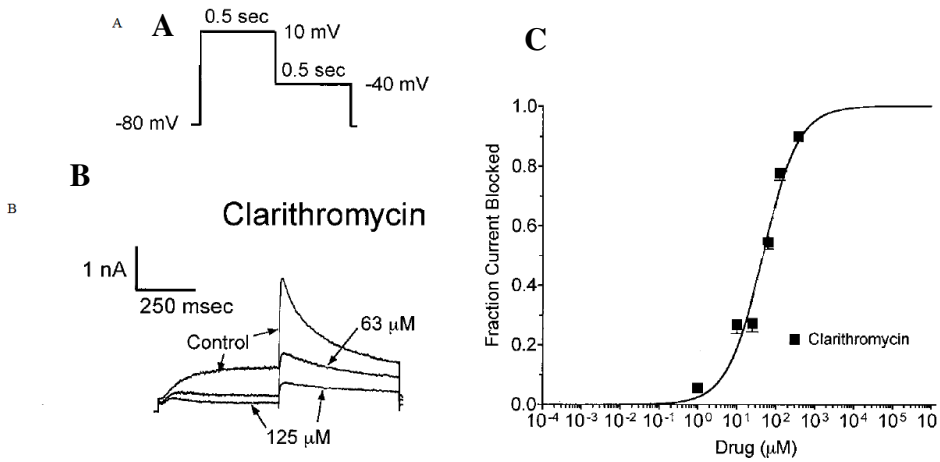

Figure 2.2: Pulse protocol where 500msec step depolarization to +10mV is used to activate the hERG current, followed by a 500msec step to -40mV to invoke a tail current (cycle length 10sec, -80mV holding potential) (A); superimposed currents recorded from one cell under control conditions and after steady state effect was achieved in the presence of 63μM and 125 μM clarithromycin (B). Sigmoidal curve obtains from non linear fitting on the experimental data.

The IC50 value for Clarithromycin which corresponds to the concentration producing 50% of K^+ current reduction, is 45.7±1.1 μM. Their experiments suggest that under condition similar to those occurring *in vivo*, clarithromycin can produce a significant inhibitory effect on the human I_{Kr} at clinically relevant plasma concentrations.

The effect of clarithromycin is also studied in FLG 29.1 (ALL) cell line where hERG are expressed endogenously. (**Figure 2.3**)

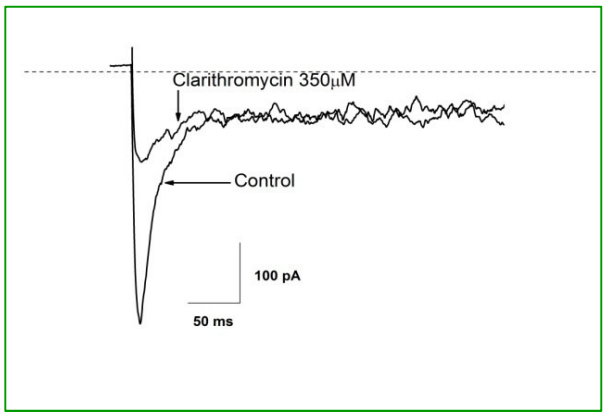

Figure 2.3: hERG potassium current recorded in FLG 29.1 before and after the treatment with Clarithromycin (350 μM).

Patch clamp experiments allow to establish that this antibiotic strongly reduced hERG potassium channel. The trend obtained from these pharmacological experiments is similar to that observed for HEK 293 stably transfected with hERG. In turn, clarithromycin determines a progressive reduction of K^+ current and experimental data fitted with Hill1 curve allow to obtain an IC_{50} value equal to 34±9.6 μM.
These experimental evidences are extremely encouraging to use clarithromycin as a potential hERG blocker. Indeed it is well established that hERG reduction in cancer enhances the decrease of invasiveness and migration of leukemic cells, but at the same time the major side effect of hERG inhibition is ventricular arrhythmia that could cause patient death. At present, the proarrhythmogenic effect of clarithromycin, on the human heart, has not been documented. Therefore this drug is designed for practical use in human patients, not only as an antibiotic but also as a coadjuvant of chemotherapy in chronic myeloid leukemia. In this study we demonstrate its effect in acute promyelocitic leukemia *in vitro* (HL60 cell lines) and subsequently *in vivo. In vitro* we study the effect of clarithromycin and also its capability to reduce chemoresistance due to the presence of MSCs, through its pharmacological effect on hERG channel.
In vivo experiments carried out by Dott.ssa Marika Masselli, allow to study the effect of clarithromycin alone and in combination with cytarabine.

Chapter 3

3.1 *In vitro* experiments

One of the main purposes of this thesis is the study of new antineoplastic drugs, targeting hERG *in vitro*. As discussed in the previous chapter the drug selected for this work is clarithromycin, a macrolide antibiotic which inhibits hERG potassium current. Our aim is testing this drug alone and in combination with cytarabine to investigate if clarithromycin can increase the sensitivity of leukemia cells toward this chemotherapic drug. Previous works demonstrate the positive effect of clarithromycin on K562 cells and on patients affected by CML.[95,96] Therefore we attempt to study its effect on the promyelocitic acute leukemia cell line HL60, where hERG is abundantly expressed.[72]

3.2 Materials

3.2.1 Drug used in the treatment

Clarithromycin used in our experiments was purchased by Sigma-Aldrich. The empirical formula is $C_{38}H_{69}NO_{13}$ with molecular weight 747.95 g/mol; the powder is solubilized in Dimethylsulfide (DMSO, Sigma-Aldrich).
Cytarabine used in the treatments was purchased by Sigma-Aldrich. The empirical formula $C_9H_{13}N_3O_5$ with molecular weight 243.22g/mol, the powder is solubilized in sterile water.

3.2.2 Cell cultures

HL60 cells (promyelocitic cell line) were cultured in RPMI with 10% fetal bovine serum (FBS, HyClone) in flasks (Corning) of 25mm maintained at 37°C, in humified atmosphere with 5% of CO_2. Medium renewal was performed every 2 - 3 days. For cryopreservation, HL60s are stored in fetal bovine serum (90%) and DMSO (10%) in liquid nitrogen.

Human bone marrow-derived MSCs, immortalized by telomerase reverse transcriptase transduction[98], were maintained in RPMI 1640 medium supplemented with 2mM/L glutamine, 10% FBS (HyClone), 10^{-6} M hydrocortisone (Sigma-Aldrich), 100U/mL

penicillin, and 100 μg/mL streptomycin. These line were obtained from professor Dario Campana, (Department of Oncology and Pathology, St. Jude Children's research hospital, Memphis, USA).
MSCs were usually maintained in flasks (Corning) of 25mm, at 37°C, in air with 5% of CO_2. Medium renewal was carried out every 2 – 3 days. For cryopreservation, MSCs were stored in fetal bovine serum (90%) and DMSO (10%) in liquid nitrogen.

3.3 Methods

3.3.1 Cell treatment

In order to investigate the effect of clarithromycin alone and in combination with cytarabine, the experiments were conducted on HL60 in suspension and in co-colture.
One day before treatment, fibronectin (1μg/well) was distributed on the bottom of 96 well plates (Costar, Corning), where MSCs were seeded till 90% confluence. After 24 hours, the medium of MSCs was removed and adherent cells were washed 7 times with AIM-V tissue culture medium (Invitrogen). The leukemic cells previously starved in medium without serum were centrifuged and resuspended in AIM-V medium. 10^{-5} leukemic cells in 100uL were placed in each well with or without MSC layer. Subsequently 100 μL of AIM-V medium containing appropriate concentrations of clarithromycin, cytarabine (or their combination), were added to the cells.
Cultures were maintained 48 hours at 37°C, 5% CO_2 and 90% humidity, prior to flow cytometry assays. (**Figure 3.1**).

3.3.2 Flow cytometry assay

After drug treatment, leukemic cells were separated from the MSCs and processed for apoptosis analysis. Annexin-V- FLUOS staining kit (Roche) was used to recognize apoptotic cells from necrotic cells through different dyes: Annexin-V fluorescein and Propidium Iodide (PI). The first one is a Ca^{2+}-dependent phospholipid-binding protein with high affinity for phosphatidylserine (PS) that translocate from the inner part of the plasma membrane to the outer layer, in the early stages of apoptosis. In turn, PI is a fluorescent dye that binds double-stranded DNA when cell membranes are compromised, remaining excluded from viable cells.
Leukemic cells were washed twice with phosphate buffered saline solution (PBS) and centrifuged at 200 g for 5 min. After this, the pellet was resuspended in 100uL of labeling solution containing Annexin V fluorescein and PI. Samples were incubated 10-15 min at room temperature and analyzed with FACSanto flow cytometer (Becton Dickinson) using 488nm excitation and 515 nm bandpass filter for fluorescein detection and a filter > 600 nm for PI detection.

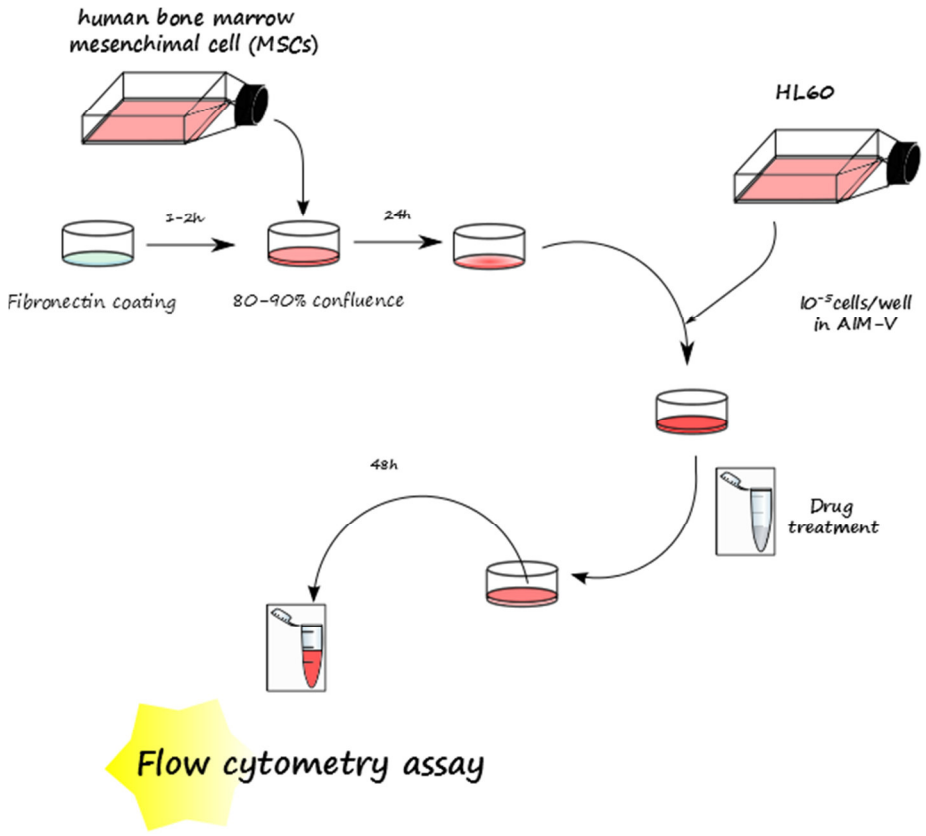

Figure 3.1: Protocol used for *in vitro* experiments.

3.3.3 IC50_Dose-effect curve

The half maximal lethal dose (LD_{50}) is a measure of the lethality of a substance. This parameter indicates the quantity of a given drug or other substance (inhibitor) needed to induce 50% of cell death. LD_{50} also represents the concentration of a drug required for inducing 50% of necrotic or apoptotic cells *in vitro*.
The LD_{50} value is determined by analyzing dose-effect curve and fitting the measured response of a system at increasing concentration of the drug. Normally the curve, used to fit the experimental data has a sigmoidal shape. Here, we chose non-linear fitting curve (NLFit, Hill1) and using Origin 6 software we determined the dose that caused the apoptosis of 50% of leukemic cells.

3.3.4 Chou-Talay method and its application in CalcuSyn

Drug combination is widely used to treat the most dreadful disease, such as cancer. The main purpose is to obtain synergistic therapeutic effect, dose and toxicity reduction, while minimizing or delaying induction of drug resistance.[99] Synergism in pharmacology is the term applied to the phenomena exhibiting by the combination of

two or more drugs in which pharmacodynamics effect produced by the mixture is not a simple addition of the effects produced by the two or more individual components. More simply, synergism is more than an additive effect and antagonism is less than an additive effect.[100] In order to study the combination existing between two or more drugs, Chou and Talay elaborated a method.[101] based on the median-effect equation where the dose of the drug is correlated with its effect as indicated below:

$$\frac{f_a}{f_u} = \left(\frac{D}{D_m}\right)^m$$

where D is the dose of the drug, D_m is the median-effect dose signifying the potency, f_a is the fraction affected by the dose, f_u is the fraction unaffected, $f_u = 1 - f_a$ and the exponent m indicate the shape of the dose-effect curve. The median-effect equation for a single drug can be extended to multiple drugs.[102] On the basis of these equations, Chou and Talay introduced the term *combination index* (CI) for quantification of synergism and antagonism:

$$CI = \frac{(D)_1}{(D_x)_1} + \frac{(D)_2}{(D_x)_2}$$

where CI<1, =1, >1 indicate synergism, additive effect, and antagonism. In the denomination, $(D_x)_1$ is for D_1 "alone" that inhibits a systems x%, and $(D_x)_2$ is for D_2 "alone" that inhibits a system x%. In the numerators, $(D)_1 + (D)_2$ "in combination" also inhibit %.[103]

The application of this method was greatly facilitated by the development of a specific software[104], "CalsuSyn" allowing to study the combinatorial effect between two or more drugs. We used this software in order to investigate the combinatorial effect of clarithromycin and cytarabine on the HL60 cell line in suspension and in the presence of MSCs.

3.4 Results and discussion

The pharmacological effect of the hERG blocker was determined for clarithromycin and its combinatorial effects with a conventional chemioterapic cytarabine, on HL60 in suspension and in co-colture. These experiments allowed to clarify the role of hERG potassium channel in leukemia chemioresistance induced by the presence of bone marrow microenvironment.

In previous experiments, HL60 were treated with increasing concentration of clarithromicin in two conditions: (i) suspension and (ii) co-colture with MSCs. Non-linear fitting allowed to obtain the LD_{50} values of clarithromycin for HL60 shown in **Table 3.1.**

	Clarithromycin			
Cellular line	Suspension		MSCs	
	% upon	LD_{50}	% upon	LD_{50}
HL60	50±2	37±5	28±2	67±5

Table 3.1: LD_{50} of clarithromycin for HL60 in suspension and in co-colture with MSCs.

The LD_{50} value for HL60 in suspension is 37 ±5 μM while for those in co-colture is 67 ±5 μM. As we expected LD_{50} value for HL60 in co-colture is higher than in suspension. This meant that MSCs prevent the effect of clarithromycin, protecting them from the antibiotic. As expected, the bone marrow microenvironment protected leukemia cells from clarithromycin effects.

In the second set of experiments HL60 were exposed to clarythromicin with or without cytarabine, both in suspension and on MSCs. The dose used in these experiments corresponded to the LD_{50} of each drug, i.e. 37μM for clarithromycin and 45nM for cytarabine.(**Figure 3.2**).

Overall, the effect of each drug decreased in cultures containing MSCs, as it is reported in literature. In fact the percentage of apoptotic cells after clarithromycin treatment, was 28% for HL60 in co-colture and 50% in suspension. The same effect was also obtained after exposure with cytarabine, since the % of apoptotic cells for HL60 was 50% in suspension and 20% in co-colture. This showed that the addition of clarithromycin LD_{50} dose to cytarabine, essentially abrogated the protective effect of MSCs, potentiating the pro-apoptotic effect of chemotherapy.

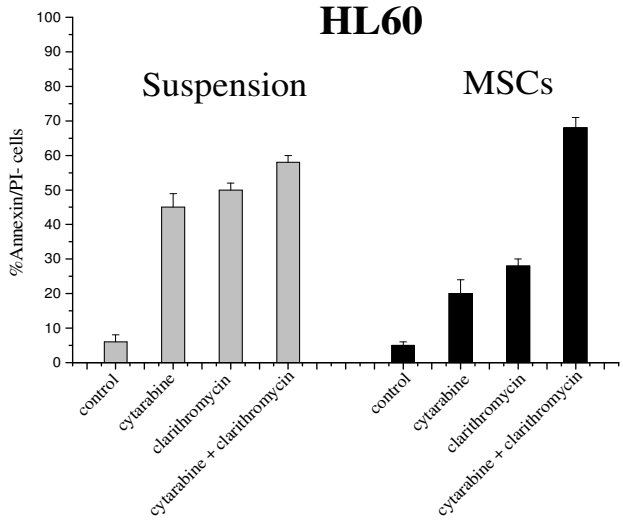

Figure 3.2: Effect of different drugs on HL60 in suspension or co-colture MSCs. Cells were treated with cytarabine and clarithromycin in concentration corresponding to their LD_{50}: i.e. 67μM and 37nM respectively.

Introducing LD_{50} values obtained from the single drug alone and from their combination in Calcusyn software it was possible to evaluate if the two drugs combination is synergic (CI<1), additive (CI=1) or antagonism (CI>1). As we could see in **Table 3.2** the effect of cytarabine in addition to clarithromycin is synergic on HL60 in co-colture. The effect of hERG blocker prevent the chemoprotective effect of bone marrow microenviroment restoring the sentivity to cytarabine.

	clarithromycin+cytarabine		
Cellular line	Suspension	MSCs	p
HL60	>1	0.657	0.009

Table 3.2: CI value obtained from the treatment with cytarabine and clarithromycin in HL60 cell line in suspension and in MSCs.

Chapter 4

4.1 *In vivo* experiments

The encouraging data obtained from *in vitro* experiments led to *in vivo* experiments on Severe Combined Immunodeficiency Disease (SCID) mouse, injected with HL60 cells tagged with luciferase. These experiments were performed by Dott.ssa Marika Masselli and allowed to study the effect of clarithromycin alone or in combination with cytarabine.

4.2 Materials

4.2.1 Drugs used in the treatment

In *in vivo* experiments we used MACLADIN® (Clarithromycin) that is resuspended in sterile water.
In turn, Cytarabine, produced by Hospira, was kindly provided by Dott. Rigacci Luigi (Unità Funzionale di Ematologia, Azienda Ospedaliera di Careggi).

4.2.2 Cell cultures

HL60 cell lines were stably transfected with pGL4.51[*luc2*/CMV/Neo] (**Figure 4.1**) plasmid (Promega, Cat. #E1320) encoding the luciferase reporter gene *luc2* (*Pothinus pyralis*), which has been codon-optimized for mammalian expression. This vector is also engineered with fewer consensus regulatory sequences for reduced backgrounds and decreased risk of anomalous transcription. It presents the following features:

- *luc2* reporter gene for expression in mammalian cells;
- *CMV* promoter for high translational expression;
- *SV40* late poly(A) signal sequence positioned downstream of *luc2* to provide efficient transcription termination and mRNA polyadenilation;
- binding region for RV primer 3 and RV primer 4;
- synthetic poly(A) signal/transcription start site;
- synthetic Neomycin-resistance gene for mammalian cell selection of the plasmid;

- plasmid replication origin;
- Ampicillin resistance gene for bacterial selection in vector amplification.

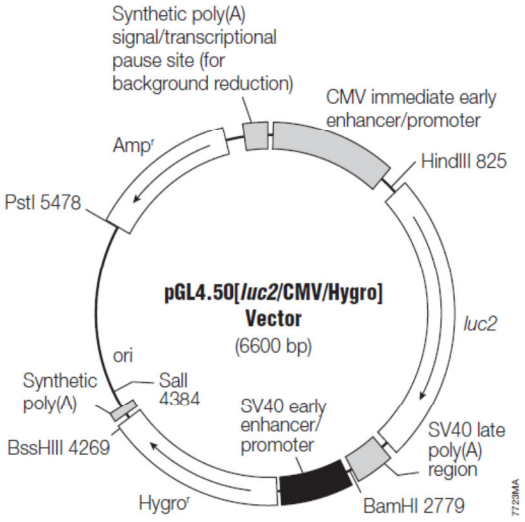

Figure 4.1: pGL4.51[*luc2*/CMV/Neo] plasmid

This vector is supplied in 10mM Tris-HCl (pH 7.4), 1 mM EDTA.[105]

HL60-*luc2* cell line were stably transfected with pGL4.51[*luc2*/CMV/Neo] by Marika Masselli. They were cultured in RPMI 1640 (Euroclone) with 10% fetal bovine serum (FBS, HyClone) and neomycin (Sigma-Aldrich, 2.8 mg/mL) and maintained in flasks (Corning) of 25 mm, at 37 °C, in humified atmosphere with 5% of CO_2. Medium renewal was performed every 2 - 3 days. For cryopreservation, HL60s are stored in fetal bovine serum (20%), in complete serum (70%) and DMSO (10%) in liquid nitrogen.

4.3 Methods

4.3.1 Bioluminescence assay

The method that we have used in *in vivo* experiments is based on animal bioluminescent imaging (BLI). This method is nowadays one of the most used by researchers with diverse backgrounds due to its low cost, high throughput, and relative ease of operation in visualizing a variety of cellular events *in vivo*.[106] BLI allows to continually monitor cellular processes or other biological interactions in a single individual, reducing the amount of inter-animal variation, thus leading to higher resolution and less data loss.
The mainstay of this method is the light generated by luciferase enzymes. In our case, light produced by firefly luciferase (FLuc) was exploited for bioluminescence assay. Fluc is the major luciferase protein studied and it was discovered in *Photinus pyralis*.

This enzyme catalyzes the oxidation of reduced luciferin in the presence of ATP-Mg^{2+} and oxygen to generate CO_2, AMP, PP_i, oxyluciferin, and yellow-green light at wavelength of 562 nm (**Figure 4.2**).[107,108]

Figure 4.2: Bioluminescence reaction promoted by Firefly Luciferase

In our experiments Fluc gene was stably transfected in tumor cells with the purpose to follow the bioluminescence produced by tagged cells, previously injected into an animal model. In this way bioluminescent cells were used to determine the kinetics of tumorigenesis and evaluate the efficacy of a chemioterapic treatment, by monitoring over time if light output increased or decreased, compared to the initial state. This method allowed to follow changes within individual animals without requiring the subject to be sacrificed.[109] Therefore, the detection of bioluminescence signals within a tissue sample was dependent on several factors, including flux of photons from the reporter, total number of functional reporters in the cells and location of the reporter cells within the tissue sample itself.

The major challenge in detecting and locating bioluminescent light emission within living subjects is represented by an optical imaging device based on highly sensitive cooled charge coupled device (CCD) cameras.[110,111] CCD detectors are made of sliced silicon crystals with high sensitivity to light, able to detect light in the visible and near-infrared range (400 – 1000 nm). CCD cameras operate by converting light photons that strike a pixel with energy of just 2-3eV into electrons. An electrical charge pattern, corresponding to the intensity of incoming photons, is read out of the CCD into an output register and amplified at the edge of the CCD for digitalization. Thermal noise is dramatically reduced since CCD cameras are refrigerated at -90÷ -150 °C.

4.3.2 Procedure

Experiments in SCID mouse were performed at the Laboratory of Genetic for the Production of Animal Models (LiGeMA) at the Animal House of the University of Florence. 1x 10^6 HL60-*luc2* cells were intraperitoneally injected in female 5-week old mice. Three days after inoculation, the distribution of HL60-*luc2* was monitored, in order to divide mice in different groups in which subjects possess the same signal. On the 5th day after inoculation mice were treated daily for two weeks with:

- physiological solution (intraperitoneal) as a control;
- cytarabine (6.25mg/kg, intraperitoneal);
- clarithromycin (15mg/kg, gavage)
- cytarabine+clarithromycin.

Images were acquired with Photo Acquisition software (Biospace Lab, Paris, France) and processed with M3 Vision sofware (Biospace Lab). Bioluminescence was detected at 9, 16, 23, 30 and 37 days after HL60-*luc2* inoculation.

4.4 Results and discussion

Figure 4.3 shows the effect of treatment with cytarabine and clarithromycin after HL60-*luc2* inoculation in SCID mice. Three days after inoculation, 12 mice were divided in three groups on the basis of the bioluminescence signal.

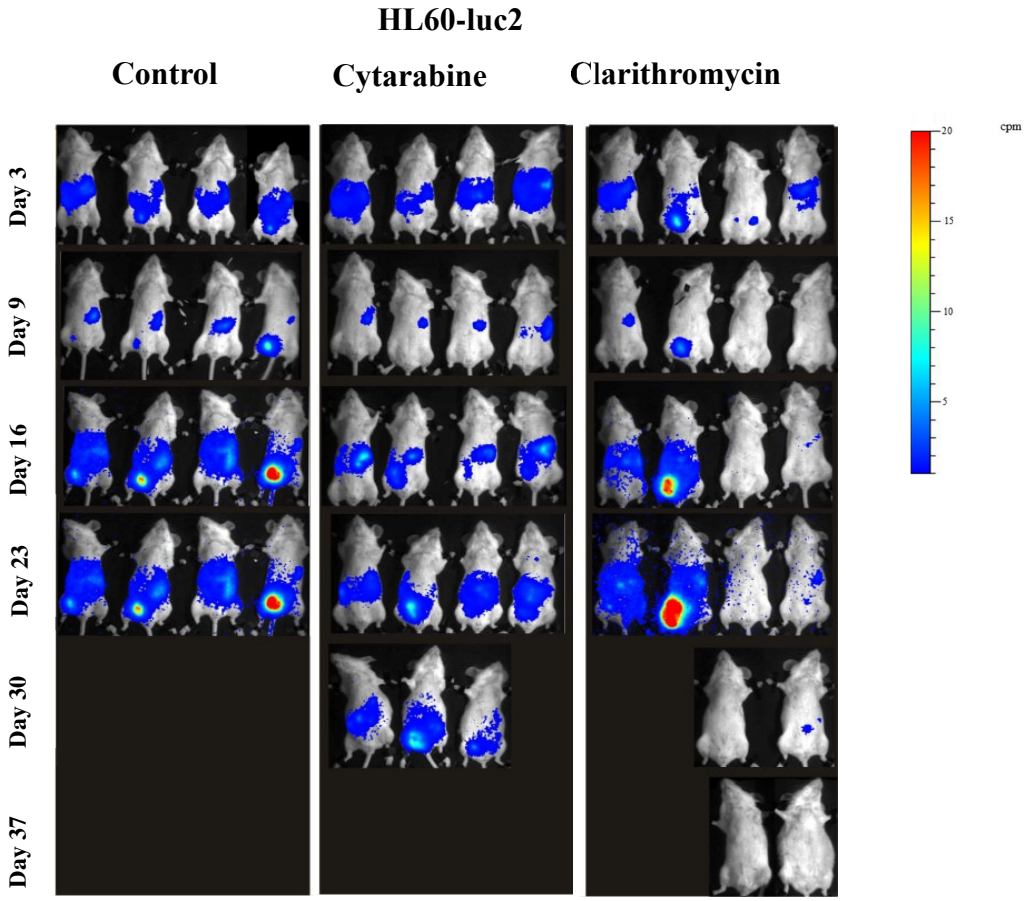

Figure 4.3: Clarithromycin reduces leukemia burden in leukemia model. SCID mice were injected with HL60-luc2 cell line (5 10^6 cells). Starting from day 5, animals were treated daily for fourteen consecutive days with physiological solution (Control, n=4), cytarabine 6.25 mg/kg, n=4 and clarithromycin 15mg/kg, n=4. Images were acquired with Photo Acquisition Software (Biospace Lab, Paris, France) and processed with M3 Vision software (Biospace Lab). Color bars represent light intensity levels from a minimum of 0.1 counts per minute (cpm) to a maximum of 20 cpm with a smoothing parameter equal to 1.295cpm.

On the 5th day, treatment with cytarabine or clarithromycin started. Mice were daily treated intraperitoneally with cytarabine (6.25mg/kg) and clarithromycin (15mg/kg) for two weeks.
On the 16th day, a considerable reduction of HL60 signal in SCID mice was noticed after treatment with clarithromycin, in contrast to what happened to control animals and those treated with cytarabine.
On the 23rd day HL60-luc2 diffused and spread in the body of control mice, as well as in mice treated with cytarabine. In contrast with the other two group, 2 mice treated with claryhtormicin showed regression of tumor diffusion and survived until 37 days after inoculation.
On the 30th day all mice in the control group died; 1 mouse in the cytarabine group died and 2 in the clarythromcin group died. Only 2 mice treated with clarithromycin survived, compared with the others. This experimental evidence showed the capability of clarithromycin to block tumor development and invasiveness.
In the second set of experiments 16 mice were divided into 4 groups, each containing four animals. The procedure was the same as explained before: after five days from inoculation, cytarabine and clarithromycin, alone or in combination were administered to mice. Mice in the control group were treated only with PBS.
The results of this treatments are presented in **Figure 4.4,** where the survival of each experimental group is reported through Kaplan-Meier curves.[112] The length of the horizontal lines along the X-axis of serial times represent the survival duration for that interval.

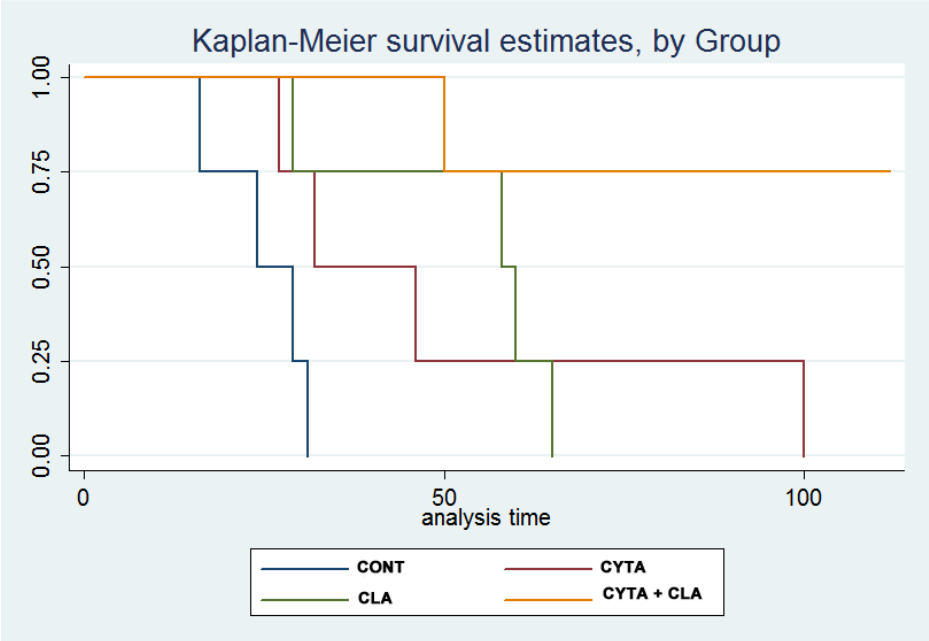

Figure 4.4: Kaplan-Meier analysis for each group in the experiment. Blue line underlines the survival of the control group, green line is referred to the group treated with clarithromycin, red line to the group treated with cytarabine, and orange line to the group treated with cytarabine and clarithromycin.

Comparing survival curves is important for visualizing the variability within groups treated with different drugs. Mice in the control group rapidly died and approximately in 30 days tumor invaded all the organs, causing mice death. After treatment with clarithromycin and cytarabine the survival increased in comparison with the control up to 65 and 100 days, respectively.

The combination of clarithromycin and cytarabine is thus particularly synergic, causing the survival of the mice for more than 100 days. The experiment is ongoing and three mice still alive.

As supported by the literature, clarithromycin increases the leukemia sensibility to cytarabine and increases the survival of mice until 120 days. Therefore clarithromycin, unlike other hERG blockers, present scarce antiarrhythmic effects and is a promising candidate for inclusion in clinical trials.

References

[1] Harmar A.J., Hills R.A., Rosser E.M., Jones M., Buneman O.P., Dunbar D.R, Greenhill S.D., Hale V.A., Sharman J.L., Bonner T.I., Catterall W.A., Davenport A.P., Delagrange P., Dollery C.T., Foord S.M., Gutman G.A., Laudet V., Neubig R.R., Ohlstein E.H., Olsen R.W., Peters J., Pin J.P., Ruffolo R.R., Searls D.B., Wright M.W., Spedding M.. IUPHAR-DB: The IUPHAR database of G proteincoupled receptors and ion channels. *Nucleic Acids Res.* **2009**, 37 (Database issue): D680-685.

[2] Hibino H., Inanobe A., Furutani K., Murakami S., Findlay I., Kurachi Y. Inwardly rectifying potassium channel: their structure, function, and physiological roles. *Physiol Rev*. **2010**, 90: 291-366

[3] Katz B. Les constantes eletriques de la membrane du muscle. *Arch. Sci. Physiol*. **1949**, 3: 285-299.

[4] Noble D. Electrical properties of cardiac muscle attributable to inward going (anomalous) rectification. *J. Cell. Comp. Physiol.* **1965**, 66: 127-136.

[5] Williams J.T., Colmers W.F., Pan Z.Z. Voltage- and ligand- activated inwardly rectifying currents in dorsal raphe neurons in vitro. *J. Neurosci*. **1988**, 8: 3499-3506

[6] McKinney L.C., Gallin E.K. Inwardly rectifying whole-cell and single-channel K^+ currents in the murine macrophage cell line J774.1. *J. Membr Biol.* **1988**,103: 41-53.

[7] Sims S.M., Dixon S.J. Inwardly rectifying K^+ current in osteclasts. **1989**, *Am. J. Physiol Cell Physiol.* 256: C1277-C1282.

[8] Silver M.R., DeCoursey T.E. Intrinsic gating of inward rectifier in bovine pulmonary artery endothelial cells in the presence or absence of internal Mg^{2+}. **1990**, *J. Gen Physiol.* 96: 109-133.

[9] Kuffler S.W., Nicholls J.G. The physiology of neuroglial cells. **1966**, *Ergeb Physiol* 57: 1-90.

[10] Hebert S.C., Desir G., Giebisch G., Wang W. Molecular diversity and regulation of renal potassium channels. *Physiol Rev.* **2005**, 85: 319-371.

[11] Hagiwara S., Takahashi K. The anomalous rectification and cation selectivity of the membrane of a starfish egg cell. **1974**, *J Membr Biol.* 18: 61-80.

[12] Ho K., Nichols C.G., Lederer W.J., Lytton J.,Vassilev P.M., Kanazirska M.V., Hebert S.C.; Cloning and expression of an inwardly rectifying ATP-regulated potassium channel. *Nature*. **1993**, 362(6415): 31-38.

[13] Kubo Y., Baldwin T.J., Jan Y.N., Jan L.Y. Primary structure and functional expression of a mouse inward rectifier potassium channel. *Nature.* **1993**, 362(6416):127-33

[14] Ishihara K., Mitsuiye T., Noma A., Takano M. The Mg2+ block and intrinsic gating underlying inward rectification of the K+ current in guinea-pig cardiac myocytes. *J Physiol.* **1989**, 419: 297-320.

[15] Lopatin A.N., Makhina E.N., Nichols C.G. Potassium channel block by cytoplasmic polyamines as the mechanism of intrinsic rectification. *Nature*. **1994**, 372(6504): 366-369.

[16] Hagiwara S., Miyazaki S., Rosenthal N.P. Potassium current and the effect of cesium on this current during anomalous rectification of the egg cell membrane of a starfish. *J Gen Physiol.***1976**, 67(6): 621-638.

[17] Imredy J.P., Chen C., MacKinnon R. A snake toxin inhibitor of inward rectifier potassium channel ROMK1. *Biochemistry.* **1998**, 37(42): 14867-14874.

[18] Enyedi P., Czirják G. Molecular background of leak K^+currents: two-pore domain potassium channels. *Physiol. Rev.* **2010**, 90: 559-605.

[19] Fink M., Duprat F., Lesage F., Reyes R., Romey G., Heurteaux C., Lazdunski M. Cloning, functional expression and brain localization of a novel unconventional outward rectifier K^+ channel. *EMBO J.***1996**, 15: 6854-6872.

[20] Leonoudakis D., Gray A.T., Winegar B.D., Kindler C.H., Harada M., Taylor D.M., Chavez R.A., Forsayeth J.R., Yost C.S. An open rectifier potassium channel with two pore domains in tandem cloned from rat cerebellum. *J. Neurosci.* **1998**, 18: 868-877..

[21] Alvarez- Baron C.P., Jonsson P., Thomas C., Dryer S.E., Williams C. The two-pore domain potassium channel KCNK5: Induction by estrogen receptor alpha and role in proliferation of breast cancer cells. *Mol Endocrinol*. **2011**, 25(6): 1326- 1336.

[22] Ohya S., Kimura K., Niwa S., Ohno A., Kojima Y., Sasaki S., Kohri K., Imaizumi Y. Malignancy grade–dependent expression of K+-channel subtypes in human prostate cancer. *J. Pharmacol Sci.* **2009**, 109 (1): 148-151.

[23] Huang L, Li B, Li W, Guo H, Zou F. ATP-sensitive potassium channels control glioma cells proliferation by regulating ERK activity. *Carcinogenesis*. **2009**, 30(5): 737-44.

[24] Miller M.R., Zou B., Shi J., Flaherty D.P., Simpson D.S., Yao T., Maki B.E., Day V.W., Douglas J.T., Wu M., McManus O.B., Golden J.E., Aubé J., Li M. Development of a Selective Chemical Inhibitor for the Two-Pore Potassium Channel, KCNK9.SourceProbe Reports from the NIH Molecular Libraries Program [Internet]. Bethesda (MD): National Center for Biotechnology Information (US); 2010-.2012 Apr 16 [updated 2013 Feb 28].

[25] Wei A.D., Gutman G.A., Aldrich R., Chandy K.G., Grissmer S. and Wulff H.. International Union of Pharmacology. LII. Nomenclature and Molecular Relationships of Calcium-Activated Potassium Channel. *Pharmacol Rev*. **2005**, 57: 463-472, 2005.

[26] Berkefeld H., Fakler B., Shulte U. Ca^{2+} -activated K^+ channel s: from protein complexes to function. *Physiol Rev*. **2010**, 90: 1437-1459.

[27] Sah P. Ca^{2+}-activated K^+ currents in neurones: types, physiological roles and modulation. *Trend Neurosci.* **1996**, 19: 150-154.

[28] Meredith A.L., Thorneloe K.S., Werner M.E., Nelson M.T., Aldrich R.W. Overactive bladder and incontinence in the absence of the BK large conductance Ca^{2+} -activated K^+ channel. **2004**, *J Biol Chem* 279: 36746-36752.

[29] Ahluwalia J., Tinker A., Clapp L.H., Duchen M.R., Abramov A.Y., Pope S., Nobles M., Segal A.W. The large conductance Ca^{2+} -activated K^+ channel is essential for innate immunity. **2004**, Nature, 427: 853-858.

[30] Yazejian B., Sun X.P., Grinnell A.D. Tracking presynaptic Ca^{2+} dynamics during neurotransmitter release with Ca^{2+}-activated K^+ channels**.** *Nat Neurosci.* **2000**, 3: 566-571.

[31] Gu N., Vervaeke K., Storm J.F. BK potassium channels facilitate high-frequency firing and cause early spike frequency adaptation in rat CA1 hippocampal pyramidal cells. *J Physiol.* **2007**, 580: 859-882.

[32] Golding N.L., Jung H.Y., Mickus T., Spruston N. Dendritic calcium spike initiation and repolarization are controlled by distinct potassium channel subtypes in CA1 pyramidal cells. *J Neurosci.* **1999**, 19: 8789-8798.

[33] Brown A., Cornwell T., Korniyenko I., Solodushko V., Bond C.T., Adelman J.P., Taylor M.S. Myometrial expression of small conductance Ca^{2+}-activated K channels depresses phasic uterine contraction. *Am J Physiol Cell Physiol.* **2007**, 292: C832–C840.

[34] Taylor MS, Bonev AD, Gross TP, Eckman DM, Brayden JE, Bond CT, Adelman JP, Nelson MT. Altered expression of small conductance Ca^{2+}-activated K (SK3) channels modulates arterial tone and blood pressure. *Circ Res*. **2003**, 93: 124–131.

[35] Zhang M., Houamed K., Kupershmidt S., Roden D., Satin L.S. Pharmacological properties and functional role of K slow current in mouse pancreatic beta-cells: SK channels contribute to K slow tail current and modulate insulin secretion. *J Gen Physiol*. **2005**, 126: 353-363.

[36] Hoffman J.F., Joiner W., Nehrke K., Potapova O., Foye K., Wickrema A. The hSK4 (KCNN4) isoform is the Ca^{2+} -activated K channel (Gardos channel) in human red blood cells. *Proc Natl Acad Sci.* **2003**, 100: 7366–7371.

[37] Fay A.J., Qian X., Jan Y.N., Jan L.Y. SK channels mediate NADPH oxidase-independent reactive oxygen species production and apoptosis in granulocytes. *Proc Natl Acad Sci.* **2006**, 103: 17548–17553.

[38] Jensen B.S., Odum N., Jorgensen N.K., Christophersen P., Olesen S.P. Inhibition of T cell proliferation by selective block of Ca^{2+}- activated K^+ channels. *Proc Natl Acad Sci.* **1999**, 96: 10917–10921.
[39] Lin M.T., Luján R., Watanabe M., Adelman J.P., Maylie J. SK2 channel plasticity contributes to LTP at Schaffer collateral-CA1 synapses. *Nat Neurosci.* **2008**, 11: 170–177.
[40] Ngo-Anh T.J., Bloodgood B.L., Lin M., Sabatini B.L., Maylie J., Adelman J.P. SK channels and NMDA receptors form a Ca^{2+}-mediated feedback loop in dendritic spines. *Nat Neurosci.* **2005**, 8: 642-649.
[41] Meera P., Wallner M., Song M., Toro L. Large conductance voltage- and calcium- dependent K^+ channel, a distinct member of voltage-dependent ion channels with seven N-terminal transmembrane segments(S0-S6), an extracellular N-terminus, and an intracellular (S9-S10) C terminus. *Proc Natl Acad Sci*. **1997**, USA 94: 14066-14071.
[42] D'Amico M., Gasparoli L. and Arcangeli A. Potassium channels: novel emerging biomarkers and targets for therapy in cancer. *Recent patents on anti-cancer drug discovery.* **2013**, 8: 53-65.
[43] Hirschberg B., Maylie J., Adelman J.P., Marrion N.V. Gating of recombinant small-conductance Ca-activated K^+ channels by calcium. *J Gen Physiol* **1998**, 111: 565-581.
[44] Swartz K.J. Towards a structural view of gating potassium channels. *Nature Rev. Neurosci.* **2004**, 5: 905-916.
[45] Bezanilla F. Ion channels: from conductance to structure. *Neuron.* **2008**, 60: 465-468.
[46] Bezanilla F. How membrane proteins sense voltage. *Nature Rev. Mol. Cell Biol.* **2008**, 9: 323-332
[47] Chandy, K.G. Wulff H., Beeton C., Pennington M., Gutman G.A., Cahalan M.D. Potassium channels as targets for specific immunomodulation. *Trends Pharmacol. Sci.* **2004**, 25: 280–289.
[48] Feske S., Gwack Y., Prakriya M., Srikanth S., Puppel S.H., Tanasa B., Hogan P.G., Lewis R.S., Daly M., Rao A. A mutation in Orai1 causes immune deficiency by abrogating CRAC channel function. *Nature*. **2006**, 441: 179–185.
[49] Pardo, L.A. Del Camino D., Sánchez A., Alves F., Brüggemann A., Beckh S., Stühmer W. Oncogenic potential of EAG K^+ channels. *EMBO J.* **1999**, 18: 5540–5547.
[50] Wulff H., Zhorov B.S. K^+ channel modulators for the treatment of neurological disorders and autoimmune diseases. *Chem. Rev.* **2008**, 108: 1744-1773.
[51] Bruhova I., Zhorov B. S. Monte Carlo-energy minimization of correolide in the Kv 1.3 channel: possible role of potassium ion in ligand- receptor interactions. *BCM Struct. Biol.* **2007**, 7: 5.
[52] Lu Q. Peevey J., Jow F., Monaghan M.M., Mendoza G., Zhang H., Wu J., Kim C.Y., Bicksler J., Greenblatt L., Lin S.S., Childers W., Bowlby M.R. Disruption of $K_v1.1$ N-type inactivation by novel small molecule inhibitors (disinactivators). *Bioorg. Med. Chem.* **2005**, 16: 1009-1017.
[53] Kaplan W. D., Trout W. E. 3rd The behavior of four neurological mutants of Drosophila. *Genetics*. **1969**, 61: 399-409.
[54] Warmke J.K., Ganetzky B. A family of potassium channel genes related to *eag* in *Drosophila* and mammals. *Proc. Natl. Acad. Sci.* **1994**, 91: 3438-3442.
[55] Farrelly A.M., Ro S., Callaghan B.P., Khoyi M. A., Fleming N., Horowitz B., Sanders K. M., Keef K. D. Expression and function of KCNH2 (HERG) in the human jejunum American Journal of Physiology - Gastrointestinal and Liver. *Physiology*. **2003**, 284: 883-895.
[56] Chiesa N., Rosati B., Arcangeli A., Olivotto M., Wanke. E. A novel role for HERG K+ channels: spike-frequency adaptation. *J Physiol.* **1997**, 501: 313-318.
[57] Wimmers S., Wulfsen I., Bauer C. K., Schwarz J. R. Erg1, erg2 and erg3 K channel subunits are able to form heteromultimers. *Pflugers Arch.* **2001**, 441:450-455.
[58] Wulff H., Castle N.A., Pardo L.A. Voltage- gated potassium channels as therapeutic targets. *Nature reviews.* **2009**, 8: 982-1001.
[59] Arcangeli A, Rosati B, Cherubini A, Crociani O, Fontana L, Ziller C, Wanke E, Olivotto M. HERG and IRK-like inward rectifier currents are sequentially expressed during neuronal development of neural crest cells and their derivatives. *Eur J Neurosci*.**1997**, 9: 2596-2604.

[60] Crociani O., Cherubini A., Piccini E., Polvani S., Costa L., Fontana L., Hofmann G., Rosati B., Wanke E., Olivotto M., Arcangeli A. Erg gene(s) expression during development of the nervous and muscular system of quail embryos. *Mech Dev* **2000**, 95: 239-243.
[61] Wang L., Dennis A. T., Trieu P., Charron F., Ethier N., Hebert T.E., Wan X., Ficker E. Intracellular potassium stabilizes human ether-a-go-go-related gene channels for export from endoplasmic reticulum. *Mol Pharmacol* **2009**, 75: 927–937.
[62] Claycomb W.C., Lanson N.A. Jr, Stallworth B.S., Egeland D.B., Delcarpio J.B., Bahinski A., Izzo N.J. Jr. HL-1 cells: a cardiac muscle cell line that contracts and retains phenotypic characteristics of the adult cardiomyocyte. *Proc Natl Acad Sci* **1998**, 95: 2979–2984.
[63] Cherubini A., Taddei G.L., Crociani O., Paglierani M., Buccoliero A.M., Fontana L., Noci I., Borri P., Borrani E., Giachi M., Becchetti A., Rosati B., Wanke E., Olivotto M., Arcangeli A. HERG potassium channels are more frequently expressed in human endometrial cancer compared with non-cancerous endometrium. *Br J Cancer*. **2000**, 83: 1722–1729.
[64] Akbarali H.I., Thatte H., He X.D., Giles W.R., Goyal R.K. Role of HERG-like K currents in opossum esophageal circular smooth muscle. *Am J Physiol Cell Physiol* **1999**, 277: C1284–C1290.
[65] Arcangeli A., Bianchi L., Becchetti A., Faravelli L., Coronnello M., Mini E., Olivotto M., Wanke E. A novel inward-rectifying K current with a cell-cycle dependence governs the resting potential of mammalian neuroblastoma cells. *J Physiol*. **1995**, 489: 455–471.
[66] Fortunato A., Gasparoli L., Falsini S., Boni L., Arcangeli A. An analytical method for the quantification of hERG1 channel gene expression in human colorectal cancer. *Diagn. Mol. Pathol.* **2013**, 22(4):215-221.
[67] Lastraioli E., Guasti L., Crociani O., Polvani S., Hofmann G., Witchel H., Bencini L., Calistri M., Messerini L., Scatizzi M., Moretti R., Wanke E., Olivotto M., Mugnai G., Arcangeli A. herg1 gene and HERG1 protein are overexpressed in colorectal cancers and regulate cell invasion of tumor cells. *Cancer Res.* **2004**, 64: 606–611.
[68] Pillozzi S., Brizzi M.F., Bernabei P.A., Bartolozzi B., Caporale R., Basile V., Boddi V., Pegoraro L., Becchetti A., Arcangeli A. VEGFR-1 (FLT-1), beta1 integrin, and hERG Kchannel for a macromolecular signaling complex in acute myeloid leukemia: role in cell migration and clinical outcome. *Blood.* **2007**, 110: 1238–1250.
[69] Cherubini A., Hofmann G., Pillozzi S., Guasti L., Crociani O., Cilia E., Di Stefano P., Degani S., Balzi M., Olivotto M., Wanke E., Becchetti A., Defilippi P., Wymore R., Arcangeli A. Human ether-a-go-go-related gene 1 channels are physically linked to beta1 integrins and modulate adhesion-dependent signaling. *Mol Biol Cell.* **2005**, 16: 2972–2983.
[70] Masi A., Becchetti A., Restano-Cassulini R., Polvani S., Hofmann G., Buccoliero A.M., Paglierani M., Pollo B., Taddei G.L., Gallina P., Di Lorenzo N., Franceschetti S., Wanke E., Arcangeli A. hERG1 channels are overexpressed in glioblastoma multiforme and modulate VEGF secretion in glioblastoma cell lines. *Br J Cancer* **2005**, 93: 781–792.
[71] Pillozzi S., Brizzi M.F., Balzi M., Crociani O., Cherubini A., Guasti L., Bartolozzi B., Becchetti B., Wanke E., Bernabei P.A., Olivotto M., Pegoraro L., Arcangeli A. HERG potassium channels are constitutively expressed in primary human acute myeloid leukemias and regulate cell proliferation of normal and leukemic hematopietic progenitors. *Leukemia*. **2002**, 16, 1791-1798.
[72] Pillozzi S., Brizzi M.F., Bernabei P.A., Bartolozzi B., Caporale R., Basile V., Boddi V., Pegoraro L., Becchetti A. and Arcangeli A. VEGFR-1 (FLT-1), $\beta_1$integrin, hERG K^+ channel for a macromolecular signaling complex in acute myeloid leukemia: role in cell migration and clinical oucome. *Blood.* **2007**, 110: 1238-1250.
[73] Pillozzi S., Masselli M., De Lorenzo E., Accordi B., Cilia E., Crociani O., Amedei A., Veltroni M., D'Amico M., Basso G., Becchetti A., Campana D., Arcangeli A., Chemotherapy resistance in acute lymphoblastic leukemia requires hERG1 channels and is overcome by hERG1 blockers. *Blood*. **2011**, 11: 902-914.
[74] Pillozzi S. Accordi B., Rebora P., Serafin V., Valsecchi M.G., Basso G., Arcangeli A. Differential expression of hERG1A and hERG1B genes in pediatric acute lymphoblastic

leukemia identifies different prognostic subgroups, *Leukemia*, **2014**, DOI: 10.1038/leu.2014.26. Accepted for publication.
[75] Omura S., Tsuzuki K., Sunazuka T., Marui S., Toyoda H., Inatomi N., Itoh Z. Macrolides with gastrointestinal motor stimulating activity. *J. Med. Chem.* **1987**, 30: 1941-1943.
[76] Sturgill M.G., Rapp R.P. Clarithromycin: review of new macrolide antibiotic with improved microbiologic spectrum and favorable pharmakocinetic and adverse effect profile. *Ann Pharmacothe.* **1992**, 26:1099-1108.
[77] Hansen L.H., Mauvais P., Douthwaite S. The macrolide-ketolide antibiotic binding site is formed by structures in domain II and V of 23S ribosomal RNA. *Mol Microbiol* **1999**, 31 (2): 623-631.
[78] Hardy D.J., Guay D.R., Jones R.N. Clarithromycin, a unique macrolide: a pharmacokinetic, microbiological, and clinical overview. *Diagn Microbiol Infect Dis.* **1992**, 15: 39-53.
[79] Hardy D J, Hensey D.M., Beyer J.M., Vojtko C., McDonald E.J., Fernandes P.B. Comparative in vitro activities of new 14-, 15-, and 16-membered macrolides. *Antimicrobial Agents and Chemotherapy*. **1988**, 32: 1710-1719.
[80] Chu S.Y., Grannerman G.R., Pichotta P.J., Decourt J.P., Girault J., Fourtillan J.B. Effect of moderate or severe hepatic impairment of clarithromycin pharmacokinetics. *J. Clin Pharmacol.* **1993**, 33: 480-485.
[81] Guay D.R., Gustavson L.E., Devcich K.J., Zhang J., Cao G., Olson C.A. Pharmacokinetics and tolerability of extended-release clarithromycin. *Clin Ther.* **2001**, 23: 566-577
[82] Ogawa M., Suzuki J-I, Hishikari K., Takayama K., Tanaka H. and Isobe M. Clarithromycin Attenuates Acute and Chronic Rejection Via Matrix Metalloproteinase Suppression in Murine Cardiac Transplantation. *J Am Coll Cardiol.* **2008**, 51:1977-1985.
[83] Basyigit I, Yildiz F, Ozkara SK, Yildirim E, Boyaci H, Ilgazli A. The effect of clarithromycin on inflammatory markers in chronic obstructive pulmonary disease: preliminary data. *Ann Pharmacother*. **2004**, 38:1400-1405.
[84] Abbott Laboratories. Biaxin (Clarithromycin): prescribing information.2008; 2008 (12/23). Available at: http://www.rxabbott.com/pdf/biapi.PDF. Accessed, August **2009**
[85] Mikasa K., Sawaki M, Kita E., Hamada K., Teramoto S., Sakamoto M., Maeda K., Konishi M. and Narita N. Significant survival benefit to patients with advanced non-small lung cancer for treatment with clarithromycin. *Chemotherapy.* **1997**, 43: 288-296.
[86] Sassa K. Mizushima Y., Fujishita T., Oosaki R. and Kobayashi M. Therapeutic effect of clarithromycin on a transplanted tumor in rats. *Antimicrobial agents and chemotherapy*. **1999**, 43: 67-72.
[87] Yatsunami J., Turuta N. Wakamatsu K., Hara N., Hayashi S. Clarithromycin is a potent inhibitor of tumor-induced angiogenesis. *Res Exp Med.* **1997**, 197: 189-197
[88] Coleman M., Leonard J., Lyons L., Szelenyi H. and Niesvizky R. Treatment of Waldenstrom's macroglobulinemia with clarithromycin low-dose thalidomide, and dexamethasone. Semin Oncol. 2003, 30: 270-274.
[89] Niesvizky R., Jayabalan D.S., Christos P.J., Furst J.R., Naib T., Ely S., Jalbrzikowski J., Pearse R.N., Zafar F., Pekle K., Larow A., Lent R., Mark T., Cho H.J., Shore T., Tepler J., Harpel J., Schuster M.W., Mathew S., Leonard J.P., Mazumdar M., Chen-Kiang S., Coleman M. BiRD (Biaxin [clarithromycin]/Revlimid [lenalidomide]/dexamethasone) combination therapy results in high complete- and overall-response rates in treatment-naive symptomatic multiple myeloma. *Blood*. **2008**, 111:1101-1109.
[90]Gay F., Rajkumar S.V., Coleman M., Kumar S., Mark T., Dispenzieri A., Pearse R., Gertz M.A., Leonard J., Lacy M.Q., Chen-Kiang S., Roy V., Jayabalan D.S., Lust J.A., Witzig T.E., Fonseca R., Kyle R.A., Greipp P.R., Stewart A.K., Niesvizky R. Clarithromycin (Biaxin)-lenalidomide-low-dose dexamethasone (BiRd) versus lenalidomide-low-dose dexamethasone (Rd) for newly diagnosed myeloma. *Am J Hematol*. **2010**, 85: 664-669.
[91] http://clinicaltrials.gov/ct2/show/NCT00461084?term=clarithromycin&rank=8
[92] http://clinicaltrials.gov/ct2/show/NCT00445692?term=clarithromycin&rank=11

[93] Kroemer G. and Jaattela M. Lysosomes and autophagy in cell death control. *Nat Rev. Cancer.* **2005**, 5: 886-897.
[94] Nakamura M., Kikukawa Y., Takeya M., Mitsuya H., Hata H. Clarithromycin attenuates autophagy in myeloma cells. *International journal of oncology*. **2010**, 37: 815-820.
[95] Carella A.M., Beltrami G., Pica G., Carella A. and Catania G. Clarithromycin potentiates tyrosine kinase inhibitor treatment in patients with resistant chronic myeloid leukemia. *Leukemia & Linphoma*. **2012**, 53: 1409-1411.
[96] Schafranek L., Leclerq T.M., White D.L. and Hughes T.P. Clarithromycin enhances dasatinib-induced cell death in CML cells, by inhibition of late stage autophagy. *Leukemia & Linphoma*. **2012** Accepted for publication. DOI:10.3109/10428194.2012.698737.
[97] Abbott G.W., Sesti F., Splawski I., Buck M.E., Lehmann M.H., Timothy K.W., Keating M.T., Goldstein S.A. MiRP1 forms IKr potassium channels with HERG and is associated with cardiac arrhythmia. *Cell.* **1999**, 97: 175-187.
[98] Mihara K., Imai C., Coustain-Smith E., Dome J.S., Dominici M., Vanin E. and Campana D. Development and functional characterization of human bone marrow mesenchymal cells immortalized by enforced expression of telomerase. *Br. J. Haematol*. **2003**, 120: 846-849.
[99] Greco W.R, Bravo G., Parsons J.C. The search for synergy: a critical review from response surface perspective. *Pharmacol. Rev.***1995**, 47: 331-385.
[100] Chou T.C. What is synergy? *Scientist.* **2007**, 21:15.
[101] Chou T.C. Drug combination studies and their synergy quantification using the Chou-Talaly method. *Cancer Research.* **2010**, 70: 440-446.
[102] Chou T.C., Talay P. Quantitative analysis of dose-effect relationships: the combined effects of multiple drugs or enzyme inhibitors. *Adv Enzyme Regul.* **1984**, 22: 27-55.
[103] Chou T.C. The median-effect principle and the combination index for quantification of synergism and antagonism. In:Chou T.C., Rideout D.C., editors. Synergism and antagonism in chemotherapy. San Diego: Academic Press, **1991**, 61-102.
[104] Chou T.C. Theoretical basis, experimental design, and computerized simulation of synergism and antagonism in drug combination studies. Pharmacol Rev. **2006**, 68: 621-681.
[105] Promega pGL4.51[luc2/CMV/Neo] Vector Product # 9PIE132. Information avaible in: http://ita.promega.com/~/media/Files/Resources/Protocols/Product%20Information%20Sheets/A/pGL4%2051%20Vector.pdf.
[106] Baker M. The whole picture. *Nature*, **2010**, 463: 977-988.
[107] Fraga H. Firefly luminescence: A historical perspective and recent developments. *Photochem. Phtobiol. Sci.* **2008**, 7: 146-158.
[108] Lee B.I. and Min J.-J. Molecular Imaging Using Bioluminescence. *The Open Nuclear Medicine Journal*, **2010**, 2: 157-165.
[109] Kim J.B., Urban K., Cochran E., Lee S., Ang A., Rice B., Bata A., Campbell K., Coffee R., Gorodinsky A., Lu Z., Zhou H., Kishimoto T.K., Lassota P. Non-invasive detection of a small number of bioluminescent cancer cells in vitro. *PLoS One,* **2010** DOI: 10.1371/journal.pone.0009364
[110] Rice B.W., Cable M.D., Nelson M.B. In vivo imaging of light-emitting probes. *J. Biomed. Opt.* **2001**, 6: 432-434.
[111] Spibey C.A., Jackson P., Herick K. A unique charge-coupled device/xenon arc lamp based imaging system for the accurate detection and quantitation of multicolour fluorescence. *Electrophoresis*. **2001**, 22: 829-836.
[112] Rich J:T., Neely J.G., Paniello R.C., Voelker C.C.J., Nussenbaum B. and Wang E.W. A practical guide to understanding Kaplan-Meier curves. *Otolaryngology-Head and Neck Surgery*. **2010**, 143: 331-336.

Second Part

Targeting hERG channels: a molecular approach through RNA interference

Chapter 1

1.1 RNAi mechanism and discovery

The discovery of noncoding double-stranded RNA (dsRNA) molecules, capable of regulating gene expression in eukaryotic cells by post-transcriptional gene silencing, is one of the most relevant advances in molecular genetics.[1] Sequence-specific gene silencing, known as interference of RNA (RNAi), is a natural occurring molecular process that can be experimentally exploited to knock-down any gene of interest. RNAi is a molecular technique that allows rapid and cost-effective screening of gene function in model organisms[2] and mammal cells.[3] Moreover, RNAi could have a considerable importance in medicine because it may allow the development of treatments against a large array of pathologies nonresponsive to conventional therapies.

RNAi was first observed in petunia flowers by plant biologists. Jorgenesen and collaborators introduced the chimeric chalcone synthase (CHS) gene in petunia, in order to increase the flowers anthocyanin biosynthesis catalyzed by CHS.[4] Contrarily to their expectations, the introduction of the transgene blocked the pigment production. The concomitant silencing of both ectopic transgenes and endogenous homologous genes was called "co-suppression". A similar phenomenon was evidenced in *Neurospora crassa* two years later. In this case, the post-transcriptional mechanism of gene silencing was called *quelling*, as its relationship with co-suppression in petunia flowers was not immediately recognized.[5]

Eventually, the post-transcriptional mechanism of gene silencing was clarified in *Caenorhabditis elegans* by Fire and Mello (1998),[6] who recognized dsRNAs, but not the single strand RNAs, as responsible for gene silencing. The first evidence of this mechanism in mammals, was described two years later in mouse early embryos, opening the possibility for RNAi human application.[7] Finally, in 2001, the discovery

that small dsRNA of 21bp (siRNA) were capable of inducing gene-specific-silencing in mammalian cells without activating immune-response turned RNAi into one of the most promising techniques to control post-transcriptional gene expression in mammals.[8]
Although many types of small RNAs have been reported, the three main classes of natural small dsRNAs involved in eukaryote gene silencing are: microRNAs (miRNAs), small interfering RNAs (siRNAs) and piwi-interacting RNAs (piRNAs).

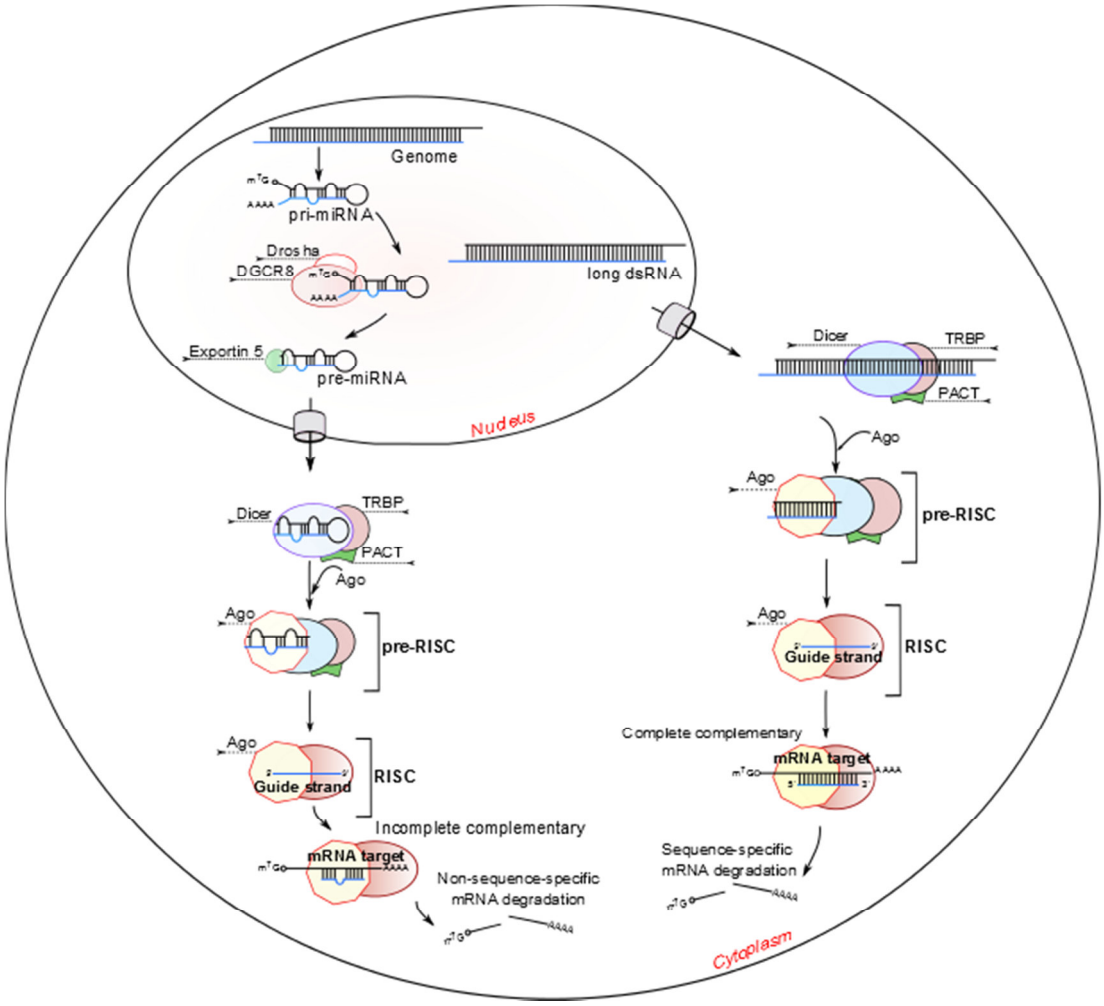

Figure 1.1: RNA interference mechanism mediated by miRNA and siRNA molecules.

miRNAs are endogenous products of genome and play an important role in post-transcriptional regulation of gene-expression. They are initially transcribed by RNA polymerase II as a part of a long primary RNA molecule called pri-miRNA, characterized by a stem loop structure.[9] As shown in **Figure 1.1**, pri-miRNAs are processed by the RNase III enzyme, Drosha, in a pre-miRNA hairpin about 70 nt in length, with interspersed mismatches along the duplex and with 2-nt 3'overhang. Pre-miRNAs are transported in the cytoplasm by the nuclear export factor. In the cytoplasm, pre-miRNAs, are processed into miRNA duplexes by a protein complex containing Dicer and other functional subunits. Dicer binds and cleaves the pre-miRNA removing the terminal loop and leaving a staggered end. Then miRNA duplexes interact with the

Argonaute (Ago) protein contained in the pre-RNA Induced Silencing Complex (pre-RISC). In the mature RISC, the passenger strand is removed and the guide strand is integrated in the RISC complex to bind the mRNA target which is cleaved by Ago.[10]
siRNAs originate from pseudogenes and from exogenous genes, such as transposons or virus, suggesting a role in the control of the genome integrity in response to invasive genomes. At variance with miRNAs, the interaction between siRNA and mRNA target is fully complementary.[11] miRNAs and siRNAs share similarities in size and sequence specific inhibitory functions, suggesting a correlation in their biogenesis and silencing mechanism.[12]
piRNAs are a complex and largely uncharacterized category of silencing inducing RNAs. piRNAs play a critical function in protecting germ line cells from invasive transposable elements but also have a role in non-gonadal cells.[13]
Synthetic siRNA delivery is a well established technique *in vitro*. However, the major challenge for the application of RNAi in molecular medicine is their *in vivo* infusion. For efficient systemic delivery, it is necessary to develop vehicles which can provide protection and selective transport to the cells of interest. Currently, the most used delivery agents *in vivo* are lipid-based vectors.[14-20]

1.2 Importance of delivery procedures

In vivo administration of siRNAs has some limitations, such as crossing the plasma-membranes of target cells, unwanted enzyme degradation and activation of immune response. Vectors specifically tailored for RNAi were introduced to enhance the efficacy of RNAi therapeutics.
Naked siRNAs is usually employed only in local applications, due to the presence of endonucleases in the blood stream and tissues. Examples include delivery to the eye, lung, joint and mucosa.[21,22] Therefore, the association of siRNAs to carriers is imperative for systemic administration to (i) protect the cargo from nuclease degradation, (ii) reach the target while avoiding off-target tissues, (iii) facilitate cellular uptake.
Vectors used in gene silencing have been classified as viral or non-viral. Viral-mediated delivery exploits the infection ability of retrovirus and adenovirus, and are usually employed to induce sustained gene silencing *in vitro.* However, *in vivo* applications are affected by a number of flaws, such as immune response, insertion mutagenensis, toxicity and uncontrolled virus replication. Another limitation is the difficult large scale preparation of viruses.[23]
On the other hand, for siRNA delivery non-viral vectors can be easily prepared and scaled-up, do not provoke immune response and can be safely handled by medical operators, without concern for their own health. Non-viral transfection can be performed by physical (e.g. electroporation) or by chemical methods. For this latter purpose different complexing agents may be used. Examples include inorganic, “hard”, nanoparticles (mainly of noble metals, calcium phosphate, or magnetic materials), and

"soft" nanoparticles made by polymers or lipids, peptides or aptamers possibly linked to siRNA with covalent bonds. In all cases, the pharmacodynamic behavior and cytotoxicity of these formulations need to be investigated to establish the risk-benefits of each delivery technique.
In the next paragraph we focalize on the most used non-viral systems, i.e. lipid-based carriers, which are biocompatible and can be prepared in a wide range of formulations.[24] Their peculiarities originate from the striking variety of shape and size shown by lipid polymorphism. Indeed, lipids can be arranged in many different aggregates, whose final structure results from the balance of intermolecular forces, geometrical constrains, counterion binding and hydration.[25,26]

1.3 Lipid based vectors for nucleic acid delivery

Micelles are the simplest nanosized aggregates of amphiphilic molecules and are spontaneously formed in aqueous media. The nonpolar portions (hydrophobic tails) of the constituent monomers are located in the interior, while the polar portions (hydrophilic heads) are exposed to water, as schematically shown in **Figure 1.2**. The inside of micelles is a liquid-like hydrocarbon milieu, in contrast with the surface, where the monomers are tightly packed.[27]

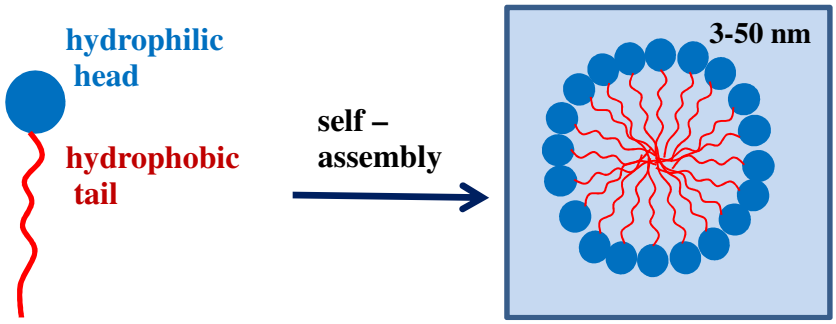

Figure 1.2. Schematic draw of an amphiphilic molecule and of a micelle

Drugs can be encapsulated in different micellar regions, according to their polar/non polar characteristics. In particular, non polar lipophilic molecules tends to concentrate into the core, whereas polar or amphiphilic compounds are included among the monomers or associated to the head region. As aggregates at thermodynamic equilibrium, micelles are easily rearranged if the environmental conditions change. Thus, the micellar cargo may not been efficiently vehiculated and, in fact, simple micelles are scarcely used in drug delivery, at variance with their polymeric analogues, which are structurally stable.[28] A noticeable exception is the transport of genetic material. In this case micelles of cationic amphiphiles, especially di- or tri-valent ones,

have proven to be an efficient tool for nucleic acid delivery, since the micelle easily deformable shape provides flexible complexing pathways.[29]

Liposomes are lipid vesicles in which one or more concentric bilayers are organized around an aqueous inner compartment. At variance with micelles, they can't usually be obtained by self-assembling and are not thermodynamically stable. However, easy preparation procedures can be devised for liposomes and, due to their biocompatibility and versatile formulation, they have been extensively used as carriers for biomolecules (**Figure 1.3**).[30-32]

A remarkable advance for intra venous administration has been the production of stealth liposomes, which are able to resist blood stream clearance.[33,34] Stealth liposomes are usually formulated adding PEG (polyethylene-glycol) modified lipids to the other starting components or to preformed liposomes. It has been established that the $(CH_2\text{-}O\text{-})_n$ units of PEG, being substantially hydrophilic, are located at the liposome surface. In practice, PEG is able to exert steric hindrance toward opsonization and reticular endothelial recognition.[35,36]

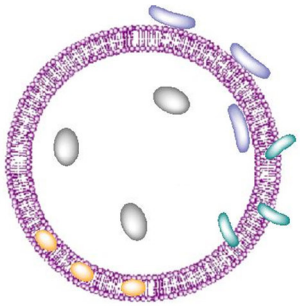

Figure 1.3: Possible loading modalities of drug into liposomes: hydrophobic and amphipatic compounds are taken up by the lipid bilayer, where they are embedded to varying extent; hydrophilic molecules are trapped inside the inner aqueous core.

Cationic liposomes are routinely used in nucleic acid delivery, thanks to the electrostatic complexation of positive charged lipids with the negative phosphate backbone of siRNAs. The balance between positive and negative (amine/phosphate) charge of the complex is a prominent factor for transfection efficacy. The overall positive surface charge loaded liposomes is also important for the interaction with cell membranes and for endosomal escape. It is known that cationic lipids may have toxic side effects. In order to decrease toxicity, the surface charge can be reduced by inserting ionizable cationic lipids in the bilayer. These lipids have a pKa of 7 or lower.[37]

Another improvement concerns the systematic use of cholesterol and of helper lipids (1,2-dioleoyl-sn-glycero-3-phosphoethanolamine, DOPE; 1,2-dioleoyl-sn-glycero-3-phosphocholine, DOPC; etc.), which stabilize the complex, mediate membrane fusion and facilitate the cargo release in the cytosol.[19,25]

Solid lipid nanoparticles (LNPs) have entered the practice of gene delivery more recently with respect to other lipid vectors, but their proven efficiency and easy preparation has made them very popular.[38-40] Additionally, solid lipid nanoparticles

possess good storage stability and can be steam-sterilized or lyophilized. These are important issues when experiments proceed from the laboratory to a pharmaceutical context.

Since about 2005 a number of sophisticatedly engineered particles have been proposed for RNAi therapeutics (SNALP, Stable Nucleic Acids Lipid Nanoparticle). They are positively charged and consist of lipid bilayers made with DLin-DMA (1,2-dilinoleyloxy-N,N-dimethyl-3-aminopropane), PEG-C-DMA (3-N-[ω-methoxypoly(ethylene glycol)$_{2000}$carbamoyl]- dimyristyloxy-propylamine), DSPC (1,2-distearoyl-*sn*-glycero-3-phosphocholine) and cholesterol tightly intertwined with genetic material.[41] Further development of SNALPs lead to formulation which include cationic alternatives to DLin-DMA for improving the dose-effect ratio in clinical siRNA delivery.

An example of well characterized SNALP is reported in **Figure 1.4**. In this work[42] a microfluidic mixing technology was used by Leung et al. to prepare lipid nanoparticles where siRNA is protected by binding to cationic lipids in a tightly arranged core. Zwitterionc lipids, some of which modified with PEG, and cholesterol are also part of this formulation. Their role is to provide a suitable interface which is at the same time biocompatible and not recognizable by the immunosystem. Detailed structural investigation was carried out by computing and spectroscopy techniques to establish the arrangement of different SNALP components. It is expected that a precise knowledge of structural details may be of valuable help for biomedical applications.

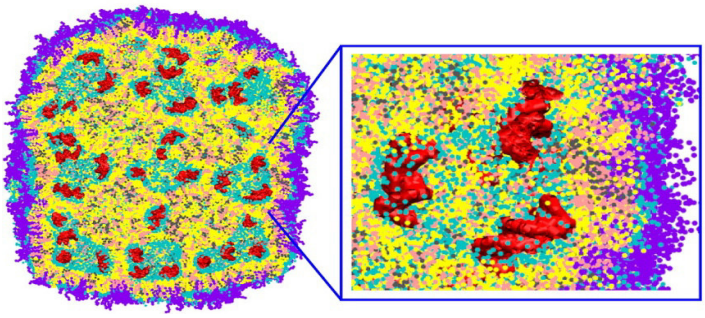

Figure 1.4. Cross-section and zoom-in views of LNP contains short nucleic acids (in red) bound to phospholipid bilayers (cationic lipid DLinKC2-DMA, 2,2-dilinoleyl-4-(2-dimethylaminoethyl)-[1,3]-di-oxolane in yellow, cholesterol in pink, DSPC in gray, PEG-lipid in violet). Lipid polar region is shown in cyan. The lipid composition was DLinKC2-DMA/DSPC/cholesterol/PEG-lipid (4:1:4:1; mol/mol) and DNA to lipid ratio ~0.05 wt/wt.

The complex arrangement of components in solid lipid nanoparticles hampers unambiguous classification of these vectors. For example, SNALPs may correspond to a variety of structures and formulations if they are obtained by different procedures. As a general remark, it can be observed that the scenario of lipid-based nanocarriers has dramatically evolved since the first non-viral tranfection agents were obtained from liposomes and nucleic acids. These complexes were named lipoplexes by Felgner[43] and their layered structure was clarified by Safinya and coworkers.[44] These Authors evidenced a subtle mechanism by which the small, highly hydrated polar head of

phosphatidyl ethanolamines can change its volume as a response to environmental stimuli. In practice, losing or binding water molecules allows to modify the local curvature of the vector, favoring cargo release during membrane fusion or endosomal escape.
For the sake of clarity we followed the nomenclature given by the Authors, joint to a brief description of each systems.
The most relevant physico-chemical properties of lipid vectors, size and surface charge, are routinely measured by benchtop dynamic light scattering and Zeta potential. Finer structural details require more sophisticated investigation by small angle scattering of neutron and x-rays, microscopy or spectroscopy (e.g. Magnetic Resonance, Florescence, Infra-red).
Thermodynamic techniques, such as isothermal titration calorimetry, give valuable information on the strength of the interactions leading to complex formation and preventing cargo release. This is a crucial factor which governs the complex stability in different conditions and determines cargo release.[45-47]

1.4 RNAi therapeutics

Many diseases are characterized by mutated genes, some of which are over-expressed or down-expressed, while others encode truncated or fusion proteins. RNAi could be exploited to knock-down over expressed or mutated genes in clinical therapy.
Synthetic carriers are mainly used for siRNA delivery, whereas engineered viruses are used to carry shRNA constructs. Alternatively, siRNA effectors may result in potent dose dependent gene silencing, but the overall effect is only transient. In a clinical setting this means that repeated treatments have to be administered, requiring large amounts of costly drugs. On the other hand, shRNA constructs have the potential of being incorporated in cell genome by viral vectors, which allows, in principle, a single treatment.[14] In clinical applications, viral carrier containing shRNAs are delivered *ex vivo* to the target cells, and then these modified cells are re-infused to patients. On the contrary, synthetic carriers are well suited for systemic delivery, due to high biocompatibility and safety. In the following sections we present a survey on clinical trials where lipid-based carriers have been used for siRNA delivery.[15, 16, 48, 49]

1.4.1 Genetic and systemic disorders

A dominant negative genetic disorder is an abnormal state in which a mutant allele prevails over its second normal copy. In this context RNAi can be used for selective inhibition of the mutant gene expression.
The usefulness of this strategy has been demonstrated for several genetic disorders, such as amyotrophic lateral sclerosis, Huntington's and Alzheimer's disease, slow channel congenital myasthenic syndrome, spinocerebellar ataxia type 3, and sickle cell anemia.[50,51] Although none of these studies have progressed into human trials yet, they

show the utility of RNAi technology as a new class of therapies for genetic disorders in preclinical models.

TransDerm (Santa Cruz, California, USA) is performing a clinical trial for the treatment of Pachyonychia Congenita. The pharmaceutical protocol is based on a local injection of naked siRNA against *keratine 6a* gene. To overcome pain and low toleration, TransDerm is currently developing an alternative delivery method that includes topical ointment with lipid-based carriers (GeneCreme).[52]

Tekmira Pharmaceuticals Corporation (Burnaby, British Columbia, Canada) has developed a number of SNALP formulations currently undergoing clinical trials. In particular, TKM-ApoB against hypercholesterolemia is based on PEG-C-DMA, DLin-DMA, DSPC and cholesterol in a 2/40/10/48 molar percent ratio. The size of the resulting vector is 77-83 nm and siRNA encapsulation efficiency is 92-97%.[53] To reduce hypercholesterolemia the chosen siRNA is designed to specifically silence the expression of Apolipotrotein B (Apo B) into liver. ApoB is the main component of low-density lipoproteins (LDL), carrying cholesterol and triglycerides through the blood stream to various tissues, where ApoB enhances the uptake of LDL particles into cells. A Phase I trial involved 23 subjects. In the two patients that received the highest dosage, ApoB protein and the correlated LDL concentration were temporarily reduced by about 20%. This trial was terminated because one subject developed flu symptoms suggesting immune system stimulation.

Another vector, classified as Lipidoid-nanoparticles (LNP), was developed by Alnylam (Cambridge, MA, USA) against hypercholesterolemia. It is made with $98N_{12}$-5 • 4HCl (**Figure 1.5**),[54] cholesterol and methoxypoly(ethylene glycol)- 1,2-dimyristoyl-sn-glycerol, $mPEG_{2000}$-DMG

(42/48/10 in ethanol). siRNA is incorporated into LNP at weight ratio siRNA/total lipids 1/7.5 (ALN-PCS). Particle diameter is about 50 nm, and siRNA entrapment is >95%.[55]

In this study siRNA targets PCSK9 (proprotein conventase subtilisin/kexin type 9), a serum protein regulating LDL metabolism. Knockdown of this protein is associated with increased LDL uptake by the liver. A Phase I trial involved 32 subjects with dose ranging from 0.015 to 0.400 mg/kg. Intravenous administration resulted in rapid, dose-dependent, and durable silencing of PCSK9 level in plasma (84%) and correlated reduction of Low Density Lipoprotein cholesterol, LDL-c (50%), in the highest dose group.[56]

Alnylam has also developed two different SNALPs for the amyloidosis disease, where the mutant transthyretin protein (TTR) causes deposit of amyloid fibrils in extracellular space of various tissues. In both SNALPs the siRNA sequence was the same and silenced TTR protein. In collaboration with Teckmira, Alnylam formulated a first generation SNALP (ALN-TTR01), based on DLinDMA, specifically designed to be taken up by liver hepatocytes. The phase 1 is now completed and ALN-TTR01 was well tolerated with 25-81% TTR suppression from a single 1 mg/kg dose with no serious toxicity or immune-response.[57]

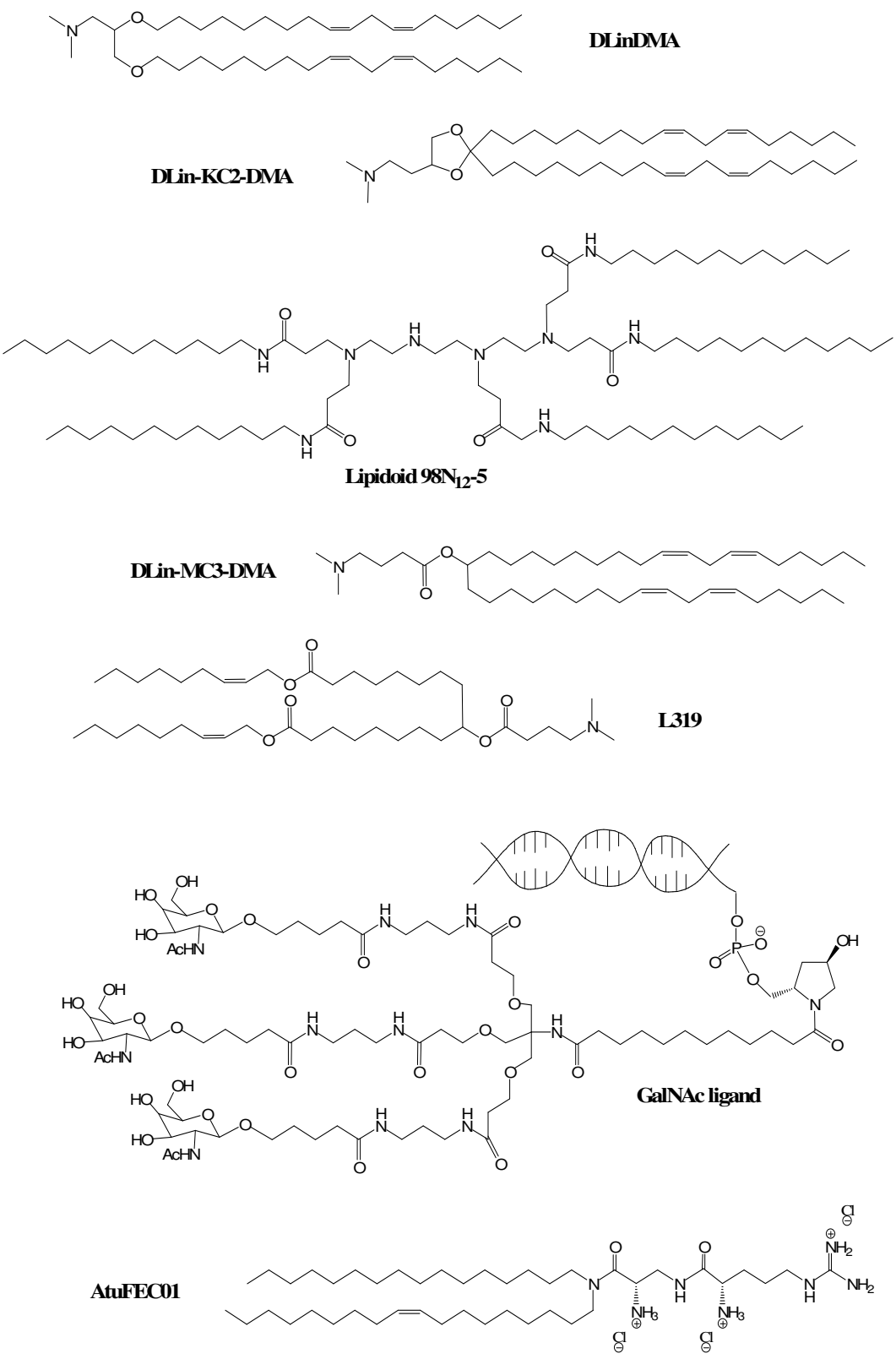

Figure 1.5: Chemical formulations of DLinDMA, DLin-KC2-DMA, Lipidoid 98 N_{12}-5, DLin-MC3-DMA, L-319, GalNac conjugate to siRNA and ATUFECT01.

The second SNALP is based on the newly synthesized lipid DLin-MC3-DMA, dilinoleylmethyl-4-dimethylaminobutyrate (**Figure 1.5**) (ALN-TTR02), developed by

Jayaraman et al.[58] This lipid was mixed with DSPC, cholesterol and PEG lipid in molar ratio 50/10/38.5/1.5. In phase 1 trial a reduction of 82% was found with the lowest dose (0.15 mg/kg), showing that the knockdown effect is enhanced by one order of magnitude with respect to ALN-TTR01. Phase II results show that multiple doses of ALN-TTR02 led to robust and statistically significant knockdown of serum TTR protein levels of up to 93%.[59]

Considering the good results obtained with DLIn-MC3-DMA, this second generation LNP technology is used to delivery PCSK9 siRNA (ALN-PCS02). With this new formulation in phase I a reduction of LDL-c of 50% with 0.25 mg/kg dose, instead of 0.4 mg/kg, was found.[60]

For the treatments of amyloidosis, Alnylam has developed another RNAi drug called ALN-TTRsc targeting transthyretin. ALN-TTRsc is characterized by siRNA conjugated to a triantennary N-acetylgalactosamine (GalNAc) a lipid like ligand which enables hepatocytes uptake by the asialoglycoprotein receptor. This compound was administered to non-human primates, resulting in a 80% reduction of TTR at doses as low as 2.5 mg/kg. Upon completion of the Phase I trial, concluded only in UK, Alnylam is planning to start a Phase II clinical study of ALN-TTRsc in patients by the end of 2013. Considering the effective dose, the solubility of GalNAc-siRNA Alnylam proposes a subcutaneous administration ALN-TTRsc in human study at volume of approximately 1mL.[61]

A novel class of third generation of LNPs, called rapid elimination lipid nanoparticles (reLNPs) was develop in order to enhance biodegradability and facilitate the elimination to deliver siRNA to the appropriate intracellular milieu. L319 (Di((Z)-non-2-en-1-yl) 9-((4-(dimethylamino)butanoyl)oxy)heptadecanedioate) in the biocleavable component of reLNP-siTTR which allowed to obtain10-fold improvement compare with second generation LNPs.[62]

1.4.2 Viral infections

There are numerous studies that underline efficacy of RNAi against hepatitis viral infection *in vitro*[63] and *in vivo*.[64] In animal models, the usual delivery method is hydrodynamic intravenous injection. However, this is not applicable in the treatment of human hepatitis.[65]

Herpes simplex virus infection is treated in a mice model by siRNA microbicide with distinct viral targets. Vaginal applications of lipid encapsulated siRNAs have been used to block the infection with no apparent toxicity.[66, 67]

Tekmira corporation has developed SNALPs (TKM-Ebola) against the Zaire species of Ebola virus (ZEBOV) that induce hemorrhagic fever with mortality rates as high as 90%. This SNALP is made with cholesterol, dipalmitoylphosphatidylcholine (DPPC), and DLinDMA and incorporates a combination of modified siRNAs targeting the ZEBOV L polymerase (EK-1 mod), viral protein 24 (VP24-1160 mod) and VP35 (VP35-855mod). The particle size is between 81-85nm. Pre-clinical studies were conducted on two groups of macaques: the first one (n=3) received four subsequent

administrations of TKM-Ebola at 2 mg/kg per dose (bolus intravenous infusion), while the second group (n=4) received seven doses, after ZEBOV infection. These post-exposure treatments protected two of three monkeys in the first group and all macaques in the second group from ZEBOV infection.[68] Considering the good results obtained in non-human primates, Tekmira started Phase I clinical trial in February 2012.[69]

1.4.3 Cancer

The most promising RNAi application is in cancer therapy, where it may offer precise genetic control and provide a viable alternative to conventional drugs. In fact despite enormous effort has made in biological research, cancer pathology remains one of the most common cause of death in the world.

The advent of the new "-omics" technologies open the possibility to individuate specific biomarkers allowing the creation of cancer molecular profile for each patient. Biomarkers include mutated and overexpressed genes, as well as genes encoding fusion proteins.[70] The corresponding mRNAs should be siRNA targets. Moreover, the possibility exist to design vectors carrying different siRNAs for a multi-target therapy with the advantage of reducing the capacity of cancer cells to develop resistance. Another possibility is silencing genes involved in the resistance to chemotherapic drugs, in order to restore their sensitivity.[71]

In latest years, cancer therapies provide new formulations of lipid based vectors for siRNA delivery as a valid alternative to conventional therapy. In addition to the classical characteristics of lipid vectors, it is possible to exploit the nanoparticle tendency to accumulate in cancer tissue rather than in healthy ones (Enanched Permeability and Retention effect).[72] In fact, after activating a neo-angiogenesis process, cancer cells produced blood vessels with abnormal form and architecture, which present wide fenestrations. This enhanced permeability leads to the transport of supply nutrients, oxygen and macromolecules larger than 40 kDa, allowing rapid tumor development. Thus vectors with size range of 50-200 nm have an easy access to cancer cells.

Current clinical trials with siRNA and lipid-based vectors for anti-cancer therapy are summarized in **Table 1.1**.

Sood and coworkers have shown that Ephrin type-A receptor 2, EphA2 is frequently expressed in ovarian and other solid cancers, but it is present at low levels in normal tissues. So, this protein is an attractive therapeutic marker.[73] The same group developed a neutral liposome for siRNA targeting EphA2.[74] The use of zwitterionic lipids, such as DOPC, allows efficient uptake of siRNA-complexes into the cell. DOPC was mixed with siRNA at weight ratio 1/10 siRNA/DOPC in terbuthanol. The tween-20 surfactant was added in weight ratio 1/19 tween-20/ siRNA complex. This complex was administered to an orthotopic mouse model of ovarian cancer. After three weeks of treatment, tumor growth was reduced. In particular, the effect was dramatically increased in combination with paclitax.

Atugen (Silence therapeutic subsidiary; AG, Berlin, Germany) has developed AtuPLEX, a siRNA-lipoplex, for the treatment of solid tumors. These liposomes are made with the novel cationic lipid AtuFECT01(β-L-arginyl-2,3-L-diaminopropionic acid-N-palmityl-N-oleyl-amide trihydrochloride), the helper lipid DPhyPE (1,2-diphytanoyl-*sn*-glycero-3-phosphoethanolamine) and the PEG_{2000}-DSPE (1,2-distearoyl-sn-glycero-3-phosphoethanolamine-N-[amino(polyethylene glycol)-2000]) in molar ratio of 50/49/1.[75] Liposome dispersions were mixed with siRNA to obtain lipoplexes at the +/- 4/1, size of ~118 nm and Zeta potential of +46 mV. In mouse model this formulation induced down-regulation of endothelia specifically expressed genes (such as CD31 and Tie2), demonstrating the applicability of this system *in vivo*.[76] The same lipid-based vector with a siRNA targeting protein kinase 3 (PKN3) named Atu027 is currently used in a Phase I clinical trial for the treatment of advanced solid tumor. Silencing PKN3 results in the inhibition of tumor angiogenesis.

Tekmira proposed a first generation SNALP TKM-PLK1 targeting polo-like kinase 1, a protein involved in tumor cell proliferation, also validated as an oncology target. LNP is composed by DLinDMA, cholesterol, DSPC and PEG-c-DMA with lipid/siRNA mass ratio 9/1.[77] Preclinical studies showed that TKM-PLK1 selectively killed cancer cells while spearing adjacent healthy tissues. TKM-PLK1 started a Phase I clinical trial in December 2010 which is now completed. This trial involved 52 subjects with advanced solid tumors. The dose range tested in this trial was 0.15-0.90 mg/kg, with a total of 105 doses administered.

Alnylam has developed a first-generation lipid nanoparticle or SNALP (ALN-VSP) to deliver two different siRNAs targeting critical genes for the proliferation and development of cancer cells: the vascular endothelial growth factor (VEGF) and kinesin spindle protein (KSP). ALN-VSP has a diameter of 80-100 nm and is essentially non-charged with a Zeta Potential of 6 mV at pH 7.4.[78] In Phase I trial the ALN-VSP was administered through intravenous injection in 41 patients with advanced solid tumors involving liver. Results demonstrate that ALN-VSP induces tumor regression (after two months of treatment) 42% of patients treated at doses of 0.4 mg/kg. ALN-VSP are well tolerated with no clinically significant changes in liver function. The same patients showed low grade of fatigue (24%), nausea (17%) and fever (17%).

Koldehoff et al. have developed anionic liposomes for siRNA delivery by targeting the fusion oncogene bcr-abl.[79] This gene results from mutual traslocation of chromosome 22 and 9, producing the so called Philadelphia chromosome, which is characteristic of chronic myeloid leukemia (CML). bcr-abl siRNA was diluted 1:10 in 10% anionic lipid solution (100 g soya been oil, 25 g glycerol, 6 g egg phospholipid per liter) forming siRNA chylomicrons in lipid solution (siRNA-DLS).[80] Anionic liposomes have less cytotoxicity compared to cationic liposomes and in this case they were able to preserve siRNA integrity in biological media. The siRNA-DLS complex was intravenously injected and subcutaneously into CML nodes of one female Imatinib resistant CML patient (clinical study sponsored by Duisburg-Essen University, Germany). This treatment didn't show severe side effects, although the knockdown of bcr-abl was not maintained 22 days after injection. Additional injection of siRNA-DLS indicated a growing resistance to siRNA therapeutics.

Table 1.1. Recent clinical trials for cancer diseases based on siRNA delivery (till 2013) from the web site www.clinicaltrials.gov

Drug	Intriduction in the body - Delivery	Vehicle	Disease	Target gene	Phase	Stage	Clinical/Trials: gov Identifier	Company
siRNA-Epha2-DOPC	Intravenous injection	DOPC liposome	advanced solid tumor	Epha2	1	Not yet recruiting	NCT01591356	MD Anderson Cancer Center
Atu027	Intravenous injection	AtuPLEX®	Advanced solid tumor	PKN3 (protein Kinase C)	1	Completed	NCT00938574	Silence therapeutic
TKM-080301	Hepatic arterial injection (HAI)	SNALP	Colorectal, Pancreas, Gastric, Breast, Ovarian and Esophageal cancer with hepatic metastasis or primary liver cancers	PLK1 (Polo-like-kinase 1)	1	Completed	NCT01437007	Tekmira Pharmacueticals Corporation
ALN-VSP02	Intravenous injection	SNALP	Solid tumors	KSP (Kinesin Spindle Protein) and VEGF	1	Completed	NCT00882180	Alnylam Pharmaceutical
Bcr-abl siRNA	intravenous injection	Anionic liposome	Chronic Myeloid Leukemia (imatinib resistance)	bcl-abl	1	Completed	N/A	University of Duisburg
pbi-shRNA™STMN1 LP/ pbi-shRNA™PDX LP	Intratumoral injection	Bilamellar invaginated vesicle	Advanced and/or Metastatic Cancer	Stathmin-1 (STMN-1)	1	Recruiting	NCT01505153	Gradilis, Inc.

Gradalis® is currently conducting two different clinical trials involving cationic liposomes encapsulating shRNA constructs. pb-shRNA™ STMN1-LP contains shRNA able to knockdown Stathmin 1, a protein critically involved in microtubule assembling and metastatic phenotype.[81]
pb-shRNA™ PDX-1 LP has been shown to silence pancreatic and duodenal homeobox factor1 (PDX-1), overexpressed in many types of solid tumors. shRNA constructs were encapsulated in two bilamellar invaginated vesicle lipoplexes (BIV-L). Extruded DOTAP (N-[1-(2,3-Dioleoyloxy)propyl]-N,N,N-trimethylammonium methyl-sulfate), cholesterol liposomes (BIVs) interact with nucleic acids which attract a second BIV to this complex. Expanding electrostatic interactions with shRNA constructs cause inversion of the larger BIV and total encapsulation of the nucleic acids in a sandwich between lipid bilayers.[82]

Chapter 2

2.1 Divalent cationic surfactant: structural description and general properties

Gemini are dimeric surfactants, made up by two amphiphilic moieties, covalently connected at the level of the head groups by a spacer (**Figure 2.1**)

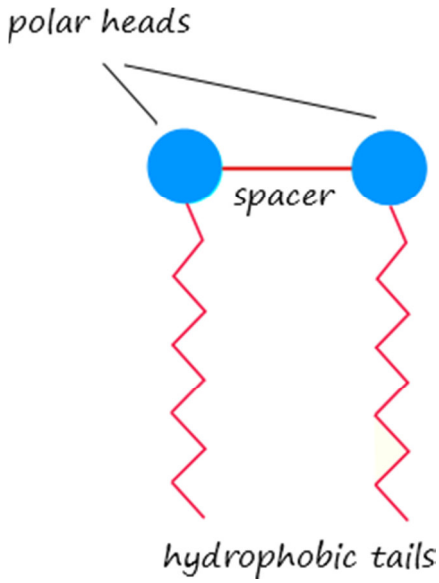

Figure 2.1: Scheme of dimeric surfactant .

In aqueous media, above a specific concentration (critical micelle concentration, cmc) dimeric surfactant self-assembly into micelles where non polar portions are located in the interior while polar heads are exposed to water.

The current interest in such surfactants arises from three essential properties. Dimeric surfactants are characterized by cmc that are one or two orders of magnitude lower than for the corresponding conventional monomeric surfactant. For example the cmc of the Gemini surfactant 12-2-12 (dymethylene-1,2-bis (dodecyldimethylammonium bromide)) is about 0.055 mol/L, whereas that of the corresponding monomeric surfactant DTAB (dodecyltrimethylammonium bromide) is 0.5 mol/L.

Dimeric surfactants are much more efficient than the corresponding monomeric surfactants at decreasing the surface tension of water. This efficiency is often characterized as the surfactant concentration (C_{20}) required for lowering the surface

tension of water by 0.02 N/m. The values of C_{20} for D2 and DTAB are 0.0083 and 0.21wt%, respectively.

Aqueous solutions of dimeric surfactants with short spacers can have very high viscosities at relatively low concentrations whereas solutions of the corresponding monomeric surfactants have low viscosities. For instance the viscosity of aqueous solutions of DTAB is larger than that of pure water up to a surfactant concentration of the least 10 wt% whereas 5 wt% solution of 12-12-12.

The different behavior of dimeric surfactant, in comparison with conventional surfactant, depends on the distribution of distances between head groups in micelles of these two type of surfactants. In dimeric surfactant this distribution depend not only on the distance between polar heads of different molecules but also on the length of the spacer. The length is determined by the bond extension and bond angle of the atoms present in the spacer group. The effect of the chemical link between the head group on the packing of surfactant alkyl chains in the micelle core are expected to affect strongly the curvature of surfactant layers and thus the micelle shape and the properties of the solution. [83, 84]

Dimeric surfactants have been also reported to have better solubilizing, wetting, foaming and lime-soap-dispersing properties than conventional surfactants.

It is possible to synthetize dimeric surfactants by using two of any type of the presently known amphiphiles, identical or different connected between a spacer of varied chemical nature, hydrophilic or hydrophobic, rigid or flexible. The enormous variety of surfactant structures that could be synthetized, leads to numerous micellar shapes with diverse physic-chemical properties, making these molecules versatile for different use.

Nowadays cationic dimeric surfactants are also studied, in order to use them in the rational design of vector for RNAi therapeutics. As previously discussed in Chapter 1 naked siRNA are not able to cross plasma membrane and it is necessary to develop new vector that can bind and deliver these molecules until the target. Since viral vectors are not safe and produce immunogenicity, the development of non-viral vectors has become urgent. In this field the use of dimeric cationic surfactants could enhance siRNA delivery not only for their capability to interact with the negative backbone of siRNA, but also for their ability to self assembly in water unlike conventional phospholipid which need energy input (by sonication or extrusion) to form liposomes.

2.2 SH14 and Gemini properties

In our work we focuse on the studies of three Gemini with general formula:

$C_{12}H_{25}$-$N^+(CH_3)_2$-C_nH_{2n}-$N^+(CH_3)_2$-$C_{12}H_{25}$, $2Br^-$

where n = 3, 6, 12 (henceforth called 12-n-12) (**Figure 2.2**):

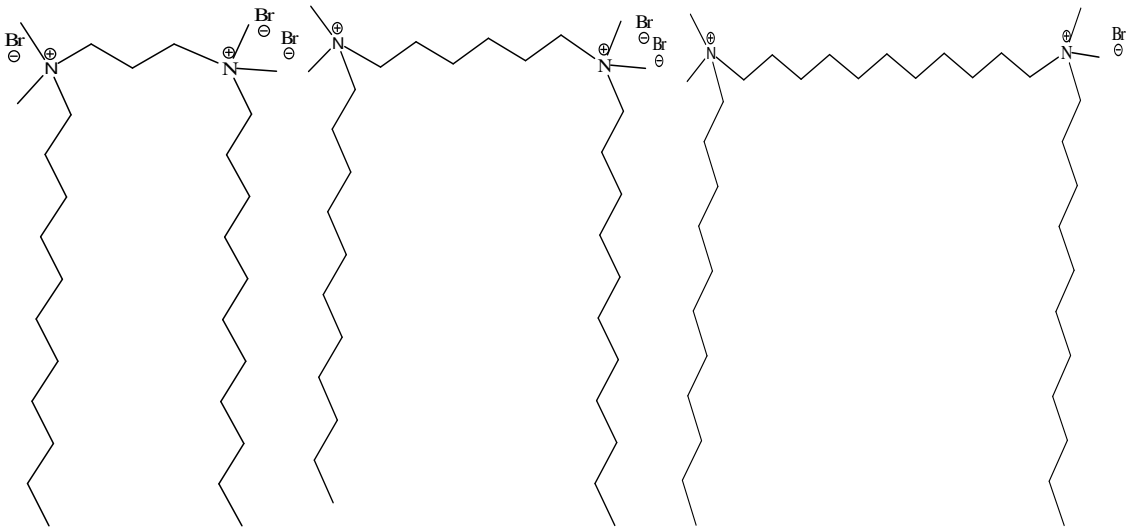

12-3-12 **12-6-12** **12-12-12**

Figure 2.2: shows the chemical structure of 12-3-12, 12-6-12 and 12-12-12

or a triazine-based surfactant (**Figure 2.3**):

$HS\text{-}C_2H_4\text{-}(N_3C_3)^{2+}\text{-}NH\text{-}C_3H_6NH_2,\ 2CF_3COO^-$

$NH\text{-}C_{14}H_{29}$

henceforth called SH14.

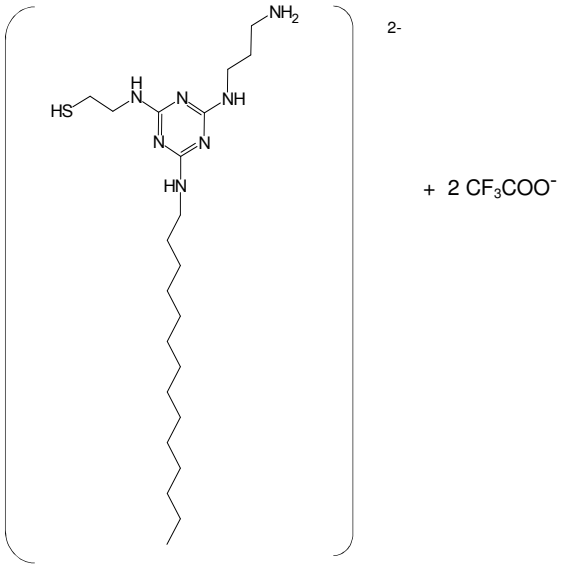

Figure 2.3: shows the chemical structure of SH14.

The three Geminis are characterized by two amphiphilic molecules, each consisting of a quaternary ammonic group and a hydrophobic chain of 12 carbons. The polar heads are

connected with a spacer group consisting of an alkyl chain of three different length $(-CH_2)_3$, D3, $(-CH_2)_6$, D6 and $(-CH_2)_{12}$, D12.
SH14 are characterized by an alkyl chain of 14C and a triazine ring with two positive charges. These molecules are characterized by a –SH group that makes possible an S-S bond between two molecules.
Gemini surfactants were synthetized at the Montpellier University by Dr. Martin In, while SH14 was synthetized at Politecnico of Milan in collaboration with the Dr. Gabriele Candiani. The synthesis of the four surfactants used in this work is reported elsewhere. [85, 86]
Powders of these surfactants are stored at room temperature and solubilized in water MilliQ RNAasi free.
Of these two surfactant classes, Geminis are the most studied.[87-90]They have been extensively investigated in research topics of therapeutic interest, such as drug delivery and gene therapy, usually in conjunction with phospholipids to form liposomes or lipid nanoparticles. In particular, both plasmids and siRNA have been successfully complexed with Gemini surfactants. The fusion process of gemini-based liposomes with model cell membranes has also been followed and elucidated by Differential Scanning Calorimetry (DSC) and fluorescence spectroscopy.[91]
Although SH14 is less studied, it appears to be a promising transfection reagent. SH14 molecules are able to dimerize forming -SS- bound upon DNA and form lipoplex, capable of realizing nucleic acids in the intracellular mielieu.[92] Alike for Gemini surfactants, SH14-based formulations have been shown to be highly effective for transfection purposes, which open the possibility to use these systems in clinical protocols.

2.3 Physico-chemical characterization of micelles

Molecular weight (g/mol) and cmc (M) values of these four surfactants are shown in **Table 2.2.**

Surfactant	Molecular Weight, g/mol	cmc, M
D3	624.37	$9.6\ 10^{-4}$
D6	666.42	10^{-3}
D12	750.52	$3.7\ 10^{-4}$
SH14	666	$1.46\ 10^{-3}$

Table 2.2: Molecular weight and cmc values determined by conductivity experiments of the four surfactants.

12-n-12 micelles are characterized also by SAXS measurements, on the ID02 beam line at the ESRF European Sinchrotron Radiation Facility, Grenoble, France. The wavelength of the incident photons was λ= 1Å and sample-detector distance was 1m, allowing for scattering wavevectors in the range 8 10^{-3} < q($Å^{-1}$) < 0.7, where q is the defined as $q = \frac{4\pi}{\lambda}\sin\theta$, θ being the scattering angle.

The measurements were performed using a two-dimensional multiwire proportional gas counter and samples are studied at room temperature in a quartz capillary.

Gemini surfactant aggregates are analyzed in function of the concentrations and linker length. Samples studied are prepared at concentrations ranging from 6 10^{-4}M to 6 10^{-2}M.

SAXS curves of micelles were analyzed by a software called GENFIT designed by Dr. Francesco Spinozzi at the University of Ancona. The best fit $I(Q)$ is written as a linear combination of *M* models chosen by the user from a wide list, $I(Q) = \sum_{m=1}^{M_c} w_m I_m\,(Q)$. The parameters of the models (such as thicknesses, scattering length densities, etc.) and the weight parameters w_m are found by minimizing the functional $\chi^2 = \left(1/N_q\right)\sum_{i=1}^{N_q} \sigma^{-2}(q_i)\,[I_{exp}\,(q_i\,) - I(q_i)]^2$, where N_q is the number of q recorded points and $\sigma(q_i)$ is the experimental standard deviation of the i-th point.

At concentrations slightly below the cmc, a weak but detectable excess scattering intensity was observed, indicating that premicellar aggregation may take place. These SAXS diagrams could not be fitted with a specific model due to low intensity and no shape features. Submicellar anomalous behavior of Gemini surfactants was also reported for surface tension and conductivity, which was explained by either premicellar aggregation or by different binding modalities between divalent surfactants and one or two counterions.

At concentration higher than the globular micelles (spherical or cylindrical) were found up to ~10^{-3}M, while above this value a shape transition took place, inducing the formation of thread like or lamellar structures.

Chapter 3

3.1 Complexation of siRNA and cationic micelles

When combined with siRNA, non-viral vectors give complexes whose structural features are from nano- to micro-scale range.[93-96] These complexes show a tendency to time evolution and are often unstable over long periods. It appears therefore that transfection agents are multifaceted systems and in depth investigation requires powerful techniques, along with more standard characterization, which provide basic physico-chemical information (e.g. overall size and surface charge). Large scale facilities offer the opportunity to perform high resolution Small Angle Scattering of neutrons and X-rays (SANS and SAXS, respectively),[97,98] that can be used to obtain insights of nanosystems, such as their internal composition.[99] In some instances, the interactions at play in the control of the system stability have also been inferred.[100] Considering that the state of the complex used for transfection strongly depends on the kinetic pathway followed during formation, time resolved experiments can give information on the mechanisms that determine the resulting structure and size. Actually, the final state of the mixture corresponds to liquid-liquid phase separation where the concentrate phase of complexes coexists with a dilute phase of released counterions. Nucleic acid-lipid complexes have been often studied after full phase separation (i.e. by analyzing the pellet),[101-103] or at the stage of their formation to point out the self-structuring of components. They are rarely studied in the early stage of formation, when they are still dispersed at the macroscopic scales. Following a previous structural study by Dynamic Light Scattering (DLS), Zeta Potential and SANS.[104]

3.2 Time resolved SAXS to study the complexation of siRNA by cationic micelles of divalent surfactants

3.2.1 Materials

We analyzed the kinetics of formation and the structural evolution of complexes obtained from a siRNA interacting with micelles of cationic divalent surfactants.
Micelles are formed by four type of cationic surfactant 12-3-12, 12-6-12, 12-12-12 and SH14 (see **Figure 2.2** and **2.3**).

The siRNA chosen for this study has the following nucleotide sequence:

sense: 5' GAUAAAGGAGCGAACCCACUU 3'
antisense: 3' UUCUAUUUCCUCGCUUGGGUG 5'

This siRNA is able to downregulate the expression of hERG1 potassium channel, which is involved in the pathogenesis of severe human diseases such as glioblastoma multiforme, leukemia, gastric and colon cancer.[105]
siRNA powder are storage at -20°C and solubilized in water Milli Q RNAasi free.

3.2.2 Methods

SAXS experiments are used to investigate the structure of the materials: solids, liquids or gels. X-rays photons interact with electrons and allow to obtain information from the distribution of electron density in the heterogeneous matter. The technique provide that a monochromatic beam of incident wave vector $\overrightarrow{k_i}$ is selected and falls on the sample. The ray interacts with the electrons and is scattered. The intensity of the scattering is collected by a detector in function of the scattering angle 2θ. Since elastic interactions do not provided energy transfer, the modulus of the final wave vector $\overrightarrow{k_f}$ is the same of the incident $\overrightarrow{k_i}$, so $|\overrightarrow{k_f}| = |\overrightarrow{k_i}| = \frac{2\pi}{\lambda}$. The relevant parameter to analyze the interaction is the scattering vector $\vec{q} = \overrightarrow{k_i} - \overrightarrow{k_f}$. The intensity of the scattering is $q = \frac{4\pi}{\lambda}\sin\theta$ and the standard unit of q is $Å^{-1}$. (**Figure 3.1**)

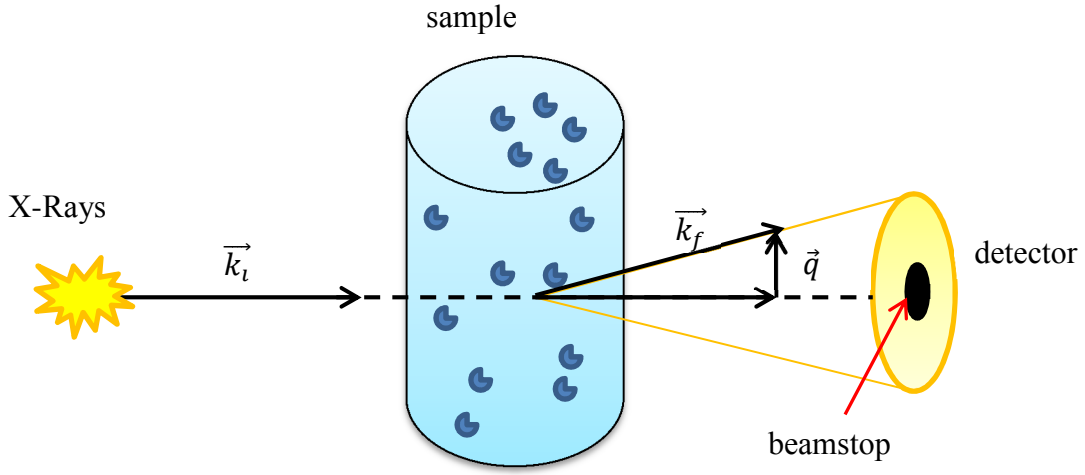

Figure 3.1: X-rays scattering scheme.

The scattered intensity I(q) is the Fourier Transform of g(r), the correlation function of the electronic density r(r), which corresponds to the probability to find a scatterer at position r in the sample if another scatterer is located at position 0: elastic x-ray scattering experiments reveal the spatial correlations in the sample. Small angle

scattering experiments are designed to measure I(q) at very small scattering vectors $q \approx \frac{4\pi}{\lambda}\theta$, with 2θ ranging from few micro-radians to a tenth of a radian, in order to investigate systems with characteristic sizes ranging from crystallographic distances (few Å) to colloidal sizes (up to few microns).
For a suspension of uniform particles, the normalized scattered intensity after substraction of solvent background is given by: [106]

$$I(q) = NV^2\,\Delta\rho^2\,P(q)\,S(q)$$

where N is the number of density of scattering particles, V is their volume, Δρ is the scattering contrast, $P(q)$ is the form factor describing the shape of the particles and $S(q)$ is the structure factor of interactions.
A typical small angle scattering intensity profile is shown on **Figure 3.2** where the intensity is plotted versus q in the range q_{min}-q_{max} defined by the experimental set-up and usually fixed by geometric limitations.

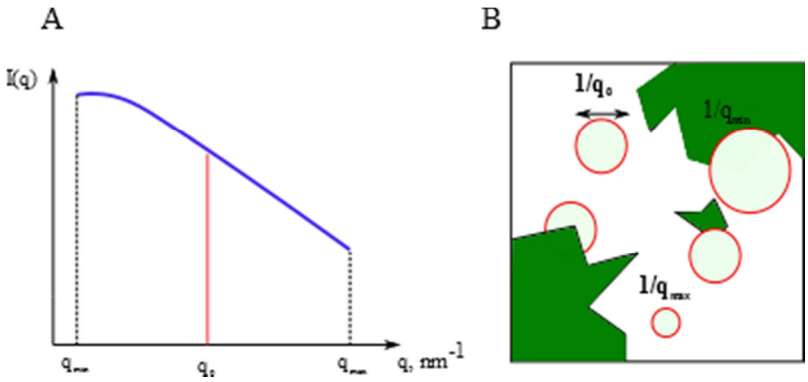

Figure 3.2: Panel A shows the feature of a typical X-ray scattering profile, panel B indicate the size of the windows in faction of q.

A measurement made at a given q_0 allows to investigate the density fluctuations in the sample on a distance scale $D = \frac{2\pi}{q_0}$. It is equivalent to observe the system through a circular window in real space of a diameter $\frac{2\pi}{q_0}$. The smallest observation window, given by $D_{max} = \frac{2\pi}{q_{min}}$ allow to determine structural characteristic of biggest objects present in solution while a largest window allow to obtain information about smallest particle.
The q range of small angle experiments is usually divided into three main domains:

- **At high q domain** the window is very small: there is a contrast only at the interface between the two media
- **At intermediary zone** is the order of the "elementary bricks" in the systems. At this level the form factor P(Q) can be measured.
- **At low q domain** the window is large and the structure factor can be obtained.[107]

Time resolved Small Angle X-ray Scattering was carried out at the high brilliance ID02 beamline of the European Synchrotron Radiation Facility (Grenoble, France). (**Figure 3.3**)

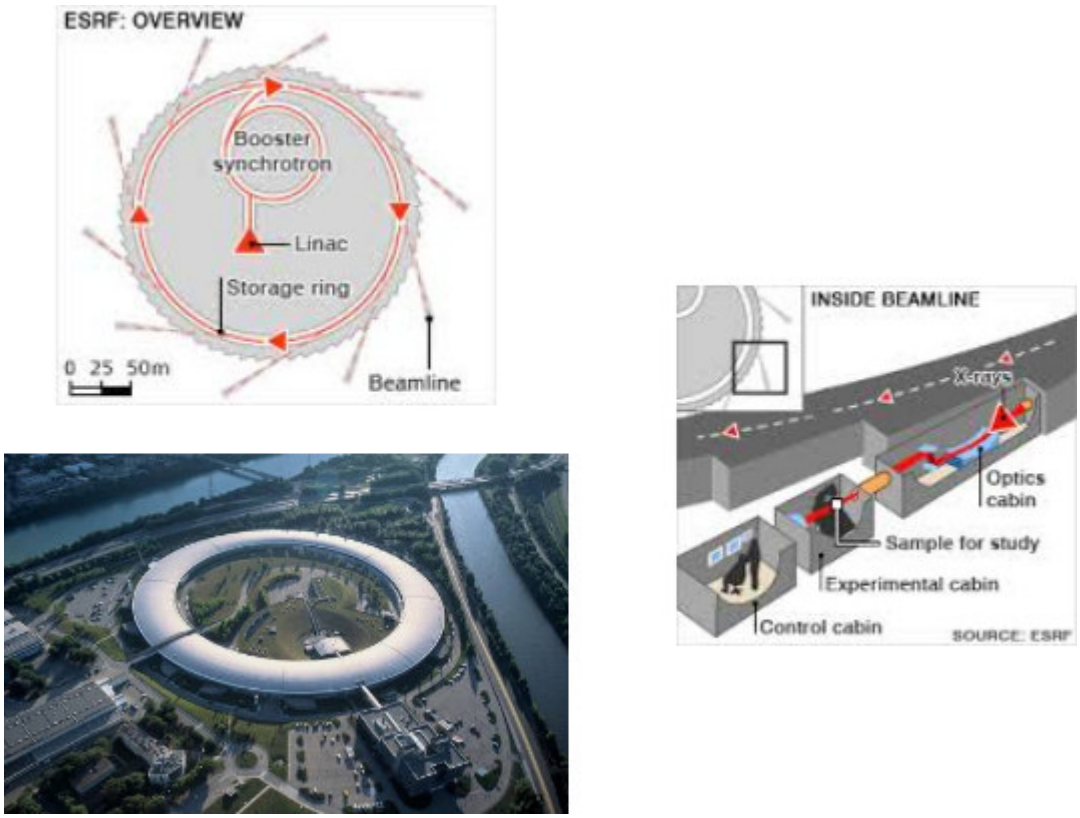

Figure 3.3. European Synchrotron Radiation Facility (Grenoble, France)

The sample to detector distance was 1.5 m, corresponding to a q (magnitude of the scattering vector) range 0.080-3.8 nm^{-1}. q is defined as $q = \frac{4\pi}{\lambda} sin\theta$ where θ is an half of the scattering angle and λ, the X-ray wavelength (λ= 0.1 nm).

siRNA/micelles complexes were prepared by mixing equal volumes (100 µL) of MilliQ grade water solutions of cationic surfactant (either 2.5 10^{-3} M or 1.25 10^{-3} M) and siRNA at the appropriate concentration to obtain the desired charge ratio: $CR = \frac{[-]}{[+]}$. From previous Zeta Potential experiments,[104] we know that at CR < 1, these complexes are positively charged, whereas at CR > 1 they are negatively charged.

In kinetic experiments the starting surfactant and siRNA solutions were mixed by a stopped-flow device (SFM-400) **Figure 3.4** from Bio-Logic (Claix, France), consisting of four motorized syringes interconnected through three mixers. The exit of the last mixer is coupled to the scattering cell, a quartz capillary with 2 mm diameter. The flow is stopped by a hard-stop placed at the end of the flow line and it is activated at the end of the mixing sequence. The dead time was primarily determined by the time to transfer

the mixture from the last mixer to the beam crossing point on the capillary cell, as described elsewhere.

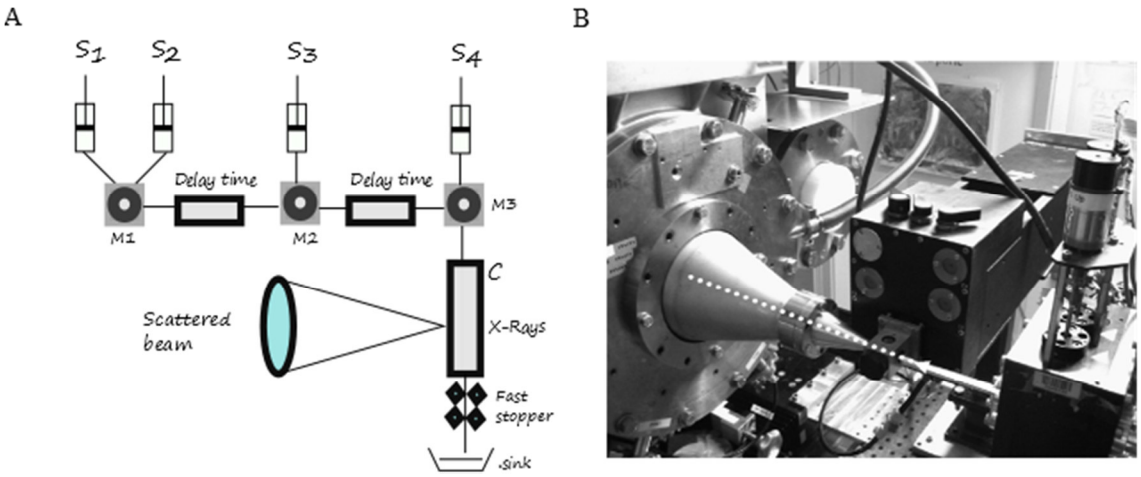

Figure 3.4: Panel A shows SFM-400 stopped-flow device. S stend for syringe (each controlled by stepper motors), M for mixers and C is the svattering cell (quartz capillary). Panel B shows stopped-flow set-up installed at the SAXS instrument with optimased cone for SAXS. White arrows indicates the X-ray beam direction.

In the present experiments all systems contained a fixed amount of surfactant, which after mixing was 1.25 10^{-3} M or 6.25 10^{-4} M, for two different sets of samples. Notably, both these concentrations are higher than the critical micelle concentration cmc [103] (see **Table 2.2**). Measurements on complexes were performed at 5 mL/s flow rate with acquisition time of 10 ms. The data acquisition cycle was triggered at the beginning of the fast mixing phase and the hard-stop was activated at the end of this phase. Each cycle consisted of a total of 80 or 60 frames, collected in three different time groups: first group each 0.15 s, second group each 2-3 s and third group each 40-60 s.

The 2-dimensional scattering patterns were normalized to an absolute intensity scale after applying the detector corrections for spatial homogeneity and linearity. Normalized SAXS patterns were azimuthally averaged to obtain the 1-dimensional scattering profiles ($I(q)$ vs q). Both sample and background (water) measurements were recorded at the same spot of the stopped-flow capillary cell to ensure an accurate subtraction of the background. On the whole, more than 5000 diagrams were recorded and analysed, since each measurement was repeated at least twice, to assure reproducibility of behaviour. This is a critical issue when describing systems like those reported in this paper, which are basically out of equilibrium.

Static experiments on micelles were also performed in a flow-through capillary of 2 mm diameter at a sample to detector distance of 0.8 m (0.1 $nm^{-1} < q < 8$ nm^{-1}). In this case the acquisition time was 100 or 200 ms.

3.3 Results and discussion

SAXS diagrams of siRNA complexed with 12-6-12 at two molar ratios, i.e. CR = 0.75 and CR = 1.25 are shown in **Figure 3.5**. The reference curves of pure siRNA and 12-6-12 are also reported in this figure for comparison. The charge ratios were chosen in order that most of the components were in the complexed form, which means close to CR=1. This simplifies the SAXS patterns as it minimize free micelles and free RNA and allows higher time resolution since most of the signal is given by the complex. Charge ratio close to neutrality might facilitate phase separation, especially when the complexing agent is a polymer or a liposome or when the nucleic acid is a high mass fragment. In general, the kinetics of phase separation depends on the size of the nucleic acid and on the concentration of starting components. Here we took advantage of the siRNA's small size and we adjusted the concentration so that the systems were stable over the whole measuring time and longer (more than 30 minutes).

In the micelle curve, the broad maximum at 2 nm^{-1} results from the shell-like structure of the counterions cloud around the hydrocarbon core, reflecting the diameter (3.14 nm) of 12-6-12 micelles.[108] Immediately after mixing, a marked increase of the intensity at low q, pointed out the formation of larger scattering objects in solution and the appearance of a quasi-Bragg peak at higher q indicated core structuring within the newly formed aggregates. Specifically, for this siRNA/12-6-12 system the peak maximum (q_{max}) was located at 1.72±0.005 nm^{-1} and 1.70±0.005 nm^{-1} for CR = 0.75 and 1.25, respectively that is slightly shifted in comparison with the maximum of the micelle curve. This suggested that siRNA is intercalated in between micelles. The q_{max} values of siRNA/12-6-12 complexes correspond to repeat distances $d = \frac{2\pi}{q}$ of 3.65±0.005 nm and 3.69±0.005 nm.

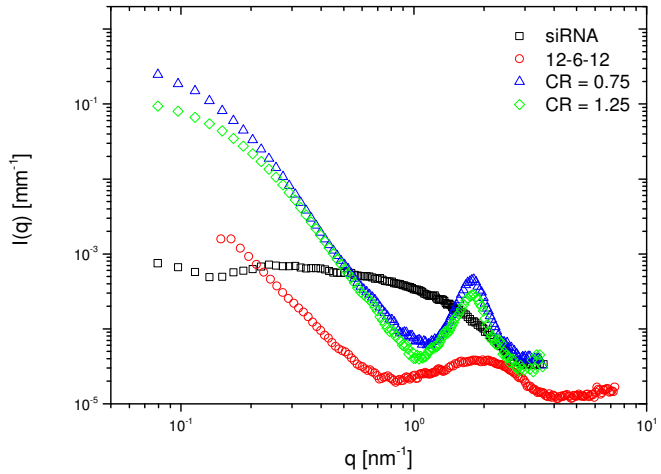

Figure 3.5: SAXS intensity diagrams of 12-6-12 micelles, siRNA and complexes at two charge ratios (CR = 0.75 and CR = 1.25) recorded after 50 ms from mixing. In the complex solution the total surfactant concentration ($1.25x10^{-3}$ M) is 1.5 times the CMC of 12-6-12. In the reference systems siRNA is $4.5x10^{-5}$ M and 12-6-12 is $1.25x10^{-3}$M.

The intensity scattered by complexes in the large q region exceeded the micelles' level by ~ 3-5x10^{-5} mm^{-1}, in agreement with the expected contribution of Br^- counterions which are transferred from the micelle surface to the bulk solvent upon complex formation. In fact, the incremental background due to ions with n electrons at molar concentration c is given by:[109]

$$I_{Br}(q)=c\ N_a f_e^2\ n^2$$

where N_a is the Avogadro number, f_e is the Thomson scattering length (2.82x10^{-13} cm), and c is the concentration of ions per unit volume released from Gemini micelles (c=1.25x10^{-3} M α).

By taking α=0.52 as the dissociation degree of 12-6-12 micelles[104] and $n = 36$, the value of 4.0x10^{-5} mm^{-1} was obtained.

Counterion release is a relevant step in the complexation of nucleic acids by positively charged nano-aggregates and, it is considered the driving force for the spontaneous nature of this process.[110-112] This behavior was observed for the three Gemini surfactants and also for SH14.

The intensity diagrams of the siRNA/SH14 systems are reported in **Figure 3.5**. These curves have a similar shape to those reported in **Figure 3.6**, indicating that complexation occurs through a similar pathway with respect to Gemini surfactants. In the SH14 case the counterions released are CF_3COO^-, which also give high SAXS contrast, due to the presence of fluorine atoms.

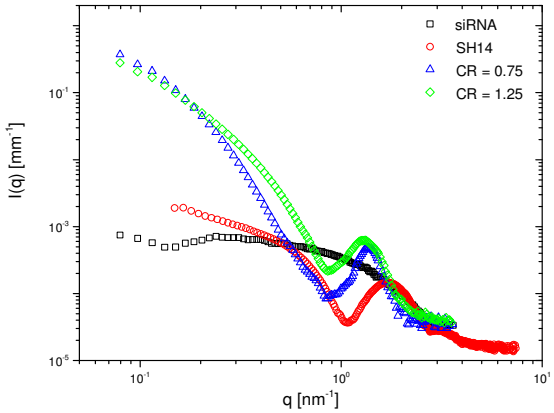

Figure 3.6: SAXS intensity diagrams of SH14 micelles, siRNA and complexes at two charge ratios (CR = 0.75 and CR = 1.25) recorded after 50 ms from mixing. The peak maxima were located at 1.38 nm^{-1} and 1.35 nm^{-1}, corresponding to repeat distances of 4.65 nm and 4.58 nm for CR = 0.75 and CR = 1.25, respectively. In the complex solution the total surfactant concentration (1.25x10^{-3} M) is approximately 3 times the CMC of SH14. In the reference systems siRNA is 4.5x10^{-5} M and SH14 is 1.25x10^{-3} M.

Selected SAXS diagrams recorded for the siRNA/12-6-12 complex (CR = 0.75 and surfactant concentration 1.25x10^{-3} M) are reported in **Figure 3.6**, as an example of time evolution. Two features common to all the investigated systems were the progressive increase of the intensity at very low q and of the quasi-

Bragg peak height, until a plateau was reached. This behavior indicated the size increase of scattering objects in solution and their progressive internal ordering, as discussed below.
The evolution of the peak position was studied during 10-15 minutes from the instant of mixing. This is a typical time interval required to prepare complexes before use and for this reason it was chosen in our experiments.

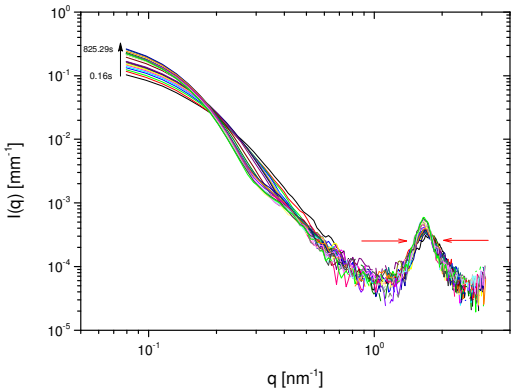

Figure 3.6: Representative SAXS intensity diagrams of the siRNA/12-6-12 complex at CR = 0.75 and surfactant concentration 1.25x10^{-3} M. in the time range 0.16-825 s after the mixing. The arrows indicate the increase of the very low q intensity and of the Bragg peak height at increasing time.

The q_{max} trend for complexes prepared at CR = 0.75 and CR = 1.25 with different surfactants is reported in **Figure 3.7**. In all systems investigated the process of complex formation, revealed by the onset of measurable periodicity, took place in less than 50 ms. This time scale agree with the one measured by stopped-flow circular dicroism in systems containing dimethyldioctadecyl ammonium bromide (DDBA), dendrimers, or 1,2-dioleoyl-3-trimetthyammonium-propane (DOTAP) unilamellar liposomes and 4.9 kbp DNA plasmid.[113] 50 ms or shorter is thus a time lapse during which cationic molecules or aggregates bind to nucleic acids, independently of their length and of their being DNA or RNA. The present study will thus access the stage of growth and reorganization of the complexes rather than their formation.
The trend followed by the peak position q_{max} depended on surfactants, as shown in **Figure 3.7**. In fact q_{max} values got constant after 5 s for 12-12-12, decreased slowly for 12-6-12 and 12-3-12 and increased slowly for SH14. However, all systems reached a plateau in 50-80 s, indicating that after this time lapse the composition of the repeat units did not change.
The repeat distance depended on the surfactant involved in complexation and was in the order:

SH14 > 12-3-12 > 12-6-12 > 12-12-12.

The longer distance in the siRNA/SH14 systems was attributed to the 2 CH_2- longer hydrocarbon chain of this surfactant, in agreement with previous SANS investigation.[104]

The difference observed in the siRNA/Gemini series followed the length of the spacer in the surfactant molecular structure and was attributed to a different hydration of the complex. The "bump" observed in the q_{max} time evolution of the siRNA/12-12-12 system (**Figure 3.7**, lower panel) is a rearrangement reflecting the flexibility of these surfactant molecules.

Interestingly, the same behavior was closely reproduced when both the concentration of surfactant and siRNA were halved, i.e. when complexes at the same CR were prepared from solution of micelles and siRNA twice more diluted (data not shown). The same bump was also observed at CR = 0.75, though in this case it was less intense, due to a smaller concentration of the complex below the neutrality point. These similarities indicate that complex formation followed reproducible path, at least in the experimental conditions of the present study. It is also worth noting that the low *d* values obtained for all systems indicate that strong squeezing of pre-existing micelles and siRNA occurs upon complex formation.

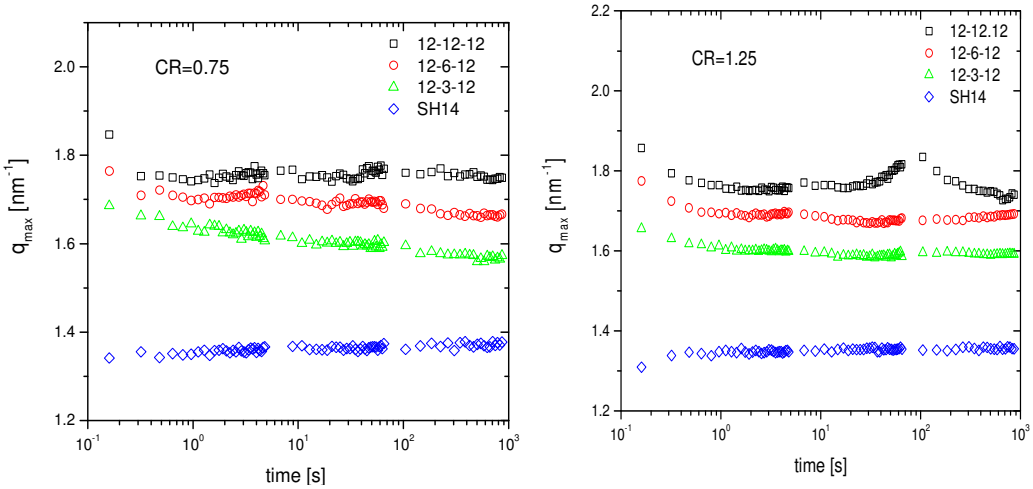

Figure 3.7: Time evolution of the quasi Bragg peak position in complexes prepared from different surfactants at the same concentration ($1.25x10^{-3}$ M) at two different charge ratios.

In the early stage (first few seconds), the evolution of Gemini complexes differed from SH14 complexes in that the repeat distance of the former systems increased, whereas SH14 complexes showed a slight internal shrinking (**Figure 3.7**). This was attributed to water intake and water expulsion, respectively, and was traced back to the higher charge density present on the Geminis' polar head, which allows for more extended hydration. Water expulsion upon siRNA complexation with cationic PAMAM-dendrimers has been described as a relevant phenomenon by MD simulation although on a shorter time-scale (~10^{-9} s).[114]

The width of Bragg peaks, usually expressed as Full Width at Half Maximum (FWHM), is another parameter which gives valuable information on the structure of complexes. In powder samples the FWHM is related to the mean size of crystallites through the Schrerrer relation[115] and in soft condensed matter it is inversely proportional to the extension of the coherence domains from which this correlation originates.[116,117] In our experimental conditions other broadening

factors, such as q-resolution, were much smaller than the measured widths and could be disregarded.

For the siRNA/12-6-12 system, the FWHM value was 0.45 nm^{-1} and 0.37 nm^{-1} at CR = 0.75 and 1.25, which correspond to coherence length ($\xi = 2\pi/q$) of 13.8 nm and 16.7 nm, respectively. For the siRNA/SH14 system (**Figure 3.8**) FWHM was 0.41 (CR = 0.75) and 0.46 (CR = 1.25), with corresponding ξ = 15.4 and ξ = 13.5, respectively.

Coherence domains were modeled as made of "sandwiches" in which siRNA and micelles are alternately repeated. By assuming this layer arrangement, the average number ⟨N⟩ of sandwiches in the complex was evaluated, in analogy with SAXS studies performed on smectic systems.[118]

$$\langle N \rangle = q_{max}/FWHM$$

Figure 3.8 shows the time evolution of siRNA/12-6-12 and siRNA/SH14 systems (CR=1.25, two different concentration). The behavior of both surfactants was in agreement with an exponential growth of the number of correlated structural units. This suggests a first order kinetics in the ordering process. The complexes containing SH14 were ordered on smaller length scale and their structure was almost unchanged at lower total surfactant concentration, while in the case of 12-6-12 a larger extent of correlation was observed for the more concentrated system. In fact, the final number of correlated layers ($\langle N_f \rangle$) was ~ 6 at [12-6-12] = 6.25×10^{-4} M and 7-8 at [12-6-12] = 1.25×10^{-3} M.

The fact that R_g and $\langle N \rangle$ vary in the same way validates the interpretation of FWHM in terms of number of repeated structural units. The long time evolution was described by an exponential increase for all systems except the 12-12-12 complexes, which underwent the structural rearrangement mentioned above in the time window 50-150 s. **Figure 3.8** reports the final number of layers $\langle N_f \rangle$ in complexes made by different surfactants at CR = 0.75 and CR = 1.25.

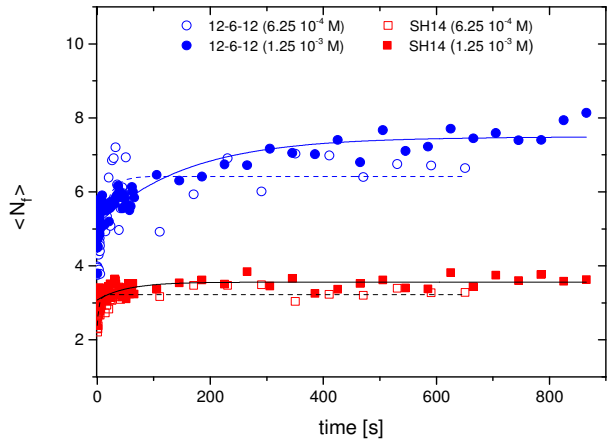

Figure 3.8: Time evolution of the number of correlated layers in siRNA/micelle complexes for surfactants 12-6-12 and SH14 at two different concentration and CR = 1.25.

To obtain information on the size of complexes $I(q)$ data were analyzed at low q by using the Guinier approximation:[119]

$$I(q) = I_0 \, exp\left(-\frac{1}{3} q^2 \, R_g^2\right)$$

where I_0 is the extrapolated $q \to 0$ intercept and R_g is the gyration radius of the scattering objects, i.e. the average squared distance of individual scatterers from the centre of the aggregate.

Surfactant	Concentration, M	CR	<N_f>
12-3-12	6 25 10^{-4}	0.75	5
		1.25	5.4
	1.25 10^{-3}	0.75	4.6
		1.25	5.3
12-6-12	6.25 10^{-4}	0.75	6.4
		1.25	5.9
	1.25 10^{-3}	0.75	6.6
		1.25	7.5
SH14	6.25 10^{-4}	0.75	3.7
		1.25	3.2
	1.25 10^{-3}	0.75	3.5
		1.25	3.6

Table 3.4: Average number of smectic layers in siRNA/micelles complexes (see text for details).

Figure 3.9 shows the Guinier fitting for the system siRNA/12-6-12 at CR=0.75 and at surfactant concentration 1.25x10^{-3}. In this system R_g grows from 11.58 nm, measured 0.32 s after mixing, to 14.42 nm in about 800 s.

The time evolution of R_g showed a rapid initial growth and an asymptotic trend, which was fitted by a stretched exponential.

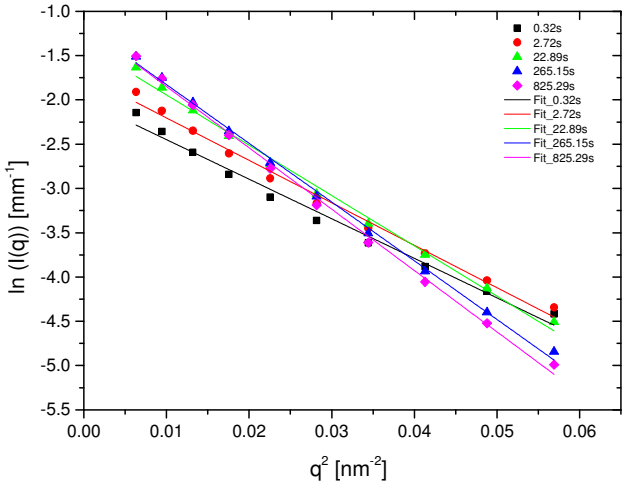

Figure 3.9: Guinier fitting of the SAXS low q region for the siRNA/12-6-12 complex at CR=1.25 and [12-6-12]=1.25x10^{-3}M. The obtained R_g value are: 11.58±0.24 nm at 0.32 s; 12±0.19 nm at 2.72 s; 13.06±0.16 nm at 22.89 s; 14.10±0.12 nm at 265.15 s; 14.42±0.14 nm at 825.29 s.

Noteworthy, a particular form of stretched exponential, the Avrami equation,[120] is conventionally used to describe nucleation and growth processes (**Figure 3.10**).[121,122] A stretched exponential behaviour was consistent with a broad set of characteristic times involved in complex formation,[123-125] which could be accounted for considering micelle deformation, association of oppositely charged aggregates, re-ordering etc., as suggested by the quasi-Bragg peak analysis. At lower surfactant content, the succession of increasing and decreasing steps was more resolved, as shown in **Figure 3.10**.
We can also notice that diluting twice the system has no marked effect either on the <N_f> or the R_g values.

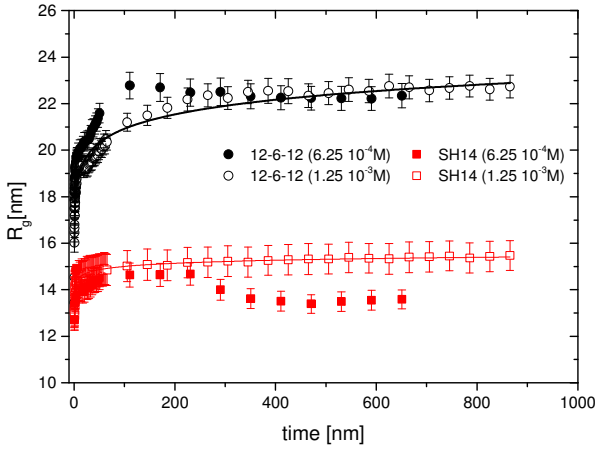

Figure 3.10: Time evolution of R_g after mixing siRNA with surfactants 12-6-12 or SH14 at two different concentration and CR = 1.25. The continuous line are fitted with a Weibull function $R_g = a - b\,e^{(-(kt)^n)}$, where a, b, k and n are best fit parameters ($n = 0.053$ and $n = 0.044$ for 12-6-12 and SH14, respectively).

Table 3.5 reports the values of R_g at the final state of siRNA/micelles nucleation. For Gemini complexes the higher values were obtained at CR = 1.25, regardless of surfactant concentration. Therefore, we hypothesize that siRNA content could be the factor limiting the aggregation process. For SH14, consistently with the results of peak analysis (**Table 3.5**), smaller variations with CR and surfactant concentration were found.

Surfactants	Concentration, M	CR	limit R_g, nm
12-3-12	6 25 10^{-4}	0.75	17.1
		1.25	19.8
	1.25 10^{-3}	0.75	14.6
		1.25	21.5
12-6-12	6.25 10^{-4}	0.75	7.3
		1.25	22.6
	1.25 10^{-3}	0.75	14.4
		1.25	23.1
12-12-12	6 25 10^{-4}	0.75	13.1
		1.25	24.4
	1.25 10^{-3}	0.75	15.2
		1.25	26.6
SH14	6.25 10^{-4}	0.75	16.6
		1.25	13.9
	1.25 10^{-3}	0.75	16.2
		1.25	15.7

Table 3.5: Long time R_g values for complexes made with different surfactant at two concentrations.

The data extracted from Bragg peaks and Guiner analysis allowed drawing the scheme reported in **Figure 3.11** to illustrate the process of complex formation. This scheme is also consistent with the mechanism proposed by Zhou et al. for

the complexation and time evolution of highly charged poly(amidoamine) (PAMAM) complexes with siRNA.[126]

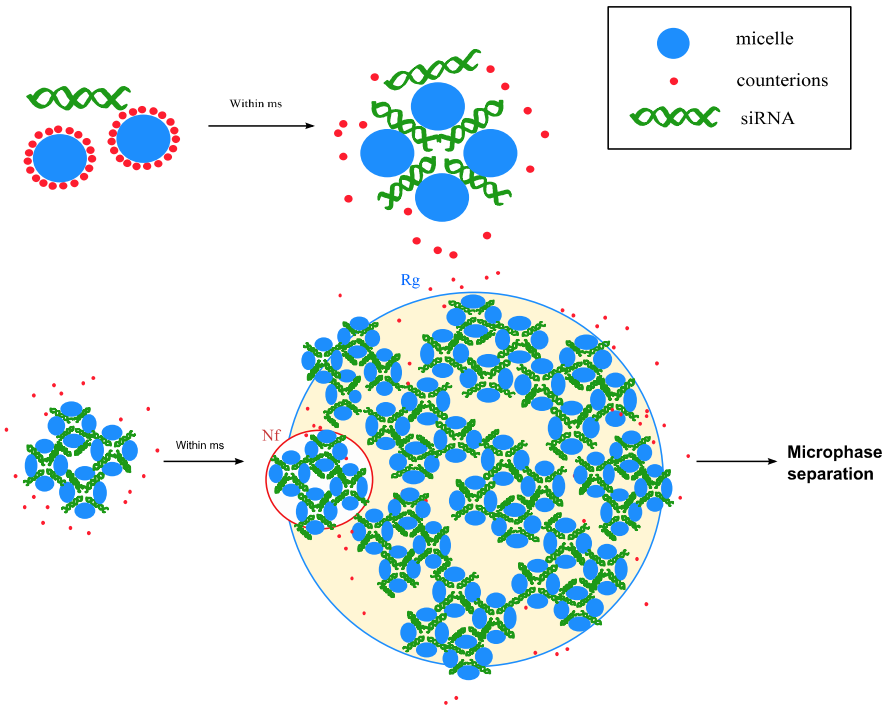

Figure 3.11: Sketch of the main steps involved in complex formation.

We studied the kinetics of self-assembly in systems containing cationic micelles and siRNA by time-dependent synchrotron SAXS.[127] These data refined and completed the structural investigation previously performed by Dynamic Light Scattering, Zeta Potential and SANS, which reported on the final state of complexes and were recorded during ~20 minutes after waiting another ~15 minutes, following a common protocol used in biological trials.

SAXS allowed following the structural evolution of complexes from few ms till 10-15 minutes after mixing. These time resolved experiments revealed that counterions release and complex formation occurs within 50 ms, as indicated by marked increase of the scattering intensity at low q and at high q (quasi-Bragg peak). In the newly formed aggregates siRNA and micelles were alternately layered in "sandwiches" with repeat distance of 3-4 nm. Further rearrangement brought to larger coherence domains made by a compact array of 4-8 units. Aggregates containing SH14 were less ordered compared to Gemini surfactants. At low q, Guiner analysis gave information on the gyration radius of the complexes, which was in the range 7-27 nm.

No larger aggregates (hundreds of nm) were detected up to 10-15 minutes from preparation. Since the transient states of complexes might be as relevant as the final state for their transfection efficiency we decided to get better inside in the

kinetic pathway of their formation. We are currently investigating complexation details by computational techniques to obtain finer insight on the siRNA/micelles complex structure. However, the obtained data are encouraging evidence in the perspective of using these systems *in vitro* or *in vivo* after preparation by simple mixing a micelle solution of the cationic surfactant and a siRNA solution, both of which are obtained without passing through irreversible steps, such as sonication or extrusion.

Chapter 4

4.1 Material and methods

4.1.1 Cell treatments.

In order to investigate whether gemini surfactants and their complexes with siRNA have cytotoxic effects on cells *in vitro*, we selected three cell lines: Human Embryonic Kidney 293 (HEK293), Human Colon Carcinoma (HCT8) and Chinese Hamster Ovary (CHO). HEK 293, HCT8 and CHO were grown respectively in DMEM (Dulbecco's Modified Eagle Medium), RPMI (Roswell Park Memorial Institute Medium) and DMEM-F12 (Dulbecco's Modified Eagle Medium-F12), supplemented with 10% fetal bovine serum (FBS), 1% L-Glutamine and 1% (penicilin/streptomicine) antibiotics. Cells were incubated at 37°C in a 5% CO_2 atmosphere. One day before treatment, 1.5×10^4 cells per well were seeded with 500 µL of growth medium into a 24-well plate for 24h.
Three different gemini surfactants (12-3-12, 12-6-12 and 12-12-12) were added to culture medium containing 10% serum at the final concentration of 10^{-4} M, $5x10^{-5}$ M, 10^{-5} M and $5x10^{-6}$ M.
We also tested the cytotoxicity of the complexes formed by Gemini surfactants and siRNA. All experiments were carried out combining equal volume of Gemini and diluted solution of siRNA in order to obtain aggregates of charge ratio (N/P) 0,25. Then complexes were added in medium with 10% serum to obtain the follow concentrations of Gemini: 10^{-4} M, $5x10^{-5}$ M, 10^{-5} M and $5x10^{-6}$ M for 24h. All experiments were performed at least in duplicate.

4.1.2 Cytoxicity Assay

To quantify the cytotoxicity effect, cells were stained with propidium iodide (PI) (P4170 Sigma Aldrich), PI is a fluorescent dye that binds to double-stranded DNA. It can penetrate the compromised cell membranes but remains excluded from viable cells. The fluorescence in the cells was detected by flow cytometry using a FACSanto cytometer (Becton Dickinson) equipped with a 488nm argon laser and a 695/40 nm band-pass filter. After gemini surfactant treatments, cells of each sample were harvested and resuspended in 500 µL phosphate buffered saline (PBS). Prior to the flow cytometric analysis, 5 µL of stock solution (10mg/mL) of PI diluted 1:400 in PBS was

added to each sample. Samples were incubated for 1 minute on ice. A total of 10.000 cells for each sample were analyzed, aggregates and debris were excluded. The percentage of PI positive cells were recorded.
To compare the effect of the three gemini surfactants in the different cell lines, we normalized the value of PI stained cells treated with gemini surfactants and the complexes (CR=0,25) by the PI stained cells of untreated controls of each cell line.

4.2 Results and discussion.

The cytometric analysis showed a different sensitivity of cells in function of gemini surfactants concentration. The two higher concentrations (10^{-4} and $5x10^{-5}$ M) of gemini surfactants were very toxic and caused the death of all the cells. On the contrary the two more diluted solution were far less toxic to cells. This trend was observed for all the three cell lines treated with gemini surfactants alone and also associated with siRNA (**Figure 4.1** and **Figure 4.2**).
The HCT8 cell lines had the higher sensitivity among the three cell lines tested to gemini surfactants at 10^{-5} M concentration. Similar results were obtain treated this cell line with complexes diluted in medium in order to obtain 10^{-5} M of Gemini.
The overall gemini surfactants citotoxicity effect seems to be proportional to the linker length at the concentration of 10^{-5} M but at the lower concentrations (5 10^{-6} M) the toxicity seems inversely proportional to the linker length. These results suggest a complex combinatorial effect of gemini surfactants concentration, cell lines and linker length of gemini surfactants that generate a different level of toxicity in relation to different experimental setting.

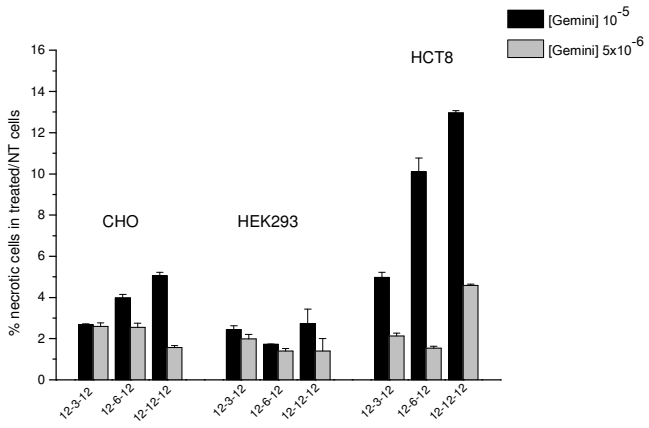

Figure 4.1: Cytotoxicity effects of three different gemini surfactant (12-3-12, 12-6-12 and 12-12-12) at 10^{-5} M and $5x10^{-6}$ M concentrations on HEK 293, HCT8 and CHO cell lines by flow cytometry analysis after staining cells with propidium iodide (PI). Values (± SEM) were normalized by PI stained cells of untreated controls.

Moreover citotoxic effect didn't change with the adding of siRNA, indeed toxicity of the complexes depends only on the type of vector. There were no peculiar differences between the effect caused by gemini surfactants alone and their aggregates with siRNA.

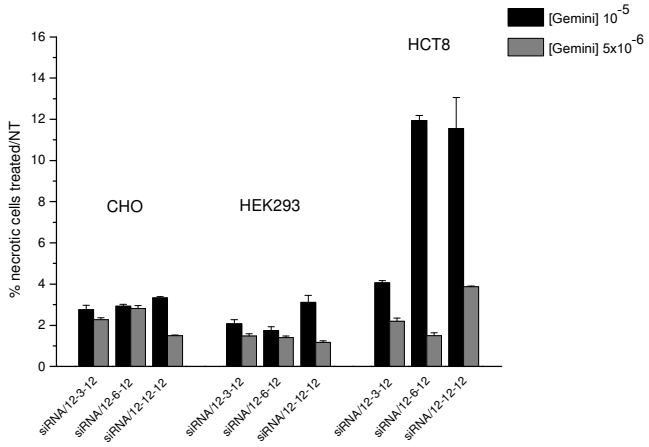

Figure 4.2: Citotoxicity effects of complexes formed by three different Gemini and siRNA(CR=0,25) on HEK 293, HCT8 and CHO cell lines. These complexes were diluted in medium with 10% of serum in order to have the follow concentrations of surfactants 10^{-5}M and $5x10^{-6}$M. Citotoxicity effect was measured by flow cytometry analysis after staining cells with propidium iodide (PI). Values (± SEM) were normalized by PI stained cells of untreated controls.

References

[1] Chen K., Mahato R.I. *Advanced delivery and therapeutic applications of RNAi*. Wiley **2013.**
[2] Fortunato, A. Quantitative high-throughput analysis of synthetic genetic interactions in *Caenorhabditis elegans* by RNA interference. *Genomics*. **2009**, 93: 392-396.
[3] Carpenter A.E., Sabatini D.M. Systematic genome-wide screens of gene function. *Nature Rev. Gen*. **2004**, 5: 11-22.
[4] Napoli C., Lemieux C., Jorgensen R. Introduction of a chimeric chalcone synthase gene into petunia results in reversibile co-suppression of homologous genes in trans. *Plant Cells*. **1990**, 2: 279-289.
[5] Romano N., Macino G. Quelling: transient inactivation of gene expression in *Neurospora crassa* by transformation with homologous sequences. *Mol. Microbiol.* **1992**, 6: 3343–3353.
[6] Fire A., Xu S., Montgomery M.K., Kostas S.A., Driver S.E., Mello C.C. Potent and specific genetic interference by double-stranded RNA in *Caenorhabditis elegans*. *Nature*. **1998**, 391: 806-811.
[7] Wianny F., Zernicka-Goetz M. Specific interference with gene function by double-stranded RNA in early mouse development. *Nature Cell Bio*. **2000**, 2: 70-75
[8] Elbashir S.M., Harborth J., Lendeckel W., Yalcin A., Weber K., Tuschl T. Duplexes of 21-nucleotide RNAs mediate RNA interference in cultured mammalian cells. *Nature*. **2001**, 411: 494-498.
[9] Borchert G.M., Lanier W., Davidson B.L. RNA polymerase III transcribes human microRNAs. *Nature Struct. Mol. Biol.* **2006**, 13: 1097-1101.
[10] Cullen B.R. Trascription and processing of human microRNA precursors. *Mol. Cell.* **2004**, 16: 861-865.
[11] Zamore P.D., Tuschl T., Sharp P.A., Bartel P.D. RNAi: double-stranded RNA directs the ATP-dependent cleavage of mRNA at 21 to 23 nucleotide intervals. *Cell*. **2000**, 101: 25-33.
[12] Nykanen A., Haley B., Zamore P.D. ATP requirements and small interfering RNA structure in the RNA interference pathway. *Cell*. **2001**, 107: 301-321.
[13] Ishizu H., Siomi H., Siomi M.C. Biology of PIWI-interacting RNAs: new insights into biogenesis and function inside and outside of germlines. *Genes Dev.* **2012**, 26(21): 2361-2373.
[14] Aagaard L., Rossi JJ. RNAi therapeutics: Principles, prospects and challenges. *Adv. Drug Deliv. Rev*. **2007**, 59: 75–86.
[15] Castanotto D., Rossi J.J. The promises and pitfalls of RNA-interference-based therapeutics. *Nature*. **2009**, 457: 426-433.
[16] Davidson B.J., McCray Jr. Current prospects for RNA interference-based therapies. *Nature Rev. Gen.* **2011**, 12: 329-340.
[17] Burnett J.C., Rossi J.J., Tiemann K. Current progress of siRNA/shRNA therapeutics in clinical trials. *Biotechnol. J.* **2011**, 6: 1130-1146.
[18] Buyens K., De Smedt S.C., Braeckmans K., Demeester J., Peeters L., van Grunsven L.A., de Mollerat du Jeu X., Sawant R., Torchilin V., Farkasova K., Ogris M., Sanders N.N. Liposome based systems for systemic siRNA delivery: stability in blood sets the requirements for optimal carrier design. *J. Contr. Release.* **2012**, 158: 362-370.
[19] Stanton M.G., Colletti S.L. Medicinal chemistry of siRNA delivery. *J. Med. Chem.* **2010**, 53: 7887-7901.
[20] Ozpolat B, Sood A.K., Lopez-Berestein G. Liposomal siRNA nanocarriers for cancer therapy. Advanced drug delivery reviews (2013) http://dx.doi.org/10.1016/j.addr.2013.12.008
[21] Kleinman M.E., Yamada K., Takeda A., Chandrasekaran V., Nozaki M., Baffi J.Z., Albuquerque R.J., Yamasaki S., Itaya M., Pan Y., Appukuttan B., Gibbs D., Yang Z., Karikó K., Ambati B.K., Wilgus T.A., DiPietro L.A., Sakurai E., Zhang K., Smith J.R., Taylor E.W.,

Ambati J. Sequence- and target- independent angiogenesis suppression by siRNA via TLR3. *Nature*. **2008**, 452: 591-597.
[22] Astor T.L. RNA Interference, RSV, and Lung Transplantation: A Promising Future for siRNA Therapeutics. *Am. J. Respir. Crit. Care Med.* **2011**, 183: 427-428.
[23] Nayerossadat N., Maedeh T., Ali P.A. Viral and nonviral delivery systems for gene delivery. *Adv. Biomed. Res.* **2012**, 1, 27.
[24] Falsini S., Ciani L., Ristori S., Fortunato A., Arcangeli A. Advances in lipid-based platforms for RNAi therapeutics. *J. Med Chem*, **2013**, DOI: 10.1021/jm400791q
[25] Cullis P.R., Hope M.J., Tilcock C.P. Lipid polymorphism and the role of lipid in membranes. *Chem. Phys. Lipids.* **1986**, 40: 127-144.
[26] Epand R. M. Eds. *Lipid Polymorphism and Membrane Properties*. Academic Press. San Diego (CA), **1997**.
[27] Ninham B. W., Lo Nostro P. Molecular Forces and Self Assembly in Colloid, Nano Sciences and Biology. *Cambridge University Press*. **2010**.
[28] Gong J., Chen M., Zheng Y., Wang S., Wang Y. Polymeric micelles drug delivery systems in oncology. *J. Control. Release*. **2012**, 159: 312-23.
[29] Wang Y., Dubin P.L., Zhang H. Interaction of DNA with Cationic Micelles: Effects of Micelle Surface Charge Density, Micelle Shape, and Ionic Strength on Complexation and DNA Collapse. *Langmuir*. **2001**, 17: 1670-1673.
[30] Lasic D.D. Ed.; Papahadjopoulus, D. Ed. Medical applications of liposomes. *Elsevier*. **1997**.
[31] Gregoriadis G., Perrie, Y. Liposomes in Nanomedicine. *Wiley*, **2012**.
[32] Musacchio T., Torchilin V.P. Recent development in lipid-based pharmaceutical nanocarriers. *Front. Biosc*. **2011**, 16: 1388-1412.
[33] Klibanov A.L., Maruyama K., Torchilin V.P., Huang L. Amphipathic polyethyleneglycols effectively prolong the circulation time of liposomes. *FEBS Lett.* **1990**, 268: 235-237.
[34] Immordino M.L., Dosio F., Cattel L. Stealth liposomes: review of the basic science, rationale, and clinical applications, existing and potential. *Int. J. Nanomedicine.* **2006**, 1: 297-315.
[35] Dos Santos N., Allen C., Doppen A.M., Anantha M., Cox K.A.K., Gallagher R.C., Karlsson G., Edward K., Kenner G., Samuels L., Webb M.S., Bally M.B. Influence of poly(ethylene glycol) grafting density and polymer length on liposomes: relating plasma circulation lifetimes to protein binding. *BBA*. **2007**, 1768: 1367-1377.
[36] Yoshino K., Taguchi K., Mochizuki M., Nozawa S., Kasukawa H. Novel analytical method to evaluate the surface condition of polyethylene glycol-modified liposomes. *Coll. Surf. A*. **2012**, 397: 73-79.
[37] Allen T.M., Cullis P.R. Liposomal drug delivery systems: from concept to clinical applications. *Adv. Drug Deliv. Rev.* **2013**, 65: 36-48.
[38] Tseng Y.C., Mozumda S., Huang L. Lipid-based systemic delivery of siRNA. *Adv Drug Delivery*. **2009**, 61: 721-731.
[39] Olbrich C., Bakowsky U., Lehr C.M., Müller R.H., Kneuer C. Cationic solid-lipid nanoparticles can efficiently bind and transfect plasmid DNA. *J. Control Release*. **2001**, 77: 345-355.
[40] Gomes-da-Silva L.C., Fonseca N.A., Moura V., Pedroso de Lima M.C., Simões S.J., Moreira N. Lipid-Based Nanoparticles for siRNA Delivery in Cancer Therapy: Paradigms and Challenges. *Acc. Che. Res.* **2012**, 45: 1163-1171.
[41] Morrissey D.V., Lockridge J.A., Shaw L., Blanchard K., Jensen K., Breen W., Hartsough K., Machemer L., Radka S., Jadhav V., Vaish N., Zinner S., Vargeese C., Browman K., Shaffer C.S., Jeffs L.B., Judge A., MacLachlan I., Polisky B. Potent and persistent in vivo anti-HBV activity of chemically modified siRNAs. *Nature Biotech*. **2005**, 23: 1002-1007.
[42] Leung A.K.K., Hafez I.M., Baoukina S., Belliveau N. M., Zhigaltsev I.V., Afshinmanesh E., Tieleman D.P., Hansen C.L., Hope M.J., Cullis P.R. Lipid Nanoparticles Containing siRNA Synthesized by Microfluidic Mixing Exhibit an Electron-Dense Nanostructured Core. *J. Phys. Chem. C.* **2012**, 116: 18440-18450.
[43] Felgner P.L. Nonviral strategies for gene therapy. *Scientific American*. **1997**, 276: 102-106.

[44] Rädler J.O., Koltover I., Salditt T. Safinya C.R. Structure of DNA-Cationic Liposome Complexes: DNA Intercalation in Multilamellar Membranes in Distinct Interhelical Packing Regimes. *Science*. **1997**, 275: 810-814.
[45] Hirst L.S. Fundamental of Soft Matter Science. *CRC Press*. **2012**.
[46] Zemb T., LindnerP., Eds. *Neutron, X-Ray and Light Scattering*. North Holland Press. **2002**.
[47] Webb G. A. *Modern Magnetic Resonance*. Springer Verlag: Berlin, **2008**.
[48] Davidson B.L., McCray Jr. P.B. Current prospects for RNA interference-based therapies. *Nature Gen.* **2011**, 12: 329-340.
[49] www.clinicaltrials.gov
[50] Amghesom A., Kaushik A., Kaushik J.J., Petros S.T. RNA interference: a futuristic tool and its therapeutic applications. *Saudi J. Bio. Sci*. **2012**, 19: 395-403.
[51] Seyhan A.A. RNAi: a potential new class of therapeutic for human genetic disease. *Hum. Genet.* **2011**, 130, 583-605.
[52] Macron D. TransDerm's RNAi-based skin dosorder drug moves into one-patient clinical trial. *RNAi News*. **2008**, 6: 10.
[53] Zimmermann T.S., LeeA.C.H., Akinc A., Bramlage B., Bumcrot D., Fedoruk M.N., Harborth J., Heyes J.A., Jeffs L.B., John M., Judge A.D., Lam K., McClintock K., Nechev L.V., Palmer L.R., Racie T., Röhl I., Seiffert S., Shanmugam S., Sood V., Soutschek J., Toudjarska I., Wheat A.J., Yaworski E., Zedalis W., Koteliansky V., Manoharan M., Vornlocher H.P., MacLachlan I. RNAi-mediated gene silencing in non-human primates. *Nature*. **2006**, 44: 111-114.
[54] Akinc A., Zumbuehl A., Goldberg M., Leshchiner E.S., Busini V., Hossain N., Bacallado S.A., Nguyen D.N., Fuller J., Alvarez R., Borodovsky A., Borland T., Constien R., de Fougerolles A., Dorkin JR., Jayaprakash K.N., Jayaraman M., John M., Koteliansky V., Manoharan M., Nechev L., Qin J., Racie T., Raitcheva D., Rajeev K.J., Sah D.W.Y., Soutschek J., Toudjarska I., Vornlocher H.P., Zimmermann T.S., Langer R., Anderson D.G., A combinatorial library of lipid-like materials for delivery of RNAi therapeutics. *Nature Biotech.* **2008**, 26: 261-269.
[55] Frank-Kamenetsky M., Grefhorst A., Anderson N.N., Racie T.S., Bramlage B., Akinc A., Butler D., Charisse K., Dorkin, R., Fan Y., Gamba-Vitalo C., Hadwiger P., Jayaraman M., John M., Jayaprakash K.N., Maier M., Nechev L., Rajeev K.G., Read T., Röhl I., Soutschek J., Tan P., Wong J., Wang G., Zimmermann T., de Fougerolles A., Vornlocher H.P., Langer R., Anderson D.G., Manoharan M., Koteliansky V., Horton J.D., Fitzgerald K. Therapeutic RNAi targeting PCSK9 acutely lowers plasma cholesterol in rodents and LDL cholesterol in nonhuman primates. *PNAS*. **2008**, 105: 11915–11920.
[56] Alnylam Pharmaceutics. Alnylam Reports Positive Clinical Results for ALN-PCS, an RNAi Therapeutic Targeting PCSK9 for the Treatment of Severe Hypercholesterolemia. *News Release*. **2012**, www.alnylam.com.
[57] Alabi C., Vegas A., Anderson D. Attacking the genome: emerging siRNA nanocarriers from concenpt to clinic. *Curr. Op. Pharmac.* **2012**, 12: 427-433.
[58] Jayaraman M., Ansell S.T., Mui B.L., Tam Y.K., Chem J., Du X., Butler D., Eltepu L., Matsuda S., Narayanannair J.K., Rajeev K.G., Hafez I.M., Akinc A., Maier M.A., Tracy M.A., Cullis P.R., Madden T.D., Manoharan M., Hope M.J. Maximizing the potency of siRNA lipid nanoparticles for hepatic gene silencing in vivo. *SiRNA deliv*. **2012**, 51: 8529-8533.
[59] Alnylam Pharmaceutics. Alnylam Reports Positive Phase II Data for ALN-TTR02, an RNAi Therapeutic Targeting Transthyretin (TTR) for the Treatment of TTR-Mediated Amyloidosis (ATTR). *News Release*. **2013**, www.alnylam.com.
[60] Alnylam Pharmaceutics. Alnylam Reports positive clinical results for ANL-PCS, an RNAi therapeutic targeting PCSK9 for the treatment of severe hypercholesterolemia. *News Release*. **2013**, www.alnylam.com.
[61] Alnylam Pharmaceutics. Alnylam Files Clinical Trial Application to initiate a phase I study for TTRsc, a subcutaneously administered RNAi therapeutic targeting transthyretin (TTR) for the treatment of TTR-Mediated Amyloidosis (ATTR). *News Release*. **2012**, www.alnylam.com.
[62] Maier M.A. Jayaraman M. Matsuda S. Liu J. Barros S. Querbes, W., Tam Y.K., Ansell S.K., Kumar V., Qin J., Zhang X., Wang Q., Panesar S., Hutabarat R., Carioto M., Hettinger J.,

Kandasamy P., Butler D., Rajeev K.G., Pang B., Charisse K., Fitzgerald K., Mui B.L., Du X., Cullis P., Madden T.D., Hope M.J., Manoharan M., Akinc, A. Biodegradable Lipids Enabling Rapidly Eliminated Lipid Nanoparticles for Systemic Delivery of RNAi Therapeutics. *Mol. Ther.* **2013**, DOI: 10.1038/mt.2013.124.

[63] Blight K.J., Kolykhalov A.A., Rice C.M. Efficient initiation of HCV RNA replication in cell culture. *Science*. **2000**, 290: 1972-1974.

[64] Song E., Lee S.K., Wang J., Ince N., Ouyang N., Min J., Chen J., Shankar P., Lieberman J. RNA interference targeting Fas protects mice from fulminant hepatitis. *Nat Med*. **2003**, 9: 347-51.

[65] Bonamassa B., Hai L., Liu D. Hydrodynamic Gene Delivery and Its Applications in Pharmaceutical Research. *Pharm Res*. **2011**, 28: 694–701.

[66] Palliser D., Chowdhury D., Wang Q.Y., Lee S.J., Bronson R.T., Knipe D.M., Lieberman J. An siRNA-based microbicide protects mice from lethal herpes simplex virus 2 infection. *Nature*. **2006**, 439: 89-94.

[67] Wu Y., Navarro F., Lal A., Basar E., Pandey R.K., Manoharan M, Feng Y., Lee S.J., Lieberman J., Palliser D. Durable protection from Herpes Simplex Virus-2 transmission following intravaginal application of siRNAs targeting both a viral and host gene. *Cell Host Microbe*. **2009**, 5: 84–94.

[68] Geisbert T.W., Lee A.C.H., Robbins M., Geisbert J.B., Honko A.N., Sood V., Johnson J.C., de Jong S., Tavakoli I., Judge A., Hensley L.E., MacLachlan I. Postexposure protection of non-human primates against a lethal Ebola virus challenge with RNA interference: a proof-of-concept study. *Lancet*. **2010**, 375: 1896-1905.

[69] http://www.tekmirapharm.com/Programs/Products.asp#ebola

[70] D'Amico M., Gasparoli L., Arcangeli A. Potassium channels: novel emerging biomarkers and targets for therapy in cancer. *Recent Pat. Anticancer Drug Discov*. **2013**, 8, 53-65.

[71] Navarro G., Sawant R.R., Biswas S., Essex S., Tros de Ilarduya C., Torchilin V.P. P-glycoprotein silencing with siRNA delivered by DOPE-modified PEI overcomes doxorubicin resistance in breat cancer cells. *Nanomedicine*, **2012**, 7: 65-78.

[72] Fang J., Nakamura H., Maeda H. The EPR effect: unique features of tumor blood vessels for drug delivery, factors involved, and limitations and argumentation of the effect. *Adv. Drug Deliv. Rev*. **2011**, 63: 136-151.

[73] Anderson M.D. EphA2-targeted therapy delivers chemo directly to ovarian cancer cell. *Newsroom.* MD Anderson Cancer Center. **2009**.

[74] Lander C.N., Chavez-Reyes A., Bucana C., Schmendt R., Deavers M.T., Lopez-Berestein G., Sood A.K. Therapeutic EphA2 gene targeting in vivo using neutral liposomal small interfering RNA delivery. *Cancer Res.* **2005**, 65: 6910-6918.

[75] Santel A., Aleku M., Keil O., Endruschat J., Esche V., Fisch G., Dames S., Löffler K., Fechtner M., Arnold W., Giese K., Klippel A., Kaufmann J. A novel siRNA-lipoplex technology for RNA interference in the mouse vascular endothelium. *Gene ther*. **2006**, 13: 1222-1234.

[76] Santel A., Aleku M., Keil O., Endruschat J., Esche V., Durieux B., Löffler K., Fechtner M., Röhl T., Fisch G., Dames S., Arnold W., Giese K., Klippel A., Kaufmann J. RNA interference in the mouse vascular endothelium by systemic administration of siRNA-lipoplexes for cancer therapy. *Gene Ther.* **2006**, 13: 1360-1370.

[77] Judge A.D., Robbins M., Tavakoli. I., Levi J., Hu L., Fronda A., Ambegia E., McClintock K., MacLachlan I. Confirming the RNAi-mediated mechanism of action of siRNA-based cancer therapeutics in mice. *J. Clin. Inv*. **2009**, 119: 661-673.

[78] Tabernero J., Shapiro G.I., Lorusso P.M., Cervantes A., Schwartz G.K., Weiss G.J., Paz-Ares L., Cho D.C., Infante J.R., Alsina M., Mrinal M., Gounder M.M., Falzone R., Harrop J., White A.C.S., Toudjarska I., Bumcrot D., Meyers R.E., Hinkle G., Svrzikapa N., Renta M., Hutabarat R.M., Clausen V.A., Cehelsky J., Nochur S.V., Gamba-Vitalo C., Vaishnaw A.K., Sah D.W.Y., Gollob J.A., Burris III H.A. First-in-man trial of a RNA interference therapeutic targeting VEGF and KSP in cancer patients with liver involvement. *J. Cancer Discov*. **2013**, DOI 10.1158/2159-8290.CD-12-0429.

[79] Koldehoff M., Steckel N.K., Beelen D.W., Elmaagacli A.H. Therapeutic application of small interfering RNA directed against bcr-abl transcripts to a patient with imatinib-resistant chronic myeloid leukaemia. *Clin. Exp. Med.* **2007**, 7: 47–55.
[80] Koldehoff M., Steckel N.K., Beelen D.W., Elmaagacli A.H. Therapeutic application of small interfering RNA directed against bcr-abl transcripts to a patient with imatinib-resistant chronic myeloid leukaemia. *Clin. Exp. Med*. **2007**, 7: 47-55.
[81] Rana S., Maples P.B., Senzer N., Nemunaitis J. Stathmin 1: a novel therapeutic target for anticancer activity. *Exp. Rev. Anticancer Ther*. **2008**; 8: 1461-70.
[82] Templeton N.S., Senzer N. Optimization of Non-Viral Gene Therapeutics Using Bilamellar Invaginated Vesicles. *J. Genet Syndr Gene Ther.* **2011**, DOI 10.4172/2157-7412.S5-002.
[83] Zana R. Novel Surfactant: Preparation, Applications and Biodegradable, C.Holmberg, Ed., Chap. 8, p.241. Dekker, New York, 1998.
[84] Zana R., Dimeric (Gemini) Surfactants: Effect of the Spacer Group on the Association Behavior in Aqueous Solution. *Adv. Colloid Interface Sci.* **2002**.
[85] Candiani G., Frigerio M., Viani F., Verpelli C., Sala C., Chiamenti L., Zaffaroni N., Folini M., Sani M., Panzeri W. Zanda. M. Dimerizable redox-sensitive triazine-based cationic lipids for in vitro gene delivery. *Chem. Med. Chem.* **2007**, 46: 4785-4792.
[86] In M., Bec V., Anguerre-Chariol O. Zana R. Quaternary Ammonium Bromide Surfactant Oligomers in Aqueous Solution: *Self-Association and Microstructure Langmuir*. **2000**, 16: 141-148.
[87] Wasungu L., Stuart M.C.A., Scarzello M., Engberts J.B.F.N., Hoekstra D., Lipoplexes formed from sugar-based gemini surfactants undergo a lamellar-to-micellar phase transition at acidic pH. Evidence for a non-inverted membrane-destabilizing hexagonal phase of lipoplexes. *Biochim. Biophis. Acta, Biomembranes.* **2006**, 1758: 1677-1684.
[88] Wettig S. D., Verrall R.E., Foldvari M., Gemini surfactants: a new family of building blocks for non-viral gene delivery systems. *Curr. Gene Ther*., **2008**, 8: 9-23.
[89] Bombelli C., Giansanti L., Luciani P., Mancini G., Gemini surfactant based carriers in gene and drug delivery.*Curr. Med. Chem.*, **2009**, 16: 171-183.
[90] Badea I., Virtanen C., Verrall R. E., Rosenberg A., Foldvari M., Effect of topical interferon-γ gene therapy using gemini nanoparticles on pathophysiological markers of cutaneous scleroderma in Tsk/+ mice. *Gene Ther*. **2012**, 19: 978-987.
[91] Aleandri S., Bombelli C., Bonicelli M.G., Bordi F., Giansanti L., Mancini G., Ierino M., Sennato S., Fusion of gemini based cationic liposomes with cell membrane models: implications for their biological activity. *Biochim. Biophis. Acta, Biomembranes*. **2013**, 1828: 382-390.
[92] Candiani G., Pezzoli D., Cabras M., Ristori S., Pellegrini C., Kajaste- Rudnitski A., Vicenzi E., Sala C., Zanda M. A dimerizable cationic lipid with potential for gene delivery. *J Gene Med* **2008**, 10: 637-645.
[93] Yuan X., Naguib S., Wu Z., Recent advances of siRNA delivery by nanoparticles.*Exp. Op. Drug. Del.* **2011**, 8: 521-536.
[94] Jensen L.B., Pavan G.M., Kasimova M.R., Rutherford S., Danani A., Nielsen H.M., Foged C., Elucidating the molecular mechanism of PAMAM-siRNA dendriplex self-assembly: effect of dendrimer charge density. *Int. J. Pharm.* **2011**, 416: 410-418
[95] Leung A.K.K., Hafez I.M., Baoukina S., Belliveau N.M., Zhigaltsev I.V., Afshinmanesh E., Tieleman D.P., Hansen C. L., Hope M.J., Cullis P.R., Lipid Nanoparticles Containing siRNA Synthesized by Microfluidic Mixing Exhibit an Electron-Dense Nanostructured Core. *J Phys. Chem. C Nanomater interface*, **2012**, 116: 18440-18450.
[96] Tagalakis A.D., Saraiva L., McCarthy D., Gustafsson K.T., Hart S.L., Comparison of nanocomplexes with branched and linear peptides for siRNA delivery. *Biomacromolecules*. **2013**, 14: 761-770
[97] Harroun T.A., Kučerka N., Nieh M.-P., Katsaras J. Neutron and X-ray scattering for biophysics and biotechnology: examples of self-assembled lipid systems. *Soft Matter*, **2009**, 5: 2694-2703.

[98] Jensen L.B., Mortensen K., Pavan G.M., Kasimova M.R., Jensen D.K., Gadzhyeva V., Nielsen H.M., Foged C., Molecular characterization of the interaction between siRNA and PAMAM G7 dendrimers by SAXS, ITC, and molecular dynamics simulations. *Biomacromolecules.* **2010**, 11: 3571-3577.
[99] Kornreich M., Avinery R., Beck R., Modern X-ray scattering studies of complex biological systems. *Modern Curr. Op. Biotechn.* **2013**, 24: 1-8.
[100] Weiss T.M:, Narayanan T., Wolf C., Gradzielski M., Panine P., Finet S., Helsby W. I., Dynamics of the self-assembly of unilamellar vesicles. *Phys. Rev. Lett.*, **2005**, PRL 94, 038303
[101] Martin- Herranz A., Ahmad A., Evans H.M., Ewert K., Schulze U., Safynia C.R., Surface functionalized cationic lipid-DNA complexes for gene delivery: PEGylated lamellar complexes exhibit distinct DNA-DNA interaction regimes. *Biophys. J.* **2004**, 86: 1160-1168.
[102] Gawęda S., Morán M.C., Pais A.A.C.C., Dias R.S. Schillén K., Lindman B., Miguel M.G. Cationic agents for DNA compaction. *J. Colloid Interf. Science.* **2008**, 323: 75-83.
[103] Marchini C., Pozzi D., Montani M., Alfonsi C., Amici A., Amenitsch H., Candeloro De Sanctis S., Caracciolo G. Tailoring lipoplex composition to the lipid composition of plasma membrane: a Trojan horse for cell entry? *Langmuir*, **2010**, 26: 13867-13873.
[104] Ristori S., Ciani L., Candiani G., Battistini C., Frati A., Grillo I., M. In, Complexing a small interfering RNA with divalent cationic surfactants. *Soft Matter*. **2012**, 8: 749-756.
[105] D'Amico M., Gasparoli L., Arcangeli A., Potassium channels: novel emerging biomarkers and targets for therapy in cancer. *Recent Pat. Anticancer Drug Discov.* **2013**, 8: 53-65.
[106] Panine P, Finet S, Weiss TM, Narayanan T. Probing fast kinetics in complex fluids by combined rapid mixing and small-angle X-ray scattering. *Adv Colloid Interface Sci.* **2006**, 127: 9-18.
[107] http://www-drecam.cea.fr/scm/lions/techniques/saxs
[108] Aswal V.K:, Goyal P.S., De S., Bhattacharya S., Amenitisch H., Bernstorff S., Small-angle X-ray scattering from micellar solutions of gemini surfactants. *Chemical Physics Letters*. **2000**, 329: 336- 340.
[109] Zemb T., Taché O., Né F., Spalla O. A high-sensitivity pinhole camera for soft condensed matter. *J. Appl. Cryst.* **2003**, 36, 800-805.
[110] Radler J.O., Koltover I., Salditt T., Safinya C. R., Structure of DNA-cationic liposome complexes: DNA intercalation in multilamellar membranes in distinct interhelical packing regimes. *Science*. **1997**, 275: 810-814.
[111] Bruisma I, Electrostatics of DNA-cationic lipid complexes: isoelectric instability. *Eur. Phys. Chem. B*. **1998**, 4: 75-88.
[112] Barreiro P.C.A., Lindman B., The kinetics of DNA-cationic veshicle complex formation. *J. Phys. Chem. B*. **2003**, 107: 6208-6213.
[113] Braun C.S., Fisher M.T., Tomalia D.A., Koe G.S., Koe J.G., A Stopped-Flow Kinetic Study of the Assembly of Nonviral Gene Delivery Complexes Middaugh C.R. *Biophys. J.* **2005**, 88, 4146-4158.
[114] Ouyang D., Zhang H., Herten D.-P., Parekh H.S., Smith S.C. Structure, Dynamics, and Energetics of siRNA–Cationic Vector Complexation: A Molecular Dynamics Study. *J.Phys. Chem. B.* **2010**, 114: 9220-9230.
[115] Cullity, B. D.; Stock, S. R. *Elements of X-ray Diffraction, 3rd ed.*; Prentice Hall; South Bay Books: Bellingham, WA, U.S.A. **2001**.
[116] Glatter, O.; Kratky, O. *Small Angle X-ray Scattering*, 1st ed.; Academic Press: London, **1982**.
[117] Lindner P., Zemb T., Neutrons, X-rays and Light: Scattering Methods Applied to Soft Condensed Matter, 1st edition; Elesevier: North-Holland, Amsterdam, **2002**.
[118] Segad M., Hanski S., Olsson U., Ruokolainen J., Åkesson T., Jönsson, B. Microstructural and swelling properties of Ca and Na Montmorillonite: (in situ) observation with Cryo-TEM and SAXS. *Chem Phys. C.* **2012**, 116: 7596-7601.
[119] Guinier A., Fournet G., *Small Angle Scattering of X-rays*. Wiley Interscience: New York, **1955**.
[120] Avrami M., Kinetics of Phase Change. I General Theory *J Chem Phys*. **1939**, 7: 1103.

[121] Shultz J.M., *Polymer Crystallization*. Oxford University Press: New York, **2001**.
[122] Liu Y., Spring J.D., Steinhart M., Bansil R., Pressure jump kinetics of disorder to BCC ordering in diblock copolymer micelles in a selective solvent. *Macromolecules*, **2012**, 45: 9147-9154.
[123] Lindsey C.P., Patterson G.D. Detailed comparison of the Williams-Watts and Cole-Davidson functions. *J. Chem. Phys*., **1980**, 73: 3348.
[124] Fischer B.R., Eisler H.-J., Stott N.E., Bawendi M.G. Emission intensity dependence and single-exponential behavior colloidal quantum dot fluorescence lifetimes. *J. Phys. Chem. B.* **2004**, 108: 143-148
[125] Biancaniello P.L. Kim A.J., Crocker J.C. Long-time stretched exponential kinetics in single DNA duplex dissociation. *Biophysical society*, 2008, 94: 891-896.
[126] Zhou J., Liu J., Shi T., Xia Y., Luo Y., Liang D., Phase separation of siRNA–polycation complex and its effect on transfection efficiency. *Soft Matter*, **2013**, 9: 2262-2268.
[127] Falsini S., Ristori S., Ciani L., Di Cola E., Supuran C.T., Arcangeli A., In M. Time resolved SAXS to study the complexation of siRNA with cationic micelles of divalent surfactants. Soft Matter, **2014**, DOI: 10.1039/C3SM52429A.

General conclusion

Leukemia represents an heterogeneous group of malignancies with great variability in clinical course and response to therapy. Despite numerous advances obtained in the understanding the genetic and molecular basis of the pathology, a subset of patients remain refractory to conventional therapy.

Nowadays the advent of the new "omics" like genomic, proteomic, metabolomic opens the possibility to make a molecular profile of cancer for each patient, in order to develop a personalized therapy. This molecular profile would allow to identify genes or proteins involved in the pathogenesis as possible-biomarkers for a specific therapy.

In recent years the involvement of potassium channel, and in particular hERG channel, in tumor biology has been demonstrated in our laboratory. It is well established that hERG exerts a relevant role in leukemia where it regulate cell migration and transendothelial invasiveness in acute myeloid leukemia. hERG is activated in the presence of bone marrow microenvironment, inducing chemoresistance in acute lymphoblastic leukemia.

These experimental evidences suggest that hERG is a possible target in antineoplastic therapy and that hERG inhibitors can function as anticancer drugs.

In this thesis we present a pharmacological approach to reduce the activity of overexpressed hERG channel avoiding side effects like QT long syndrome and arrhythmia and we propose innovative carriers for anti-hERG siRNA as possible molecular therapy.

For the pharmacological effect we selected clarithromycin, a commercially used antibiotic. Experimental evidences demonstrate that it is a growth inhibitor and an antiangiogenetic agent of certain cancer cells. Therefore it was demonstrated that clarithromycin induces the inhibition of the late stage of autophagy, a mechanism of chemioresistance. In fact, the use of this drug restore the sensitivity to chemotherapy in chronic myeloid leukemia.

In addition, clarithromycin reduces the activity of hERG channel in HEK293 stably transfected with hERG and FLG29.1 (ALL) where hERG is abundantly expressed.

These characteristics, linked with known anthyarritmic effect, suggest the use of clarithromycin for leukemia treatment.

Initially we tested the effect of clarithromycin on an acute promyelocitic cell line (HL60) where hERG is overexpressed, with or without bone marrow mesenchymal cell line (MSCs). It was possible to individuate the LD_{50} of clarithromycin for HL60 in suspension (37±5μM) and in co-colture (67±5μM). As expected, the effect of clarithromycin is larger for HL60 in suspension than in co-colture which underlines the protecting effect mediated by bone marrow microenvironment.

In a subsequent set of experiments we tested the effect of clarithromycin in combination with cytarabine, following the method of Chou-Talay in order to use the software Calcusyn. We tested this two drugs at their corresponding LD_{50}, 37μM for clarithromycin and 45nM for cytarabine. This experiments demonstrate that the addition of clarithromycin to cytarabine reduce the chemoprotective effect induce by the presence of MSCs (CI=0.657).

The encouraging data obtained from *in vitro* experiments led to *in vivo* experiments on SCID mice, injected with HL60 cell, tagged with luciferase. These experiments were performed by Dott.ssa Marika Masselli. In the first set of experiments it was demonstrated the capability of clarithromycin to block tumor development and invasiveness. In turn, this second set of experiments demonstrated the synergic effect of cytarabine in addition with clarithromycin. The efficacy of this therapy is evidenced by the long survival of the animal group where three are still alive (up to 200 days).

We also explore the possibility of a molecular approach to hERG silencing by developing a new lipid based vectors for RNA interference (RNAi) targeting hERG. RNAi is a specific post-transcriptional silencing mechanism induced by small interfering RNA (siRNA) of 21pb. This phenomenon can be exploited for the treatment of diseases in which an overexpressed gene is involved. Despite this potentiality siRNA based therapeutics have not displayed major success so far and still present some physiological problems. The main barriers have been: (i) inefficient delivery to the correct cells or tissues, (ii) suboptimal gene silencing activity owing to instability and poor bioavailability of RNAi agents and (iii) toxicity due to off-target effects or immune activation. One of the main improvements is therefore expected by designing a delivery agents able to vehiculate siRNA to the target cells. For this reason we selected three Gemini surfactants:12-3-12, 12-6-12 , 12-12-12 and a triazine based surfactants SH14, as possible delivery agents of siRNA. In aqueous media these surfactants self-aggregate into spherical micelles and complex siRNA molecules through electrostatic interactions. We studied the physico-chemical properties of the complexes by time resolved SAXS at ESRF (Grenoble, France). These experiments allowed to elucidate the structural evolution of complexes from few ms till 10-15min after mixing. It was found that complex formation occurs rapidly (< 50 ms), the process being driven by counterion expulsion from the water-micelle interface. In the following instants siRNA and cationic micelles aggregate into “sandwiches” with repeat distance of 3-4nm and more structured assemblies appears, until a steady state is reached after 10-15 min. The final number of layer within the complexes is of 4-8units.

Complexes obtained with SH14 are less ordered than those formed by Gemini surfactants. In all cases an estimation of the complex size, i.e. its gyration radius, give values in the range 7-27nm.

We tested the cytotoxicity of Gemini surfactant and their complexes (CR=0.25) in three cell lines: HEK293, HCT8 and CHO. The two higher concentrations (10^{-4} M and $5x10^{-5}$) were found to be toxic while the two more diluted solutions were acceptably safe toward cells. This trend was observed for all the three cell lines treated with gemini surfactants alone and in combination with siRNA. We could therefore identify a range

of concentration in which our newly designed systems can be used for transfection experiments.
In this thesis the major intent was to increase the knowledge about hERG channel role in tumor in order to exploit these new informations for designing innovative anticancer therapies.

Aknowledgments

I would like to thank:

- Noi per Voi association (referent Mr. Pasquale Tulimiero) which sustains the research project on chemoresistance in pediatric leukemia coordinated by Prof. Annarosa Arcangeli;
- Foundation Ente Cassa di Risparmio di Firenze "In memoria di Jacopo Ficai" for annual grant (2012);
- Fondazione Ente Cassa di Risparmio di Firenze for annual grant (2013).

I would like to thank my tutor Prof. Annarosa Arcangeli for giving me the opportunity to attend this PhD course, Dr. Serena Pillozzi for the supervision of *in vitro* treatments and Dr. Marika Masselli for *in vivo* experiments.

I would like to express my gratitude to my co-tutor Dr. Sandra Ristori whose expertise, understanding, and patience, added considerably to my personal experience. I appreciate her vast knowledge and skill in many areas (e.g. vision, growing, ethics), and her assistance in writing reports (i.e. scholarship applications, articles and this thesis).

I would like to thank Dr. Laura Ciani not only for her professional support but also for her friendship. Thanks her for answering my questions, helping to think rationally and even for listening to my problems.

I express my deep gratitude to Dr. Martin In for his experience and for helping us to SAXS data interpretation. Thanks also his contribution, our SAXS data took place in a publication.

I would like to express my deep gratitude to my family for always believing in me, for their continuous love and their supports in my decisions.

I would like to thanks my all friends, in particular Eleonora, Chiara and Elena for their special support.